

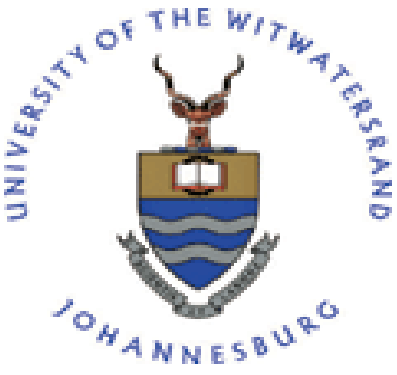
https://dspace.org/

Investigation of the effect of bio-dispersants on condenser tube fouling and thermal performance

Nagel, Louw

2020
https://hdl.handle.net/10539/31244

Downloaded from a DSpace repository. https://dspace.org/



Investigation of the Effect of Bio-dispersants on Condenser Tube Fouling and Thermal Performance

Louw Nagel

(Student number: 1884324)

School of Mechanical, Industrial and Aeronautical Engineering,

University of the Witwatersrand

Johannesburg, South Africa.

Supervisors:

Supervisor: Prof. Walter Schmitz (Wits)

Co-Supervisor: Prof. Hlanganani Tutu (Wits)

A dissertation submitted to the Faculty of Engineering and the Built Environment, University of the Witwatersrand, in fulfilment of the requirements for the degree of Masters in Engineering.

12 June 2020

SCHOOL OF MECHANICAL, INDUSTRIAL & AERONAUTICAL ENGINEERING

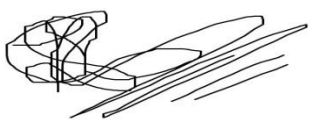
PLAGIARISM DECLARATION TO BE SIGNED BY ALL HIGHER DEGREE STUDENTS

SENATE PLAGIARISM POLICY: APPENDIX ONE

I Louw Nagel (Student number: 1884324) am a student registered for the degree of Master of Science in Engineering by Research Mechanical, Industrial and Aeronautical in the academic year 2.

I hereby declare the following:

- I am aware that plagiarism (the use of someone else's work without their permission and/or without acknowledging the original source) is wrong.
- I confirm that the work submitted for assessment for the above degree is my own unaided work except where I have explicitly indicated otherwise.
- I have followed the required conventions in referencing the thoughts and ideas of others.
- I understand that the University of the Witwatersrand may take disciplinary action against me if there is a belief that this is not my own unaided work or that I have failed to acknowledge the source of the ideas or words in my writing.

Signature:  Date: **12/06/2020**

Abstract

Bio-dispersants and biocides are currently dosed into a wet-cooled recirculating cooling water system at a coal-fired power station. Although these chemicals are being used, no improvement in the heat rate or condenser performance is observed at the power station where the research was conducted. A portable offline test facility that operates in real time was used to monitor the fouling heat transfer resistance on the water side of condenser tubes, while various bio-dispersants were dosed at various concentrations in the individual test condenser tubes. Cooling water tapped off from the main turbine condenser flowed through the test facility. The fouling factors, cleanliness factors, friction factors, mass gained and bacterial counts of the set of chemically dosed tubes in this test facility were continuously monitored against the untreated tubes in this facility. The results indicated that the dosing of two of the three bio-dispersants worsened the heat transfer across the tube walls and fouling layers of the titanium condenser tubes, at times increasing the fouling factors up to 5.2 times higher than the non-dosed controls. The fouling resistances of each test was related to the impact on cycle efficiency and it was found that load losses up to 243 MW could potentially be obtained with incorrect chemical dosing. It is recommended that further studies should be carried out to investigate the effect of combined dosing of bio-dispersants and biocides on biofilm formation and heat transfer across the tube walls and fouling layers of titanium condenser tubes.

Acknowledgements

I want thank the EPPEI program for giving me the opportunity to complete my masters in engineering and for the funding that was made available for me.

My mentor Professor Walter Schmitz, thank you for your exceptional support and guidance. Heena Madhav, thank you for your leadership, mentorship and guidance. Francois du Preez thank you for the technical knowledge you contributed.

I also want to thank the following members at the power utility for their unconditional support and guidance: Siboniso Hlatshwayo, Harry Mokabane, Ockert Augustyn, Sheldon Beangstrom, Kelley Reynolds-Clausen and Portia Maduna. Thank you, Professor Hlanganani Tutu for being my co-supervisor.

Lastly I want to thank my wife for her unconditional support.

Table of Contents

Abstract ii

Acknowledgements iii

Table of Contents iv

List of Figures viii

List of Tables xii

Nomenclature xiii

1 Background 1

2 Literature review 2

2.1 Coal fired power station 2

2.2 Wet recirculating cooling system 2

2.3 Fouling overview 3

2.4 Anti-scalants overview 5

2.5 Biofilm 6

2.6 Biocides overview 8

2.6.1 Non-Oxidising biocides 8

2.6.2 Oxidising biocides 8

2.7 Bio-dispersants overview 9

2.8 Impact of biofilms on industrial systems 10

2.9 Industry use of bio-dispersants 11

2.10 Supplier recommendations regarding bio-dispersants 11

2.11 Titanium condenser tubes 12

2.12 Effect of fouling on heat transfer 12

2.13 Impact of fouling on cycle efficiency 14

3 Methodology overview 17

4 Experimentation 18

4.1 Introduction 18

4.2 Apparatus description 19
4.3 Modifications to existing test apparatus 22
4.4 Measurement techniques 23
4.4.1 Temperature measurement 26
4.4.2 Pressure measurement 26
4.4.3 Flow measurement 28
4.4.4 Tube mass 28
4.4.5 Bacterial swabs 28
4.4.6 Cooling water quality 28
4.5 Operation and control 29
4.5.1 Tube installation 29
4.5.2 Heat transfer 29
4.5.3 Maintenance 29
4.6 Analysis 30
4.6.1 Heat transfer inside the parallel co-current heat exchanger tubes 30
4.6.2 Inside tube convection coefficient 31
4.6.3 Outside tube convection coefficient 32
4.6.4 Tube heat transfer performance analysis 33
4.6.5 Mass and energy balance checks 34
4.6.6 Experimental procedure 35
4.7 Uncertainty analysis 40
4.8 Cooling water analysis 41
5 Results and discussion 44
5.1 Fouling factor 44
5.2 Cleanliness factor 49
5.3 Friction factor 52
5.4 Mass gain 55

5.5 Bacterial counts 56
6 Relating the impact of single tube fouling to the actual main turbine condenser 59
6.1 Heat transfer inside the actual main turbine condensers 59
6.1.1 Inside tube convection coefficient 60
6.1.2 Shell side convection coefficient 60
6.1.3 Condenser heat transfer performance analysis 61
6.2 Relating the experimentally determined fouling resistances to its impact on an actual power generating unit. 61
6.2.1 Results obtained from the fouling resistances obtained from test 1: 63
6.2.2 Results obtained from the fouling resistances obtained from test 2: 66
6.2.3 Results obtained from the fouling resistances obtained from test 3: 68
7 Conclusions and recommendations 72
References 75
Appendix A 83
Appendix B 88
B.1 Fluid properties 88
Appendix C 89
C.1 Sample calculations 89
C.1.1 Measured variables: 89
C.1.2 Fluid thermodynamic properties 90
C.1.3 Flow rates 91
C.1.4 Friction factor and Reynolds numbers 93
C.1.5 Nusselt numbers and convection heat transfer coefficients 93
C.1.6 Thermal resistances 94
C.1.7 Heat transfer 96
Appendix D 98
D.1 Before increase in dosing concentration 98

D.2 After increase in dosing concentration....102
Appendix E....106
Appendix F....108
F.1 Main turbine condenser sample calculations....108
F.1.1 Fluid thermodynamic properties....109
F.1.2 Flow rates....112
F.1.3 Friction factor and Reynolds numbers....113
F.1.4 Nusselt numbers and convection heat transfer coefficients....113
F.1.5 Thermal resistances....116
F.1.6 Heat transfer....117

List of Figures

Figure 1: Basic wet recirculating cooling cycle. 3

Figure 2: Condenser inside tube precipitation fouling at a power station on the utility. 4

Figure 3: Condenser inside tube particulate fouling at a power station in the utility. 5

Figure 4: Schematic cross-sectional tube drawing showing the fouling layer. 13

Figure 5: Thermal resistances for heat transfer from the hot to the cold fluid. 14

Figure 6: Rankine power cycle: Temperature – entropy diagram 15

Figure 7: Summary of the methodology used. 17

Figure 8: The location of the test apparatus at the recirculating cooling water system. 18

Figure 9: The location of the test apparatus on the actual plant - (1) Test apparatus, (2) 10% tap - off line 19

Figure 10: Layout of the test apparatus – (1) temperature probe, (2) polypropylene supports, (3) annulus manifold, (4) hot water flow direction, (5) cooling water flow direction, (6) cooling water manifold, (7) diaphragm valve 20

Figure 11: Water flow through annuli and titanium tube – (1) hot water flow, (2) cooling water flow 20

Figure 12: Heat transfer conditions compared in the double pipe heat exchanger and the actual condenser - (1) hot water flow, (2) cooling water flow, (3) fouling layer, (4) heat transfer, (5) steam, (6) condensate (Goodenough, 2017) 21

Figure 13: Layout of double pipe heat exchanger – (1) polyurethane insolation, (2) tube gland, (3) titanium condenser tube, (4) hot water jacket, (5) pressure tapping 22

Figure 14: Layout of the cooling water entrance point – (1) cooling water manifold, (2) temperature probe, (3) chemical injection point, (4) cooling water flow direction 23

Figure 15: Piping and instrumentation diagram for the test apparatus. 25

Figure 16: Pressure tapping – (1) Pipe saddle, (2) Isolating valve, (3) PVC hose to common manifold 27

Figure 17: U-type manometer – (1) Pressure differential over the first condenser tube. 27

Figure 18: A flow chart explaining the experimental procedure. 38

Figure 19: A flow chart explaining the three fouling tests in the experimental procedure (Figure 18). 39

Figure 20: Measured fouling factors for tube 1, 2, 3, 4, 5 and 6 during test 1 – (1) Plant dosed biocide – (2) Increase dosing concentration in tube 1, 2, 3 and 6 – (3) Dosed NaOCl in strainers – (4) Dosed NaOCl in strainers 46

Figure 21: Measured fouling factors for tube 1, 2, 3, 4, 5 and 6 during test 2 – (1) Plant dosed biocide – (2) Increase dosing concentration in tube 1, 2, 3 and 6.....47

Figure 22: Measured fouling factors for tube 1, 2, 3, 4, 5 and 6 during test 3 – (1) Plant dosed biocide – (2) Increase dosing concentration in tube 1, 2, 3 and 6.....49

Figure 23: Calculated cleanliness factors for tube 1, 2, 3, 4, 5 and 6 during test 1 – (1) Plant dosed biocide – (2) Increase dosing concentration in tube 1, 2, 3 and 6 – (3) Dosed NaOCl in strainers – (4) Dosed NaOCl in strainers 50

Figure 24: Calculated cleanliness factors for tube 1, 2, 3, 4, 5 and 6 during test 2 –(1) Plant dosed biocide –(2) Increase dosing concentration in tube 1, 2, 3 and 6 51

Figure 25: Calculated cleanliness factors for tube 1, 2, 3, 4, 5 and 6 during test 3 – (1) Plant dosed biocide – (2) Increase dosing concentration in tube 1, 2, 3 and 6 52

Figure 26: Measured friction factors for tube 1, 2, 3, 4, 5 and 6 during test 1 – (1) Plant dosed biocide – (2) Increase dosing concentration in tube 1, 2, 3 and 6 – (3) Dosed NaOCl in strainers – (4) Dosed NaOCl in strainers 53

Figure 27: Measured friction factors for tube 1, 2, 3, 4, 5 and 6 during test 2 – (1) Plant dosed biocide – (2) Increase dosing concentration in tube 1, 2, 3 and 6.....54

Figure 28: Measured friction factors for tube 1, 2, 3, 4, 5 and 6 during test 3 – (1) Plant dosed biocide – (2) Increase dosing concentration in tube 1, 2, 3 and 6.....55

Figure 29: Mass gained for tube 1, 2, 3, 4, 5 and 6 during test 1, 2 and 3. 56

Figure 30: Anaerobic bacterial counts for tube 1, 2, 3, 4, 5 and 6 during test 1, 2 and 3. 57

Figure 31: Aerobic bacterial counts for tube 1, 2, 3, 4, 5 and 6 during test 1, 2 and 3. 58

Figure 32: Generated load and actual condenser saturation pressure for test 1- (D) Dosed tube-6, (ND) Non dosed tube-4 64

Figure 33: Financial impacts of chemical dosing for test 1: non-dosed tube – 4 (ND) and dosed (D) tube-6. 65

Figure 34: Generated load and actual condenser saturation pressure for test 2- (D) Dosed tube-1, (ND) Non dosed tube-4. 67

Figure 35: Financial impacts of chemical dosing for test 2: non-dosed tube – 4 (ND) and dosed (D) tube-1. 68

Figure 36: Generated load and actual condenser saturation pressure for test 3- (D) Dosed tube-3, (ND) Non dosed tube-4. 69

Figure 37: Financial impacts of chemical dosing for test 3: non-dosed tube – 4 (ND) and dosed (D) tube-3. 71

Figure 38: Cooling water tube section modelled – (1) Section where CFD was performed, (2) Proposed chemical injection point 83

Figure 39: CFD geometry as per Figure 10. 84

Figure 40: Meshed geometry as in Figure 39. 84

Figure 41: CFD results for a bio-dispersant flowrate of 1.24761e-05 kg/s (Final mixing concentration of 20 ppm). The scale indicates the bio-dispersant concentration in mg bio-dispersant per 1 L water. 86

Figure 42: CFD results for a bio-dispersant flowrate of 6.238056e-06 kg/s (Final mixing concentration of 10 ppm). The scale indicates the bio-dispersant concentration in mg bio-dispersant per 1 L water. 86

Figure 43: CFD results for a bio-dispersant flowrate of 1.24761e-06 kg/s (Final mixing concentration of 2 ppm). The scale indicates the bio-dispersant concentration in mg bio-dispersant per 1 L water. 87

Figure 44: Bio-dispersant dosing concentration: Test 1: Tube 1 (5.9 ml/h), Test 2: Tube 1 (6.2 ml/h) and Test 3: Tube 2 (5.6 ml/h)..... 98

Figure 45: Bio-dispersant dosing concentration: Test 1: Tube 2 (4.4 ml/h), Test 2: Tube 2 (4.5 ml/h) and Test 3: Tube 1 (3.6 ml/h)..... 99

Figure 46: Bio-dispersant dosing concentration: Test 1: Tube 3 (2.3 ml/h), Test 2: Tube 3 (2.6 ml/h) and Test 3: Tube 6 (1.4 ml/h)..... 100

Figure 47: Bio-dispersant dosing concentration: Test 1: Tube 6 (3.1 ml/h), Test 2: Tube 6 (4.1 ml/h) and Test 3: Tube 3 (9.2 ml/h)..... 101

Figure 48: Bio-dispersant dosing concentration: Test 1: Tube 2 (30.4 ml/h), Test 2: Tube 1 (36 ml/h) and Test 3: Tube 2 (24.5 ml/h)..... 102

Figure 49: Bio-dispersant dosing concentration: Test 1: Tube 1 (24.9 ml/h), Test 2: Tube 2 (21.3 ml/h) and Test 3: Tube 1 (22 ml/h)..... 103

Figure 50: Bio-dispersant dosing concentration: Test 1: Tube 3 (19.9 ml/h), Test 2: Tube 6 (15.5 ml/h) and Test 3: Tube 6 (16.3 ml/h)..... 104

Figure 51: Bio-dispersant dosing concentration: Test 1: Tube 6 (13.6 ml/h), Test 2: Tube 3 (14.2 ml/h) and Test 3: Tube 3 (34.8 ml/h)..... 105

List of Tables

Table 1: Properties of each bio-dispersant used during each test. (Information obtained from the different suppliers) 36

Table 2: Dosing concentrations (ppm) (DC) of each tube during each test. 37

Table 3: Uncertainty variables and values 41

Table 4: Average cooling water properties for the duration of each test. 42

Table 5: Measured variables of tube 6 during test 1 at day 8. These values are used in the sample calculations. 89

Table 6: Inputs used for the main turbine condenser sample calculations 108

Table 7: Guess values used for the main turbine condenser sample calculations 108

Table 8: Iterated values for the variables above. 119

Nomenclature

Symbols:

A_{ANN}	Annulus cross sectional inside area	m²
A_{ANN_S}	Total annulus inside area available for heat transfer	m²
A_c	Outside tube area available for heat transfer	m²
A_i	Tube cross sectional inside area	m²
A_{Nu}	Experimentally determined coefficient	-
A_s	Total tube inside area available for heat transfer	m²
A_{shell_S}	Total shell inside area available for heat transfer	m²
B_{Nu}	Experimentally determine coefficient	-
CF	Cleanliness factor	%
$Cp_{W_{ANN}}$	Water specific heat capacity (Annulus)	$\frac{J}{kg \cdot K}$
Cp_c	Water specific heat capacity (Condensate)	$\frac{J}{kg \cdot K}$
$Cp_{W_{CW}}$	Water specific heat capacity (Cooling water)	$\frac{J}{kg \cdot K}$
Cp_W	Water specific heat capacity	$\frac{J}{kg \cdot K}$
D_{ANN}	Annulus inside diameter	m
D_i	Tube inside diameter	m
D_O	Tube outside diameter	m

EB	Energy balance	%
E_{reg}	Energy rejected by main turbine condenser	MW
f_{ANN}	Friction factor (annulus)	-
F_{ANN}	Tube annulus flow rate	L/s
F_{CW}	Tube cooling water flow rate	L/s
f_{cw}	Friction factor (Cooling water)	-
F_{dose}	Chemical dosing flow rate	ml/h
g	Gravitational acceleration	$\frac{m}{s^2}$
ΔH	Cooling water tube manometric height difference	mm
h_{ANN}	Annulus convection coefficient	$\frac{W}{m^2 \cdot K}$
h_c	Condensate convection coefficient	$\frac{W}{m^2 \cdot K}$
h_{CW}	Cooling water convection coefficient	$\frac{W}{m^2 \cdot K}$
h_{fg}	Available heat of evaporation based on the saturation pressure	kJ/kg
$H_{hotwell}$	Hotwell enthalpy	kJ/kg
h_L	Enthalpy of saturated liquid water	kJ/kg
HR	Net heat rate	kWh
h_s	Steam enthalpy	kJ/kg
h_{shell}	Shell side convection coefficient	$\frac{W}{m^2 \cdot K}$
h_V	Enthalpy of saturated water vapour	kJ/kg

k_{ANN}	Annulus water thermal conductivity	$\frac{W}{m \cdot K}$
k_c	Condensate thermal conductivity	$\frac{W}{m \cdot K}$
k_{CW}	Cooling water thermal conductivity	$\frac{W}{m \cdot K}$
k_s	Steam thermal conductivity	$\frac{W}{m \cdot K}$
k_t	Tube thermal conductivity	$\frac{W}{m \cdot K}$
k_W	Water thermal conductivity	$\frac{W}{m \cdot K}$
L_{eff}	Effective heat transfer length	m
L_p	Length between pressure tapings	m
L_t	Tube length	m
m_{ANN}	Annulus water mass flow	kg/s
m_C	Condensate mass flow	kg/s
m_{CW}	Cooling water mass flow	kg/s
N_p	Number of passes	-
N_t	Number of tubes	-
Nu_{ANN}	Annulus water Nusselt number	-
Nu_{CW}	Cooling water Nusselt number	-
P_{gen}	Generated load	MW
P_L	Pressure drop over condenser tube (water)	mm H_2O

Pr_{ANN}	Annulus Prandtl number	-
Pr_c	Condensate Prandtl number	-
Pr_{CW}	Cooling water Prandtl number	-
P_{sat}	Saturation pressure	kPa
Q	Heat transfer rate	W
q	Steam quality	-
Q_{ANN}	Annulus heat transfer rate	W
Q_C	Condensate heat transfer rate	W
Q_{CW}	Cooling water heat transfer rate	W
R_{ANN}	Annulus thermal resistance	K/W
R_{CW}	Cooling water thermal resistance	K/W
Re_{ANN}	Annulus water Reynolds number	-
Re_{CW}	Cooling water Reynolds number	-
R_f	Fouling layer thermal resistance	K/W
R_{f_D}	Fouling resistance inside condenser tube as per data	K/W
R_i	Inner tube convection thermal resistance	K/W
R_O	Outer tube convection thermal resistance	K/W
$\sum$R	Total thermal resistance	K/W
R_{shell}	Shell side thermal resistance	K/W
R_{tube}	Tube thermal resistance	K/W

T	Temperature	°C
$T_{ANN_{in}}$	Annulus inlet temperature	°C
T_{ANN_m}	Annulus mean temperature	°C
$T_{ANN_{out}}$	Annulus outlet temperature	°C
$T_{cooling\ water}$	Cooling water temperature	°C
$T_{CW_{in}}$	Cooling water inlet temperature	°C
$T_{CW_{out}}$	Cooling water outlet temperature	°C
T_{CW_m}	Cooling water mean temperature	°C
T_{LM}	Log mean temperature difference	°C
T_{Sat}	Saturation temperature	°C
T_{steam}	Steam temperature	°C
T_{Wall_o}	Outside tube wall temperature	°C
U	Overall heat transfer coefficient	$\frac{W}{m^2 \cdot K}$
u_{ANN}	Annulus water axial velocity in tube	m/s
u_{CW}	Cooling water linear velocity in tube	m/s
U_t	Overall heat transfer coefficient at time t	$\frac{W}{m^2 \cdot K}$
U_{t_0}	Overall heat transfer coefficient at time 0	$\frac{W}{m^2 \cdot K}$

Greek:

ρ_{ANN}	Annulus water density	$\frac{kg}{m^3}$
ρ_c	Condensate density	$\frac{kg}{m^3}$
ρ_{CW}	Cooling water density	$\frac{kg}{m^3}$
ρ_W	Water density	$\frac{kg}{m^3}$
μ_{ANN}	Annulus water dynamic viscosity	$\frac{kg}{s \cdot m}$
μ_c	Condensate dynamic viscosity	$\frac{kg}{s \cdot m}$
μ_{CW}	Cooling water dynamic viscosity	$\frac{kg}{s \cdot m}$
μ_W	Water dynamic viscosity	$\frac{kg}{s \cdot m}$

Acronyms:

SANAS: South African National Accreditation System

1 Background

The wet cooled power stations at the utility are currently experiencing severe main turbine condenser load losses, approximately 180 MW at the power station where the research was conducted, due to fouling that occurs inside the main turbine condenser tubes. Losses due to poor cooling tower performance can also contribute substantially to the main turbine condenser load. The fouling is observed due to bad cooling water quality and non-optimized chemical dosing regimens. The load losses add extensive pressure to the South African electricity grid which increases the chances of load shedding which has a negative influence on the economy of the country.

Three types of fouling are observed in the main turbine condensers at the power station: particulate, precipitation and biological fouling. The particulate fouling is managed by maintaining the strainers in the cooling water system to prevent solid particles from entering the condenser tubes. Precipitation and biological fouling however, are managed by dosing anti-scalants and a combination of bio-dispersants and biocides respectively. The dosing of bio-dispersants and biocides happens on an irregular basis. No measurable improvement in the current condenser performance is observed with the current dosing regimen when these chemicals are dosed into the main cooling water cycle.

The research question of the study is: What is the change in fouling rate inside titanium condenser tubes as a result of chemical dosing?

2 Literature review

2.1 Coal fired power station

The utility consists of 15 coal-fired power stations of which 11 are cooled with recirculating treated raw water (Kotzé, 2015). This study has been conducted at one of these wet cooled coal-fired power stations. A steam surface condenser at the power plant which has a capacity of 500 MW consists of approximately 26000 titanium condenser tubes. The steam surface condensers are used to transfer the latent heat from the steam exiting the low-pressure turbine to the raw cooling water flowing through the inside of the condenser tubes. A lower condenser temperature will increase the cycle efficiency in a regenerative Rankine cycle (Smith, J.M , Van Ness, H.C, Abbott, 2015) (Tuo and Hrnjak, 2014). The maximum heat transfer efficiency deteriorates as a condenser tube fouls which, therefore, lead to a decrease in cycle efficiency (Love, Szybist and Sluder, 2012) (Urbaniec, Markowski and Trafczynski, 2011) (Li *et al.*, 2016) (Liengen, T., Féron, R., Basséguy, R., Beech, 2018).

2.2 Wet recirculating cooling system

A wet recirculating raw water cooling system can be explained as water recirculating from a cooling tower through a single or a set of heat exchangers where it is heated up and then returned to the cooling tower where it is cooled (Figure 1). Cooling water (make- up water from the local water source) needs to be added to the system on a regular basis to compensate for the evaporation water losses. Cooling water needs to be discarded from the recirculating cooling system (blowdown) to prevent the build-up of minerals and sediments in the recirculating system as evaporation takes place (Deziani *et al.*, 2017). A way to decrease the water consumption at the power stations is to decrease the number of blowdowns being done which then leads to higher cycles of concentrations which in turn increase the fouling and corrosion potential of the cooling water (Rahmani, 2017).

Methods to treat water in wet recirculating systems include: sedimentation, coagulation, water clarification, water softening, pH correction together with the use of anti-scalants, bio-dispersants and biocides (Rahmani, 2017).

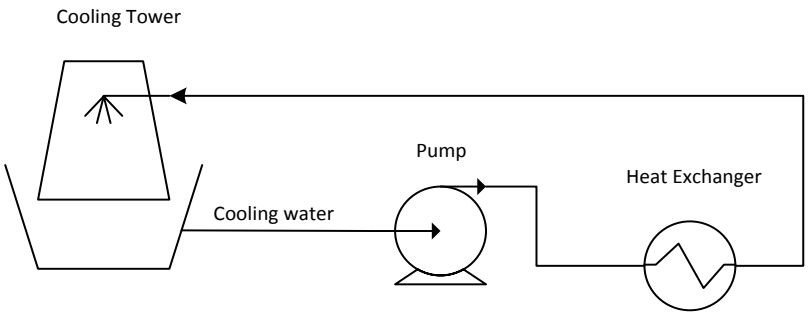


Figure 1: Basic wet recirculating cooling cycle.

2.3 Fouling overview

Fouling is defined as the process where unwanted particles deposit on a heat transfer surface that lessens the heat transfer through the surface and increases the pressure drop over the heat transfer surface (Pääkkönen *et al.*, 2015). Fouling reduces the heat transfer between the hot steam and the cooling water in power station condensers. Condenser fouling has a negative effect on the cycle efficiency of a power station which has large economic and production effects (Nebot *et al.*, 2007).

Goodenough (2017) distinguished between six types of fouling:

1. Precipitation (scaling) fouling: Precipitation of dissolved minerals in supersaturated solutions on the heat transfer surface (Goodenough, 2017). Scaling is due to precipitation of dissolved minerals due to an increase of temperature over a heat transfer surface. Precipitation fouling in a supersaturated solution takes place when a nuclei is formed and then grows into a crystal structure. (Mwaba, Golriz and Gu, 2006).
2. Biological fouling: The accumulation of living organisms on a heat transfer surface which amends the heat transfer characteristics of the surface.
3. Particulate fouling: Accumulation of solid particles suspended in the heat transfer medium on the heat transfer surface.
4. Chemical reaction fouling: Chemical reactions take place over the heat transfer surface which produce products which deposit on the heat transfer surface. The heat

transfer surface does not take part in the chemical reaction (Watkinson and Wilson, 1997).

5. Corrosion fouling: Formation of corrosion products on the heat transfer surface as a result of corrosion. The heat transfer properties of the surface are altered (Somerscales, 1997).
6. Freezing fouling: A fouling layer is formed on the heat transfer surface which is colder than the bulk fluid (due to crystallization of the bulk fluid or dissolved species) (Fernandez-Torres *et al.*, 2001).

Precipitation, particulate and biological fouling are normally observed in the utility's condensers (Goodenough, 2017). Figure 2 and Figure 3 show precipitation and particulate fouling observed inside a condenser at a power station at the utility where the research is conducted. The biological fouling appears as a transparent slime layer on the tube walls and cannot be visibly captured. Biological fouling was confirmed by a study conducted by Goodenough (2017) at the same power plant where this research was conducted. The effects of bio-dispersants on condenser fouling at a power station in the utility are investigated in this research study. This research study will not be limited to identifying other types of fouling mechanisms which may or may not occur.



Figure 2: Condenser inside tube precipitation fouling at a power station on the utility.



Figure 3: Condenser inside tube particulate fouling at a power station in the utility.

2.4 Anti-scalants overview

Scale deposition takes place when the cooling water used is supersaturated with one or more soluble salts e.g. calcium carbonate salts. Some of these soluble salts will deposit on the heat transfer surface with an increase of temperature which will form the scale layer. Anti-scalants reduces the crystals in the scaled layer and reduce nucleation and growth rates. Anti-scalants can be effective and can be used at very low dosages at affordable costs (Zaslavschi *et al.*, 2013). In a clean tube, calcium carbonate scaling has a long initial lag time before scaling occurs and this initial lag time is increased with the use of anti-scalants (Amjad and Hooley, 1994). Precipitation scaling in this study is caused by inversely soluble salts.

The effectiveness (decreasing) of calcium carbonate precipitation follows the sequence: formulated-anti-scalant (AF 1000) > sodium heaxametaphosphate (SHMP) > Poly maleic Acid (PMA) > Poly Acrylic Acid (PAA) > copolymers of acrylic acid and acrylamide (P(AA:AM)) > poly(acrylamide) (P-AM) ≈ Poly(2-acrylamido-2-methyl propane sulfonic acid) (P-SA) ≈ no anti-scalant used from a study conducted by (Amjad and Hooley, 1994). PMA was used as a calcium carbonate scale inhibitor in water conditions that has high hardness, alkalinity and temperatures (Shandong Taihe Water Treatment Technologies Co, 2013). PAA was also used to increase the lag time before scale occurs. It was identified by running a simulation on French Creek Software ™ (limited to precipitation fouling) that anti-scalants with Poly maleic Acid (PMA) or Poly Acrylic Acid (PAA) as the active ingredient

will give the best results at the power station where the research will be conducted with its unique water chemistry (French Creek Software, 2017).

2.5 Biofilm

Jamal *et al*. (2015) described a biofilm as a group of micro-organisms where the microbial cells adhere to each other or on living or non-living surfaces within a self-produced matrix of extracellular polymeric substance (EPS). The biofilm produces an extracellular polymeric substance which consists of proteins (<1-2%), deoxyribonucleic (DNA) and ribonucleic acid (RNA) (<1-2%), polysaccharides (1-2%), and water (up to 97%) and this is responsible for the flow of nutrients inside the biofilm medium (Jamal *et al*., 2015). Bacteria inside cooling water systems forms polymeric matrixes that bind the microbes providing mechanical stability inside the biofilm (Di Pippo *et al*., 2018). Biofilms compose of microorganisms which adhere to surfaces which are submerged in a self-produced matrix (Di Pippo *et al*., 2017). Biofilms consist of microbial cells which include algae, fungus and bacteria (Buckman, 2017).

Biofilm formation is dependent on the pH of the cooling water. Fungal growth has a lower optimal growth pH than bacterial growth (Horn and Richards, 2010).

Cooling water can consist of free-floating bacterial (planktonic) or bacteria that attach to the surfaces called sessile bacteria. Sessile bacteria has limps which allow the attachment to wall surfaces (Horn and Richards, 2010). The sessile bacteria form a thin layer on the surfaces which then develop into a thick layer of biofilm as the bacteria grow. The biofilm consists of a variety of bacteria species. Dissolved minerals inside the cooling water like calcium, magnesium, silica and iron react with the carboxyl groups in the polymer biofilm layer. The biofilm layer is thickened by the minerals (Horn and Richards, 2010) (Christophersen, 2006). The top layer of a biofilm normally consists of an aerobic bacteria layer depending on the cooling water conditions. The lower layer is normally oxygen deprived and consists of an anaerobic bacteria layer. The incoming cooling water stream is nutrient rich and feeds the bacteria in the biofilm layer (Horn and Richards, 2010).

Water with a high total suspended solids (TSS) count causes scaling and encourages biofilm formation (Mohseni and Berijani, 2018). A bio-dispersant will be effective in water with a

high (> 2 ppm) total organic carbon (TOC) count (Buckman, 2017). Corrosion takes place underneath the biofilms because of by-products released by the bacteria in the biofilm (Christophersen, 2006).

Wet recirculating cooling water systems are the perfect environment for bacterial growth. The average temperatures vary from 25 °C to 35 °C, the water is exposed to direct sunlight, new planktonic cells enter the system on a continuous basis, the pH is very close to neutral and the system is continuously made up by raw water (Di Pippo *et al.*, 2018).

Jamal *et al.* (2015) described biofilm formation as a very complex process in which microbial cells transform from a planktonic to sessile growth mode. Biofilm formation is described as a multi-step process with the following steps (Jamal *et al.*, 2015):

- Attachment: A reversible connection is made by a microbial cell to a surface or another microbial cell when the microbial cell nears the surface or another microbial cell. Rough, hydrophilic and coated surfaces are described as ideal surfaces for biofilm formation. Fluid velocity, temperature and nutrient concentrations influence biofilm growth.
- Micro-colony formation: The microbial cells start to multiply as soon as they have attached to the surfaces or other cells. The initially attached cells trigger the multiplication of the existing cells and the formation of the extracellular matrix.
- Three-dimensional structure formation and maturation: The micro-colonies trigger the formation of the extracellular matrix. The extracellular matrix allows for water and nutrient channels to the cells as well as removing waste from the cells.
- Detachment: Cells leave the biofilm on a regular basis, enabling rapid multiplication and dispersing of the cells. Detachment occurs naturally when the extracellular polysaccharides or exopolymeric substances (EPS) production is stopped, or due to the mechanical properties of the fluid. Detached cells have the ability to retain properties of the biofilm, such as resistance to certain chemicals, and these detached cells can quickly return to their normal planktonic states.

Cells in biofilms have the ability to communicate through a mechanism called quorum sensing. Quorum sensing enables the communication between inter and intra species which includes: food shortages and environmental conditions (disinfectants, antibiotics, bacterial colonization) (Jamal *et al.*, 2015).

It is important to note that cells from a biofilm colonize in other regions where new colonies are formed when a mature biofilm undergoes a dispersive process (Prakash, Veeregowda and Krishnappa, 2003). The bacteria inside the biofilms have exponential growth rates and can cause operational deviations in a very small period of time (Horn and Richards, 2010).

2.6 Biocides overview

The growth of microorganisms is controlled and or eliminated by the use of biocides which is also known as microbicides or inhibitors. Several types of biocides are available to control biofouling of process surfaces (Morkus *et al.*, 2018). Biocides are divided into two groups, oxidising and non-oxidising biocides (Elsmore, 1994).

2.6.1 Non-Oxidising biocides

The power plant at which the research is conducted doses 10 ppm Isothiazolinone and 10 ppm 2,2-dibromo-3-nitrilopropionamide (DBNPA) once a month on an alternating basis. Isothiazolinone is used to control the growth of microorganisms and is generally used in industrial systems. Isothiazolinone is described as a fast-acting and effective biocide (Mardones *et al.*, 2018). DBNPA is a widely used halogenated amide which is effective against planktonic organisms. DBNPA is not as effective as oxidising biocides (Mueller *et al.*, 2002).

Non-oxidising biocides are normally dosed once a week into the cooling water systems in conjunction with a continuous dosing of oxidising biocides (Rahmani, Jadidian and Haghtalab, 2016).

2.6.2 Oxidising biocides

Chlorine and or sodium hypochlorite are widely used as an oxidising biocide and are dosed in a continuous manner (Rahmani, Jadidian and Haghtalab, 2016). Chlorine dioxide is currently being used to control biofilms in: drinking water systems, desalination units, in the petrochemical industry and at power stations. Chlorine dioxide is normally dosed in cooling water systems at 0.6 to 1 ppm and is known to kill and remove biofilms by penetrating through the cellular membranes (Venkatnarayanan *et al.*, 2017). Bromine is also used as an effective biocide in industrial systems (Elsmore, 1994).

Several resistance mechanisms of biofilms to biocides have been reported. Biofilms of bacterial species have developed resistance to biocides such as Isothiazolinone, iodine and chlorine (Cloete, 2003).

2.7 Bio-dispersants overview

Bio-dispersants as an antifoulant are described by Cloete, Jacobs and Brözel (1999) as a synthetic surfactant used to control microbiological growth in cooling water systems. Olariu (2015) stated that a bio-dispersant has non-biocidal surface active ingredients which break up biofilms into smaller pieces and remove them from surfaces where they attached. The dispersed particles are easily removed by blowdowns of the cooling system (Olariu, 2015). Bio-dispersant dosing can happen either on a continuous or periodic basis. The disadvantage of bio-dispersants is that it can cause clogging of downstream equipment once the biofilm is removed from a surface (Horn and Richards, 2010). A bio-dispersant normally consists of amphiphilic molecules that consist of hydrophobic and hydrophilic parts. The polar hydrophilic part interacts with the water molecules where the non-polar hydrophilic part is in interaction with the air or nonpolar liquid. The cohesive energy of the liquid is reduced with the presence of these molecules which lowers the surface energy of the liquid (Olariu, 2015).

Cloete, Jacobs and Brözel (1999) stated that an effective bio-dispersant should disperse sessile bacteria populations into the bulk of the cooling water so that it is more exposed to the action of biocides. Bio-dispersants are also used to soften deposits on surfaces allowing the deposits to be removed from the surfaces by the turbulent fluid flowing over the surfaces. Bio-dispersants should also restrict biofilm formation on clean surfaces (Cloete, Jacobs and Brözel, 1996) (Christophersen, 2018) (Olariu, 2015).

Surfactants have biocidal effects because it is toxic to cell membranes and can change the permeability of the membranes, membrane disruption, cellular lysis, the leakage of metabolic fluids and physical alternation of the cell membranes (Olariu, 2015). The normal flow of nutrients in a cell is disturbed when a cell is exposed to a surfactant because it changes the permeability of the cell which can eventually kill the cell (Cloete, Jacobs and Brözel, 1996).

Cloete, Jacobs and Brözel (1999) stated that it is unlikely for bacteria to gain resistance against bio-dispersants but Macdonald, Santa and Bro (2001) tested a bio-dispersant over a

period of 200 days in an industrial system and has concluded that the bio-dispersant was only effective initially and then observed a decrease in biofilm removal efficiency implicating that the biofilm got resistant to the bio-dispersant.

2.8 Impact of biofilms on industrial systems

Di Pippo *et al.* (2017) described that non-treated cooling water in industrial systems can lead to significant heat transfer efficiency losses due to biofilm formation which can lead to interruptions in production. Surfaces like cooling tower fill material, tubes in heat exchangers, inside walls of pipelines and water reservoirs are available for the growth of biofilms (Di Pippo *et al.*, 2018).

Horn and Richards (2010) described microbial deposition as a common occurrence on sites where untreated groundwater is used in cooling systems. Microbial deposition is also a joint operating and maintenance challenge where the cost of the biofouling treatment can be a significant portion of the production cost (Horn and Richards, 2010). Biofilms can have the following impact on an operational plant (Horn and Richards, 2010):

- Biofilms blind bag filters which reduce their efficiencies and operating life.
- Emulsions are formed by the biofilms which clog oil and water separators.
- Strainers and screens are being clogged by the biofilms which decrease the cleaning interval times.
- Flow restrictions are observed where a biofilm is formed.

The conductive heat transfer is reduced by the biofilm which leads to severe heat exchanger efficiency losses which lead to operational inefficiencies and losses (Di Pippo *et al.*, 2018). The thermal conductivity of a biofilm can vary between 0.57 and 0.71 (W/mK) at 27 °C (Nimmons, 1979) (Goodenough, 2017).

Biofilm formation has negative health impacts. Health problems associated with pathogens like Legionella species and free-living protozoa are observed. These free living protozoa can spread over long distances (Di Pippo *et al.*, 2018).

2.9 Industry use of bio-dispersants

Dave *et al.* (2017) emphasised that the dosing success of bio-dispersants varies from site to site due to operating parameters, cooling water quality and ambient conditions. Anti-scalants and bio dispersants are commonly used in combination with biocides (Di Pippo *et al.*, 2017). Buckman (2017) showed that bio-dispersants can be effectively dosed at a continuous rate at low concentrations to remove existing biofilms in industrial systems.

Bio-dispersants used in conjunction with an oxidising biocide will reduce the time to exterminate the biofilm because it breaks the biofilm in smaller pieces for more effective biocide action (Horn and Richards, 2010). Biocides (oxidising and non-oxidising) are the most effective way to eliminate biofilms (Horn and Richards, 2010). Buckman (2017) also stated that bio-dispersants are more effective when used together with a biocide because of the fact that the bio-dispersant increases the performance efficiency of the biocides.

SUEZ (2018) proved that bio-dispersants must be applied to a cooling water system when a non-oxidising biocide is used. A study was done by Murthy *et al.* (2004) where an oxidising biocide (sodium hypochlorite) was dosed in a seawater system together with a bio-dispersant. The study showed that it is vital to use a bio-dispersant with a biocide to ensure that the biofilm is dispersed to enhance the effectiveness of the biocide. The chlorine also controlled the sulphate reducing bacteria.

Murthy *et al.* (2005) stated that there is a lack of clear understanding of biofilm behaviour and that it requires a site specific dosing regimen which allows for bio-dispersant and biocide dosing. Olariu (2015) explained that it is recommended to dose a bio-dispersant one to four hours prior to a biocide to ensure a better dispersion of the biofilms in the water mass.

2.10 Supplier recommendations regarding bio-dispersants

Chemtex: Bio-dispersant can be applied to a cooling water system with basic procedures. The bio-dispersant is non-foaming and removes biofilm while the efficiency of biocides is increased. The recommended dosage is 5 ppm to 40 ppm (Chemtex, 2018).

Chemworld.com: Bio-dispersant is used to break down biofilms. The dispersant is used in recirculating systems over a wide pH range and is dosed at concentrations of 10 ppm –

40 ppm. The product consist of alkyl dimethyl benzyl ammonium chloride, ethanol, water and C12-16 alkydimethyl amines (Chemworld.com, 2018).

Veolia: Bio-dispersants disperses the biofilms allowing for more effective penetration of biocides. Bio-dispersants are usually made up from DTEA II (2-Decylthio ethanamine) DMAD (Fatty acid amide) Dodecylamine acetate Polyquaternary amines DOSS (Dioctylsulfosuccinate) and Polyoxyalkylenes Enzymes (Christophersen, 2018).

Accepta Water Treatment: Bio-dispersant is used for once-through and re-circulating water cooling systems which can be used with chlorine and bromine oxidising biocides (Accepta Water Treatment, 2018).

Bio-source inc: Bio-dispersant can be used in open reticulating as well as once-through cooling water systems (Bio-Source, 2018).

Acuro Organics Limited: The bio-dispersant can be used in re-circulating as well as once-through cooling water systems and will improve the system efficiency, and will remove and disperse unwanted deposits (Acuro Organics Limited, 2018).

2.11 Titanium condenser tubes

The condensers in the utility are currently being replaced with titanium tubes. Titanium has a lower thermal conductivity than brass but has a high erosion and corrosion resistance and is economically feasible to procure (Mostafa, 2011). Titanium tubes were therefore used in the test apparatus during the experimental tests conducted.

2.12 Effect of fouling on heat transfer

Figure 4 shows a cross-sectional view of a tubed heat exchanger indicating the fouling layer which can consist of the different types of fouling mentioned above.

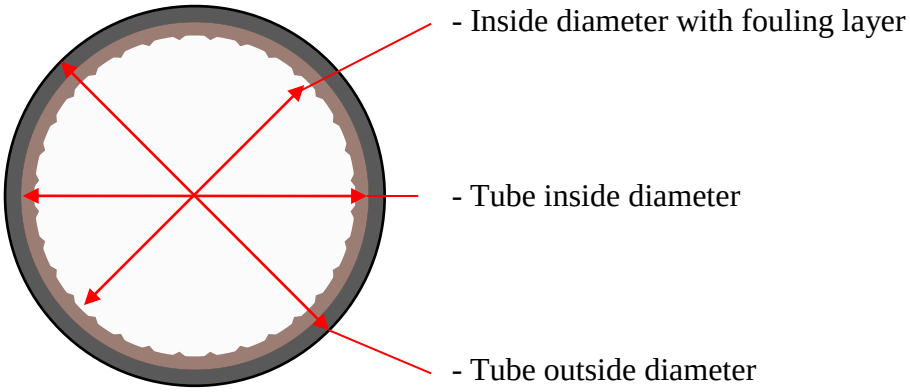


Figure 4: Schematic cross-sectional tube drawing showing the fouling layer.

Steam is condensed in a condenser by removing the latent heat of evaporation. Heat is thus transferred from the steam (hot fluid) to the cooling water (cold fluid). Fouling inside the condenser tubes decreases the conductivity of the tube wall which requires a greater temperature difference to transfer the energy from the steam to the cooling water. This requires that the steam saturation temperature rises and the resulting increase in backpressure causes a drop in cycle efficiency. The heat transfer resistances in a typical condenser tube and the heat transfer resistance network where the heat is transferred from the steam to the cooling water are shown in Figure 5. Equation (1) shows the sum of the thermal resistances in the heat transfer network as indicated in Figure 5 (Cengel and Ghajar, 2011).

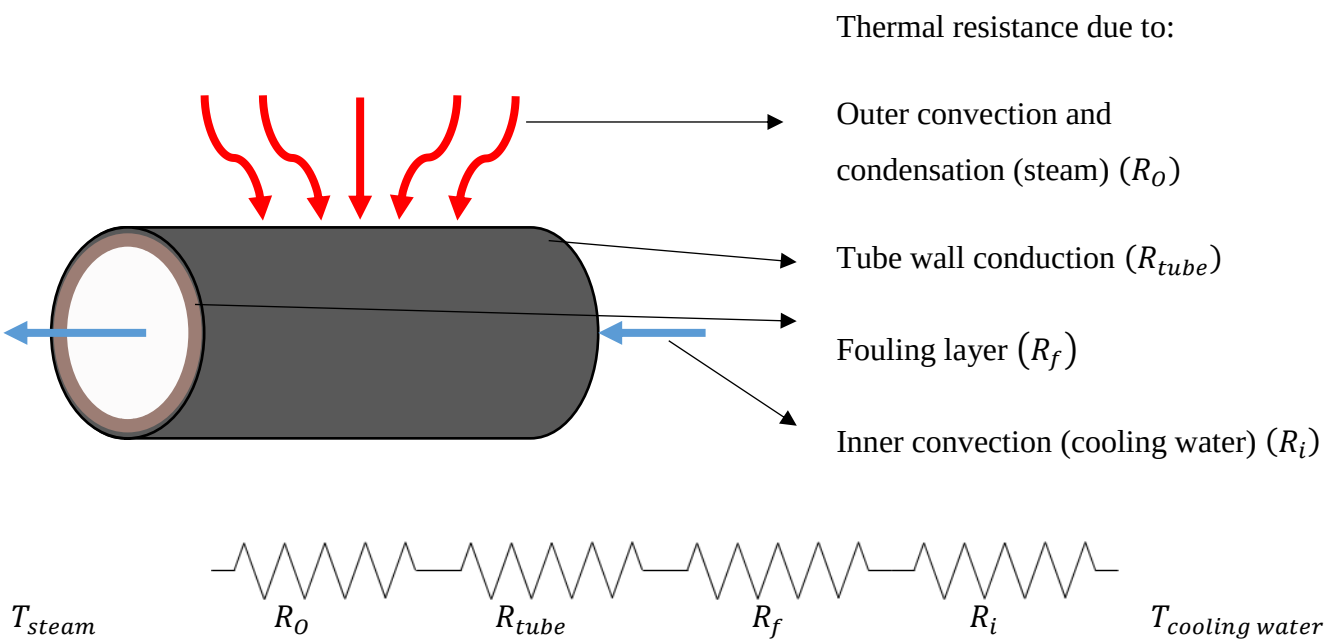


Figure 5: Thermal resistances for heat transfer from the hot to the cold fluid.

$$\sum R = R_O + R_{tube} + R_f + R_i \quad (1)$$

2.13 Impact of fouling on cycle efficiency

The main turbine condenser can be explained as the second-largest heat exchanger on the power plant (second to the boiler) and also has a significant impact on the overall cycle (Goodenough, 2017) (Vedran, Branimir and Vedran, 2018). A typical temperature- entropy diagram is shown in Figure 6. The process is explained as follows:

1 – 2: The superheated steam from the boiler is expanded through the turbine.

2 – 3: The wet steam is condensed inside the condenser.

3 – 4: The slightly subcooled liquid is pumped to the boiler.

4 - 1: The liquid is heated inside the boiler.

The area bounded in points 1 – 2 – 3 – 4 represents the net heat input and net power output to the power cycle. The net power output for a closed cycle is equal to the bounded area in points 1 – 2 – 3 – 4 from the first law of thermodynamics. It is clear that as the condenser pressure increases that the net power output decreases. The cycle efficiency is therefore directly influenced by the condenser pressure (Smith, J.M , Van Ness, H.C, Abbott, 2015) (Vedran, Branimir and Vedran, 2018)(Ibrahim and Attia, 2015).

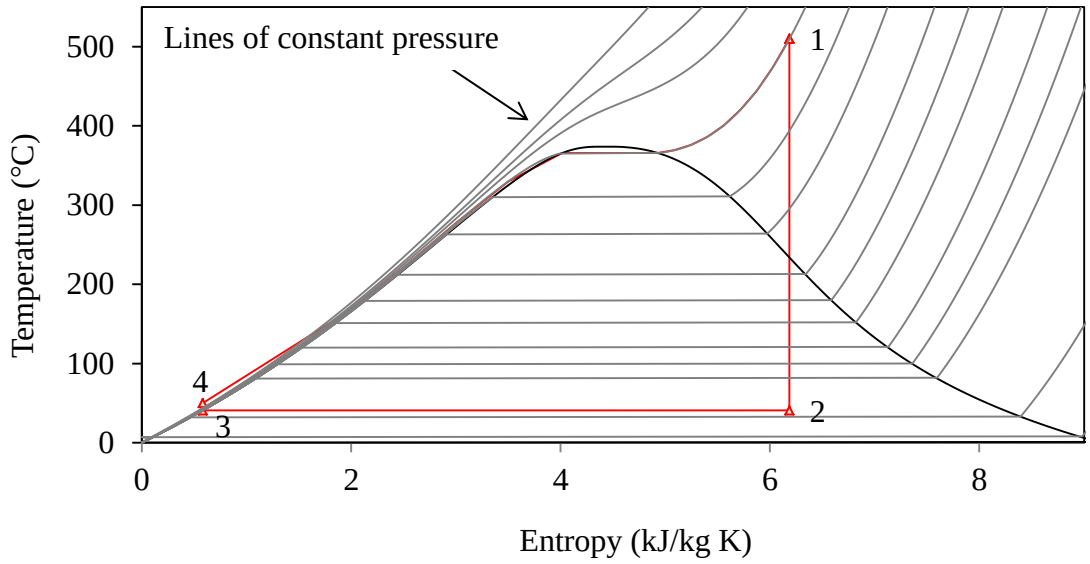


Figure 6: Rankine power cycle: Temperature – entropy diagram

The condenser pressure is influenced by:

- The heat load on the condenser.
- The condenser inlet cooling water temperature.
- The cooling water flow through the condenser.
- Air ingress into the condenser which causes blanketing around the tubes.
- Fouling inside the condenser tubes.

Condenser inside tube fouling is explained by Ibrahim and Attia (2015) as one of the most important factors effecting thermal performance which reduces heat exchanger efficiencies (Ibrahim and Attia, 2015). Fouling builds up inside the condenser tubes over a long term period which reduces the heat transfer efficiency of the condenser (Shen *et al.*, 2015). Multiple fouling mechanisms occur at the same time and have different effects on the overall fouling rate (Vedran, Branimir and Vedran, 2018).

The overall cycle efficiency decreases as the condenser temperature and corresponding pressure increase as a result of fouling. More coal needs to be burned inside the boiler to get the same generator power output which leads to an increase in production costs. The fouling can also lead to production losses due to limitations at the boiler plant or due to outages to clean the heat exchangers (Ahmed and Zubair, 2016). A study done by Walker *et al.* (2012)

indicated that the production losses due to fouling related outages are between 0.4 – 2.2 Million (USD 2009) per year (Walker *et al.*, 2012) for a 550 MW plant. Pattanayak, Padhi and Kodamasingh (2019) also indicated that 75 % of the decrease in efficiency observed was due to fouling inside the condenser tubes at a 33 MW plant (Pattanayak, Padhi and Kodamasingh, 2019).

The fouling can be addressed by a combination of chemical treatment of the cooling water and mechanical cleaning of the inside of the condenser tubes (Ahmed and Zubair, 2016). This study focuses on biological fouling inside the condenser tubes.

3 Methodology overview

A summary of the research methodology used in this study is shown in Figure 7. This is only an overview and the details in each step are explained in the sections below.

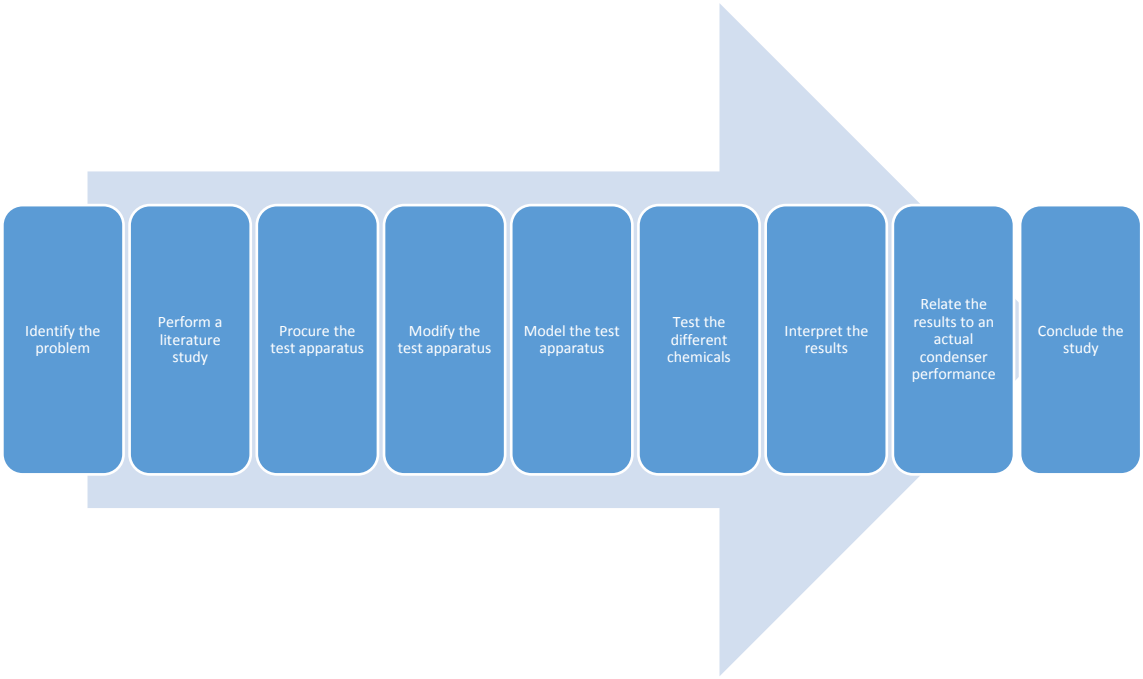


Figure 7: Summary of the methodology used.

The first step was to identify the problem at the power utility from where a literature study was conducted to determine the different fouling mechanisms inside condenser tubes as well as how it can be mitigated. A test facility was then procured and modified to chemically dose and analyse individual condenser tubes to determine the effect of the chemical dosing on the heat transfer of the condenser tubes while actual cooling water from the power plant was flowing through the facility. The analysis was done by developing a heat transfer model of the test facility. Three different bio-dispersants were dosed during three different tests from where the results were interpreted.

The actual fouling factors obtained from the test results were then used as inputs into a model to predict the losses or gains at the power utility if any one of the three bio-dispersants were dosed at the power station. The study was then concluded and recommendations were given.

4 Experimentation

4.1 Introduction

A condenser test apparatus by Goodenough (2017) was designed to monitor waterside fouling inside condenser tubes. The test apparatus was installed at a conventional coal-fired power station and was used during this study. The test apparatus was designed to test the performance of paint-based protective films inside condenser tubes. These tests were completed successfully and showed that admiralty brass tubes have lower fouling rates than titanium and stainless steel tubes.

The coal-fired power station consists of an open recirculation cooling water system with four natural draft cooling towers and six main turbine condensers. It is difficult to measure water side fouling inside the condenser tubes on the plant because of the variability and uncertainty of steam flow and cooling water flow rates through the condensers, inaccurate measurements, lack of installed measuring points and variability of process parameters such as feed heaters and inaccessibility of the condensers. The test apparatus is therefore used to monitor the relevant parameters to determine the water side fouling inside the condenser tubes.

Actual cooling water is tapped from the 10 % tap-off line (pipe transferring 10 % of the total water flow, from the main turbine condensers to the cooling towers, to the clarifiers to be treated) as it leaves the actual condensers and just before it enters the cooling towers in the cooling water system from where it flows through six condenser tubes inside the test apparatus from where it is returned to the cooling tower pond (Figure 8 and Figure 9).

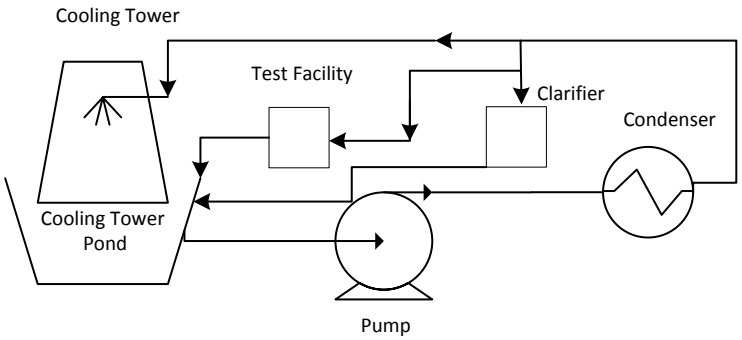


Figure 8: The location of the test apparatus at the recirculating cooling water system.



Figure 9: The location of the test apparatus on the actual plant - (1) Test apparatus, (2) 10% tap - off line

Goodenough (2017) selected the position of the test apparatus because it is the point where the water will be at its hottest and therefore has the highest scaling potential. The cooling water is supersaturated with ions (Table 4) and scaling will therefore still occur inside the test apparatus even if scaling occurred inside the actual main turbine condensers. The temperature of the cooling water entering the test apparatus is also in the temperature range for biofilm formation (35 °C and 40 °C) (Characklis and Marshall, 1990). Goodenough (2017) chose not to tap cooling water from the cooling tower pond to the test apparatus due to the lower cooling water temperature which will drastically reduce the amount of fouling that can occur inside the test apparatus.

4.2 Apparatus description

The cooling water tapped from the 10 % tap off line flows through two 100 µm parallel strainers from where it flows into the test apparatus. The cooling water is then distributed through a manifold which allows the cooling water to flow through six titanium condenser tubes. A manifold combines the cooling water exiting each of the six condenser tubes into one pipe section from where the cooling water flows out of the test apparatus into the cooling water pond. The titanium condenser tubes can be replaced with new ones as needed.

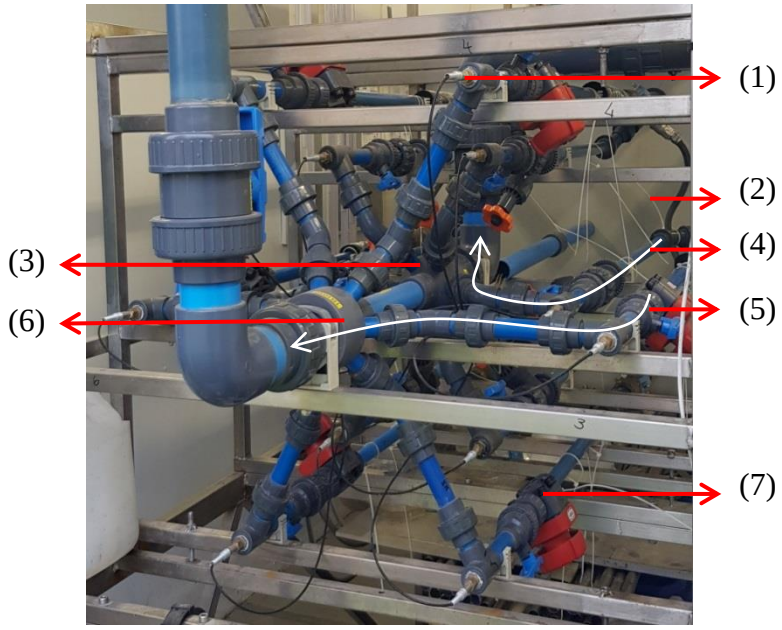


Figure 10: Layout of the test apparatus – (1) temperature probe, (2) polypropylene supports, (3) annulus manifold, (4) hot water flow direction, (5) cooling water flow direction, (6) cooling water manifold, (7) diaphragm valve

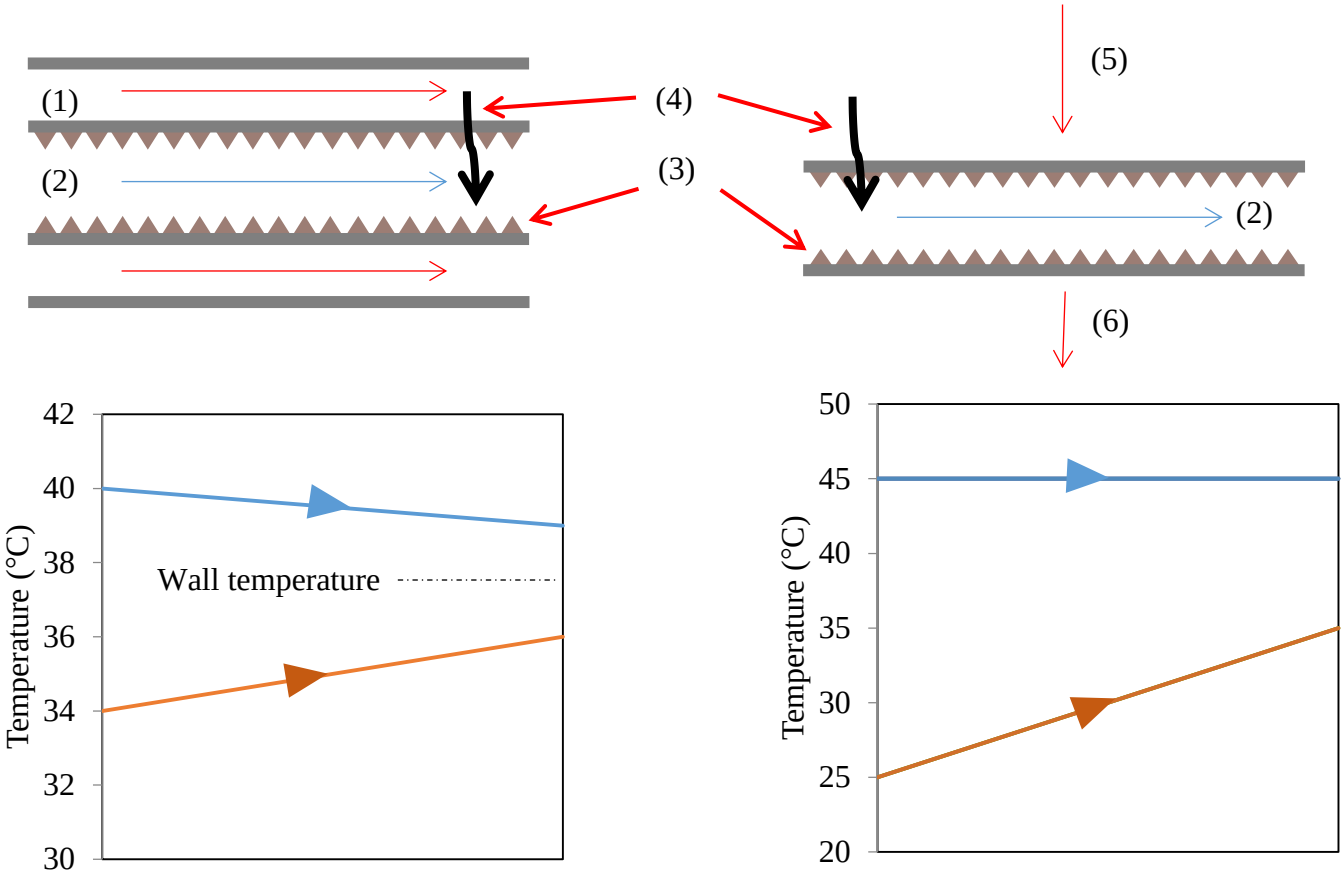


Figure 11: Water flow through annuli and titanium tube – (1) hot water flow, (2) cooling water flow

Each of the titanium condenser tubes are situated inside an annuli. Hot filtered water is pumped from a 1000 L reservoir through a manifold that distributes the water into six pipe sections which are connected to each of the six annuli. Each of the pipe sections consists of a diaphragm valve to ensure equal flow through each of the annulus sections. The hot water then combine into one pipe section from which it flows through three 8 kW electric heaters in series and then back into the 1000 L reservoir.

The annuli that heats the condenser tube acts as a double pipe co-current flow heat exchanger (Figure 11 and Figure 13). The apparatus needs to simulate similar thermal conditions as an actual condenser, therefore, a co-current fashion was selected to achieve a more uniform tube

wall temperature. The hot water velocity is controlled to have the same sensible convective heat transfer coefficient as comparable to those for condensing steam.



(1) - Double pipe heat exchanger (2) Actual condenser

Figure 12: Heat transfer conditions compared in the double pipe heat exchanger and the actual condenser - (1) hot water flow, (2) cooling water flow, (3) fouling layer, (4) heat transfer, (5) steam, (6) condensate (Goodenough, 2017)

The apparatus is housed inside an aluminium container. The container was constructed by sandwiching 40 mm polystyrene between two aluminium sheets. The temperature inside the container is controlled at 28 °C by a 5 kW air conditioner. The container has a door which is 1.2 m wide to ensure easy tube replacement and maintenance of the facility.

The annuli and condenser tubes are supported by a stainless steel frame with polypropylene plates.

The pump that circulates the hot water is a chemical pump and all wetted surfaces are made of polypropylene. PVC piping was used because it is chemically inert and has low thermal conductivity properties (Goodenough, 2017).

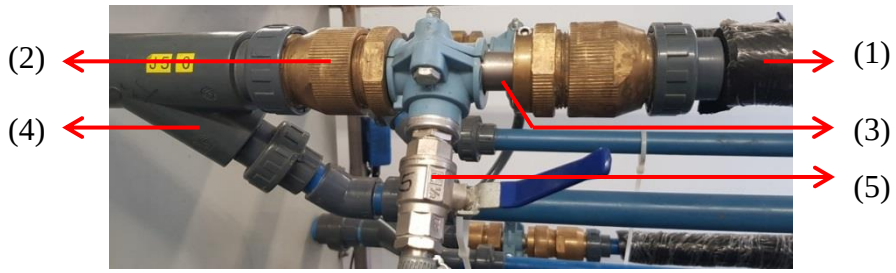


Figure 13: Layout of double pipe heat exchanger – (1) polyurethane insolation, (2) tube gland, (3) titanium condenser tube, (4) hot water jacket, (5) pressure tapping

4.3 Modifications to existing test apparatus

The bio-dispersants need to be dosed in a range between 0 ppm and 40 ppm which relates to a volumetric flow rate of 0 ml/h to 88 ml/h. These dosing ranges were recommended by the different suppliers who provided the power station, where the research is conducted, with chemicals in the past. Peristaltic pumps with a dosing rate of 0 ml/h to 120 ml/h were selected to be installed at four of the six tubes in the test apparatus. The remaining two tubes were kept as control tubes to compare the dosed and non-dosed tubes with each other.

A basic computational flow analysis (Appendix A) was done to simulate how mixing takes place inside a condenser tube once dosed with a bio-dispersant using a peristaltic dosing pump. The point at which the chemical injection point is installed is shown in Figure 14.



Figure 14: Layout of the cooling water entrance point – (1) cooling water manifold, (2) temperature probe, (3) chemical injection point, (4) cooling water flow direction

The literature survey in Section 2.10 indicated that bio-dispersants should be dosed at concentrations between 5 ppm and 40 ppm. The chemical services at the power plant typically dosed 5 ppm bio-dispersant when available.

4.4 Measurement techniques

The test apparatus is used to monitor waterside fouling in six condenser tubes by measuring the cooling water inlet and outlet temperatures, pressure differentials and flowrates at each of the tubes. The inlet and outlet temperatures and flowrates of each annulus heating a condenser tube are also measured. The waterside fouling in each of the parallel condenser tubes can thus be monitored by calculating the heat transfer parameters in each of the tubes. The heat transfer parameters of each of the individual condenser tubes can then be compared with each other. The surface roughness inside the condenser tubes has a large influence on the heat transfer in each of the tubes and is therefore calculated by using a static pressure drop measurement over each of the condenser tubes. It is assumed that the outside section of the condenser tubes are smooth and that no outside tube fouling will take place (filtered water is used in the heating side). This assumption is verified by a visual inspection of each of the condenser tubes after each test.

Each of the six condenser tubes are weighted before and after each test to obtain the mass gained due to the inside tube fouling over the test period.

Bacterial swabs of each of the six condenser tubes are taken on a weekly basis and send for analysis at a SANAS (South African National Accreditation System) accredited laboratory.

Four of the six condenser tubes can be continuously chemically dosed with peristaltic dosing pumps. These dosing pumps are calibrated by measuring the volume of chemicals pumped by each pump within an hour. This process is repeated three times for each pump to ensure that the pumps are correctly calibrated.

The piping and instrumentation diagram is shown in Figure 15.

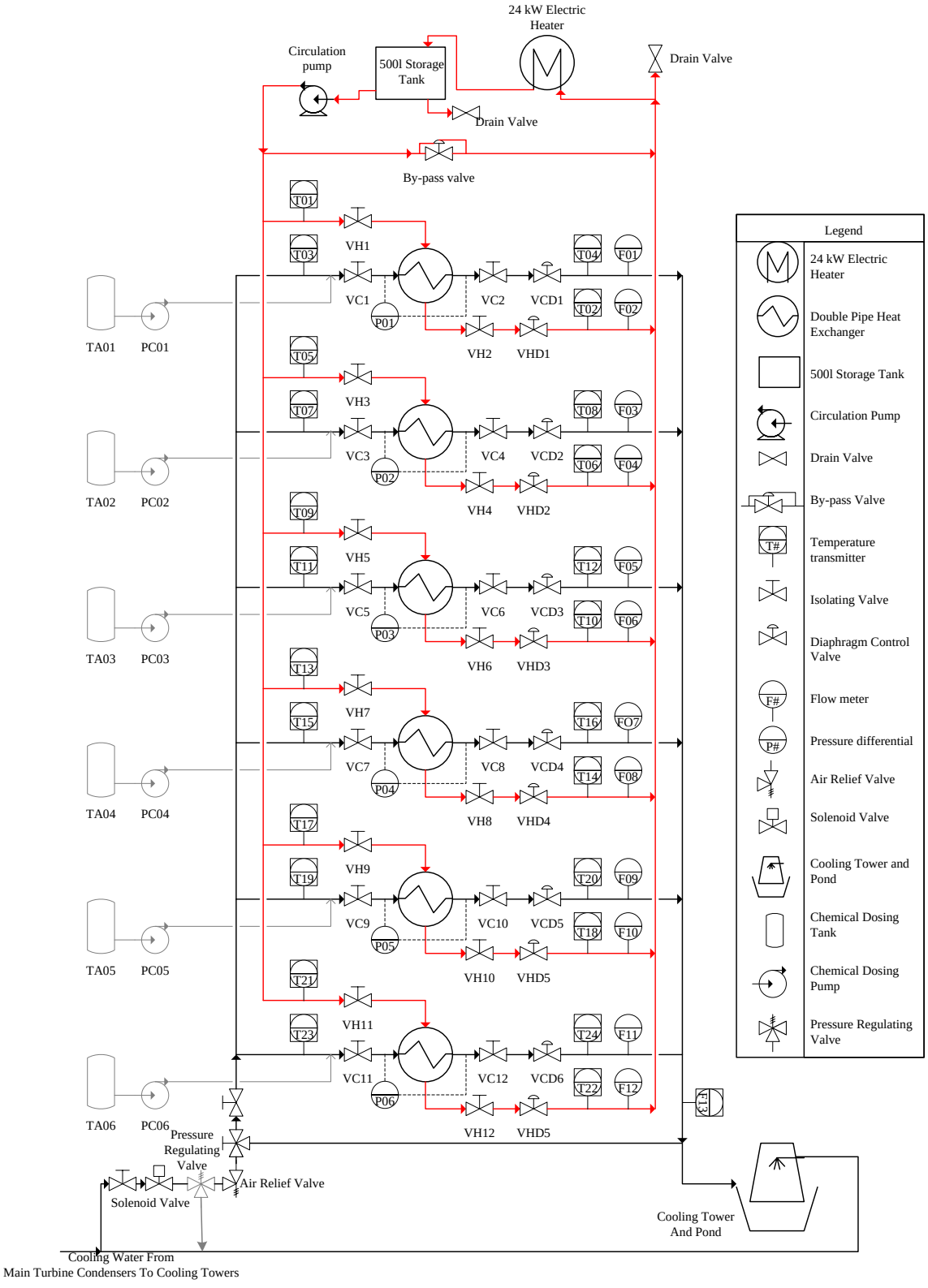


Figure 15: Piping and instrumentation diagram for the test apparatus.

4.4.1 Temperature measurement

Goodenough (2017) designed the test apparatus by using a total of 24 Class AA PT1000 stainless steel sheathed resistance temperature detectors. The high resistance of these probes allows the necessary resolution for measuring the difference in temperatures across the heat exchangers within 0.1 °C. The inlet and outlet temperature of each annulus and condenser tube are measured. Each 6.14 mm probe has a sensor size of 20 mm and is inserted to a depth of 100 mm ninety degree to the direction of the water flow. The point of insertion is shown in Figure 14. The thermocouples are connected to a data logger. It was confirmed before the first set of test that all 24 thermocouples read the same temperature value for the temperature range between 15 °C and 55 °C within a deviation of 2 %. It was, therefore, decided that it is not necessary to do any further calibrations on the thermocouples.

4.4.2 Pressure measurement

The test apparatus was designed to allow the static pressure measurement along the internal surfaces of the condenser tubes. The static pressure is measured by using u-type manometers. The manometers are connected to a common manifold. A 1 mm pressure tapping hole is drilled through the inlet as well as the outlet of the condenser tubes before it is installed. A pipe saddle is connected over the 1 mm hole to connect the pressure tapping to the manometer as described in Figure 16.

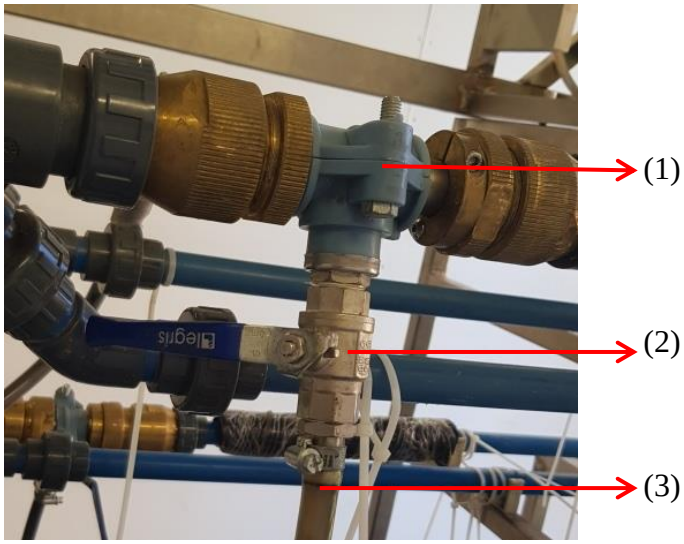


Figure 16: Pressure tapping – (1) Pipe saddle, (2) Isolating valve, (3) PVC hose to common manifold

A PVC pipe run from each of the pipe saddles vertically into a common manifold. The PVC pipes are then filled with water. Air is pumped into the manifold to form an air bubble. The pressure differential over the test section of the condenser tubes are then related to the height difference water between the inlet and outlet section of the tube as described in Figure 17.

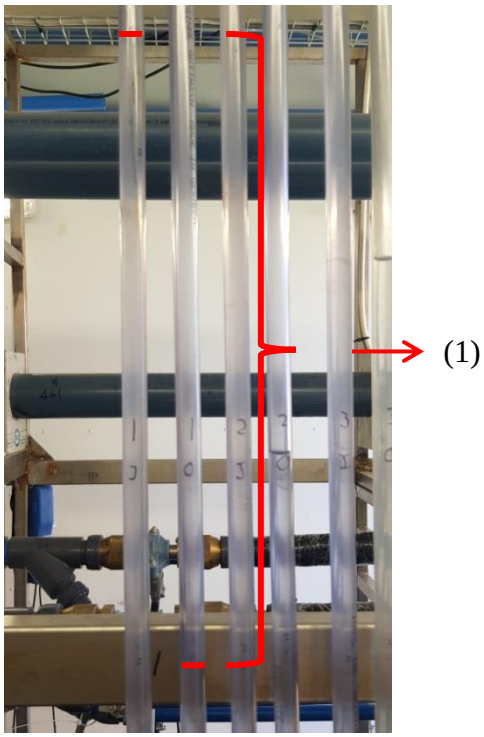


Figure 17: U-type manometer – (1) Pressure differential over the first condenser tube.

4.4.3 Flow measurement

The test apparatus has one electromagnetic flow meter (F13) which measures the flowrate of the cooling water entering the test apparatus as indicated in Figure 15. The electromagnetic flow meter has a measuring accuracy of 0.05 %. The flowrate inside the six individual condenser tubes and the six annulus sections are measured with a hand held ultrasonic flow meter with a flow deviation of +- 0.001 L/s. The readings from the electromagnetic flow meter were verified comparing the measured value to the sum of the flowrate inside the six individual tubes that were measured with the hand held ultrasonic flow meter. These readings were within 2 % of each other.

4.4.4 Tube mass

Each condenser tube is weighed before and after each test to obtain the mass gained due to inside condenser tube fouling. The tubes were weighed with a scale with an accuracy of ± 2 g after naturally drying the tubes at an angle of ± 30 degrees for 8 days at the same storage conditions which allows for comparative values.

4.4.5 Bacterial swabs

The cooling water flow rate through each of the six condenser tubes is closed on a weekly basis to allow bacterial swabs to be taken. The bacterial swabs are taken inside the condenser tubes at the outlet sections. The bacterial swabs are taken with a sterile cotton bud and by wiping it inside the condenser tube and then insert it into a saline solution. The cotton bud inside the saline solution is then transported to a laboratory and analysed within 24 hours. The analysis from the laboratory shows the amount of anaerobic and aerobic bacteria present inside each of the six condenser tubes. The laboratory is SANAS accredited.

4.4.6 Cooling water quality

Cooling water is sampled at the cooling tower ponds, analysed and logged on a daily basis by the power station. The cooling water results are shown in Section 4.8 .

4.5 Operation and control

4.5.1 Tube installation

New titanium tubes (12 m lengths) supplied by the power station are cut to the correct lengths (3.199 m) from where the entrance and exit sections of the tubes are filed smooth. The outside sections of the tubes are then cleaned with acetone to ensure that the outside oxide layer is removed and that no outside fouling resistance layer is present. The individual tubes are then centred inside the annulus sections and connected to the inlet and outlet connections of the test apparatus.

4.5.2 Heat transfer

The data logger is set to take temperature and flow readings every 30 minutes. The readings are then averaged to daily values during the data analysis to obtain smooth trends.

4.5.3 Maintenance

The following maintenance tasks needed to be performed during each test:

- The two parallel strainers to the test apparatus are cleaned when the total cooling water flow into the test apparatus dropped below 3 L/s. This is when the linear velocity in a condenser tube decreased by ± 20 %. This was approximately once a week.
- The static pressure tapping points are backwashed every four weeks or when blockages are observed.
- Other maintenance also includes checking of the hot water tank level and pipework inspections to check for water leaks.

4.6 Analysis

4.6.1 Heat transfer inside the parallel co-current heat exchanger tubes

The following assumptions are made during the analysis of the double pipe co-current heat exchangers:

1. The cooling water that flows through the heat exchangers, water in the hot circulating cycle and the bio-dispersants that are being dosed are assumed to be incompressible fluids.
2. The thermodynamic water properties for pure water are used for the cooling water. There are impurities present in the cooling water but the error on thermodynamic properties is negligible (Goodenough, 2017).
3. When the flowrates of each annulus and condenser tube are measured steady state conditions exist for a period of 60 minutes.
4. The annulus tubes and cooling water tubes are insulated and heat transfer losses are negligible.

The log mean temperature difference method is applicable to determine the heat transfer inside the parallel co-current condenser tubes when the assumptions above are made (Cengel and Ghajar, 2011). The rate of heat transfer is expressed as:

$$\mathrm{Q} = \mathrm{U}A_{ANN_S} \, \Delta \, T_{LM} \tag{2}$$

Where U the overall heat transfer coefficient, A the available heat transfer surface of the condenser tubes and $\Delta \, T_{LM}$ is the log mean temperature difference expressed in Equation (3).

$$\Delta \, T_{LM} = \frac{\left(T_{ANN_{in}} - T_{CW_{in}}\right) - \left(T_{ANN_{out}} - T_{CW_{out}}\right)}{\ln\left(\frac{T_{ANN_{in}} - T_{CW_{in}}}{T_{ANN_{out}} - T_{CW_{out}}}\right)} \tag{3}$$

Cengel and Ghajar (2011) describes that the overall heat transfer is equal to the inverse of the total thermal resistance as explained in Equation (4).

$$\mathrm{U}A_{ANN_S} = \left(\frac{1}{\sum R}\right)^{-1} \tag{4}$$

The total thermal resistance for each of the six parallel condenser tubes is the sum of the thermal resistances of the: convectional resistance of the cooling water inside the condenser tubes, conduction resistance of the tube material, fouling resistance inside the condenser tube and the convectional heat transfer resistance of the hot water flowing in the annulus side as described in Equation (1). Equation (1) is expanded to its individual variables in Equation (5).

$$\sum R = \frac{1}{h_{CW} \cdot A_s} + \frac{ln\left(\frac{D_O}{D_i}\right)}{2 \cdot \pi \cdot k_t \cdot L_{eff}} + \frac{R_f}{A_{ANN}} + \frac{1}{h_{ANN} \cdot A_{ANN}} \tag{5}$$

The fouling resistance inside the six different condenser tubes is thus calculated by solving the fouling resistance (R_f) in Equation (5).

4.6.2 Inside tube convection coefficient

The pressure drop over each of the six individual condenser tubes is measured as described in Section 4.4.2 . Cengel and Ghajar (2011) described that the pressure drop over a tube for all types of fully developed internal flows is described by Equation (6) where the pressure drop over the condenser tube is direct proportional to the Darcy friction factor.

$$\Delta P_L = f_{cw} \cdot \frac{L_p}{D_i} \cdot \frac{\rho_{CW} \cdot {u_{CW}}^2}{2} \tag{6}$$

The surface roughness inside each of the six condenser tubes will increase as the tubes foul. Equation (6) will therefore be used to calculate the friction factor inside the condenser tubes. The friction factor influence the Nusselt number (Equation (7)) which has an impact on the convectional heat transfer coefficient (Equation (8)) inside the condenser tubes (Cengel and Ghajar, 2011). Equation (7) is valid for $3000 < Re < 10^6$.

$$Nu_{CW} = \frac{\left(\frac{f_{CW}}{8}\right) \cdot (Re_{CW} - 1000) \cdot Pr_{CW}}{\left(1 + 12.7 \cdot \left(\frac{f_{CW}}{8}\right)^{0.5} \cdot \left({Pr_{CW}}^{\frac{2}{3}} - 1\right)\right)} \tag{7}$$

$$h_{CW} = \frac{Nu_{CW} \cdot k_{CW}}{D_i} \tag{8}$$

The Reynolds number for the cooling water flowing inside the condenser tubes is calculated by using Equation (9) (Cengel and Ghajar, 2015).

$$Re_{CW} = \frac{D_i \cdot u_{CW} \cdot \rho_{CW}}{\mu_{CW}} \tag{9}$$

4.6.3 Outside tube convection coefficient

The Reynolds number for the water flowing through the annulus section is calculated by using the hydraulic diameter as in Equation (10) (Cengel and Ghajar, 2015):

$$Re_{ANN} = \frac{(D_{ANN} - D_O) \cdot u_{ANN} \cdot \rho_{ANN}}{\mu_{ANN}} \tag{10}$$

Gnielinski (2009) determined that the friction factor of the water flowing through the annulus section with data in the fully developed region is determined by using Equation (11).

$$f_{ANN} = (1.8 \cdot log_{10}(Re_{ANN}) - 1.5)^{-2} \tag{11}$$

Goodenough and Reuter (2014) and Gnielinski (2009) sited that Equation (12) is the most comprehensive correlation to determine the Nusselt number inside an annulus for fully developed flow.

$$Nu_{ANN} = \frac{\left(\frac{f_{ANN}}{8}\right) \cdot Re_{ANN} \cdot Pr_{ANN}}{k_1 + 12.7 \cdot \left(\frac{f_{ANN}}{8}\right)^{0.5} \cdot \left(Pr_{ANN}^{\frac{2}{3}} - 1\right)} \tag{12}$$

$$k_1 = 1.07 + \frac{900}{Re_{ANN}} + \frac{0.63}{1 + 10 \cdot Pr_{ANN}} \tag{13}$$

It is important to note that the heat exchangers in the test apparatus have edge effects due to the transition from circular to annular areas. It is therefore necessary to measure the initial annular Nusselt numbers for a range of Reynolds numbers before each test starts. The

coefficients A_{Nu} and B_{Nu} in Equation (14) are then determined which are used during the duration of the test.

$$Nu_{ANN} = A_{Nu} \cdot {Re_{ANN}}^{B_{Nu}} \cdot {Pr_{ANN}}^{0.3} \tag{14}$$

The annular convection coefficient is then calculated by Equation (15).

$$h_{ANN} = A_{Nu} \cdot {Re_{ANN}}^{B_{Nu}} \cdot {Pr_{ANN}}^{0.3} \cdot \left(\frac{k_{ANN}}{D_{ANN} - D_O}\right) \tag{15}$$

4.6.4 Tube heat transfer performance analysis

The heat transfer performance of the condenser tubes is evaluated by solving the fouling factor, R_f, from Equation (5). This fouling factor obtained from Equation (5) can also be evaluated by comparing the difference between the inverse overall heat transfer coefficient at time t to the inverse of the overall heat transfer coefficient at $\mathrm{t} = 0$ (t_0) (Equation (16)) (Goodenough, 2017). This evaluation will be valid if assumed that there are no changes in heat transfer and cooling water and annular flow rates.

$$R_f = \frac{1}{\mathrm{U}_t} - \frac{1}{\mathrm{U}_{t_0}} \tag{16}$$

The performance of the condenser tubes can also be expressed as a cleanliness factor percentage. This is done by dividing the overall heat transfer coefficient at time t by the overall heat transfer coefficient at t_0 Equation (17).

$$CF = \frac{\mathrm{U}_t}{\mathrm{U}_{t_0}} \cdot 100 \tag{17}$$

The sample calculations are shown in Appendix C.

4.6.5 Mass and energy balance checks

The accuracy of the cooling water flow rates are evaluated before each test by measuring the flowrate through each of the six condenser tubes and comparing the sum of it by the incoming cooling water before it enters the manifold. The annular flow rates are evaluated by using the same ultrasonic flow meter. The flow distribution inside the annuli was within 6 % of each other.

The difference in inlet and outlet temperatures of each tube in the cooling water and annulus side is measured during an isothermal test before each fouling test commenced. The differences were below the uncertainty of the temperature probes which indicates that there is sufficient insolation around each tube and that there is negligibly small heat transfer to the surroundings.

The heat transfer rate over the tube wall in the cooling water side is calculated by Equation (18).

$$Q_{CW} = m_{CW} \cdot Cp_{W_{CW}} \cdot \left(T_{CW_{out}} - T_{CW_{in}}\right) \tag{18}$$

The heat transfer rate over the tube wall in the annulus side is calculated by Equation (19).

$$Q_{ANN} = m_{ANN} \cdot Cp_{W_{ANN}} \cdot \left(T_{ANN_{in}} - T_{ANN_{out}}\right) \tag{19}$$

The error in energy balance is determined by Equation (20). This error varies for each time measurements are taken and are due to uncertainties in the temperature and flow readings.

$$EB = \frac{Q_{CW} - Q_{ANN}}{\max(Q_{CW}, Q_{ANN})} \tag{20}$$

4.6.6 Experimental procedure

The experimental procedure is summarized in Figure 18. The experimental setup, no load testing, convection test and post processing is done for each of the three tests.

4.6.6.1. Experimental setup

Six new titanium condenser tubes are installed at the test apparatus and it is confirmed that no leaks are present after the tubes are installed.

4.6.6.2. No load testing

This is an important part before the fouling tests can start. It is necessary to make sure that the ultrasonic flow meter and electromagnetic flow meter readings correspond to ensure that the overall mass balance is satisfied. The next step will be to do an isothermal test to ensure that the thermocouples read the same temperatures for a variety of temperatures. This will prove that the tubes are correctly insulated and eliminate any uncertainties in the overall energy balance. The last step will be to calibrate the chemical dosing pumps as explained in Figure 19 by using the method described in Section 4.4 .

4.6.6.3. Convection test

This test is to calculate the annular Nusselt number for each of the tubes for different Reynolds numbers. Parameters A_{Nu} and B_{Nu} are then fit to Equation (14).

4.6.6.4. Fouling test

Three different bio-dispersants were tested. The three bio-dispersants were chosen because of the fact that the power station is using them on an alternating basis. The properties of the three different bio-dispersants are shown in Table 1.

Table 1: Properties of each bio-dispersant used during each test. (Information obtained from the different suppliers)

	Test		
	1	2	3
Bio-dispersant	A	B	C
pH	3 - 5	12.5	5 - 9
Specific Gravity	1.03 – 1.08	1.02	1.01 – 1.05
Viscosity (cP)	-	11	-
Colour	Colourless to light yellow	Colourless	Light yellow
Active ingredient (Weight percentage)	Alkyl aryl polyglycol ether (10 % - 45 %) Polymer (10% - 25 %)	Alkylene oxide block polymer (unknown)	Docusate sodium (3 % - 7 %) Nonylphenol, ethoxylated (3 % - 7 %) Dimethylamides of soya (1 % - 3 %) Poly(oxy-1,2-ethanediyl),α-hydro-ω-hydroxy-Ethane-1,2-diol, ethoxylated (1 % - 3 %) Glutaral (0.1 % -1 %)

The dosing concentrations of each bio-dispersant as described in Figure 19 is explained in Table 2. The supplier recommended dosing concentrations were 5 ppm and the power station is currently dosing ± 1 ppm. The dosing concentrations were increased during each test at certain time points as indicated in Table 2 to determine the effect of a higher bio-dispersant dosing concentration.

The power station only batch doses a biocide every 30 days and sometimes every 60 days with continuous bio-dispersant dosing. Only a bio-dispersant is, therefore, present in the system for approximately 30 days. The 30 days were doubled to see the effect of only dosing a bio-dispersant on the thermal performance of the condensers. The trends in Section 5 show

that an effect on heat transfer as a result of bio-dispersant dosing can be seen within the 60 day test duration.

Table 2: Dosing concentrations (ppm) (DC) of each tube during each test.

Tube	Test 1		Test 2		Test 3	
	Initial DC	Increased DC[a]	Initial DC	Increased DC[b]	Initial DC	Increased DC[c]
1	5.9	24.9	6.2	36	3.6	22.0
2	4.4	30.4	4.5	21.3	5.6	24.5
3	2.3	19.9	2.6	14.2	9.2	34.8
4	0	0	0	0	0	0
5	0	0	0	0	0	0
6	3.1	13.6	4.1	15.5	1.4	16.3

Dosing concentration increased on day 41[a], 40[b] and 44[c].

Biological swabs were taken weekly inside each of the condenser tubes. The static pressure and the annular and cooling water flowrate readings were also taken on a weekly basis.

4.6.6.5. Post processing

The fouling, cleanliness and friction factors are calculated for each tube for the test duration. The fouled condenser tubes are removed and naturally dried for eight days and weighed. The biological results from the laboratory are processed.

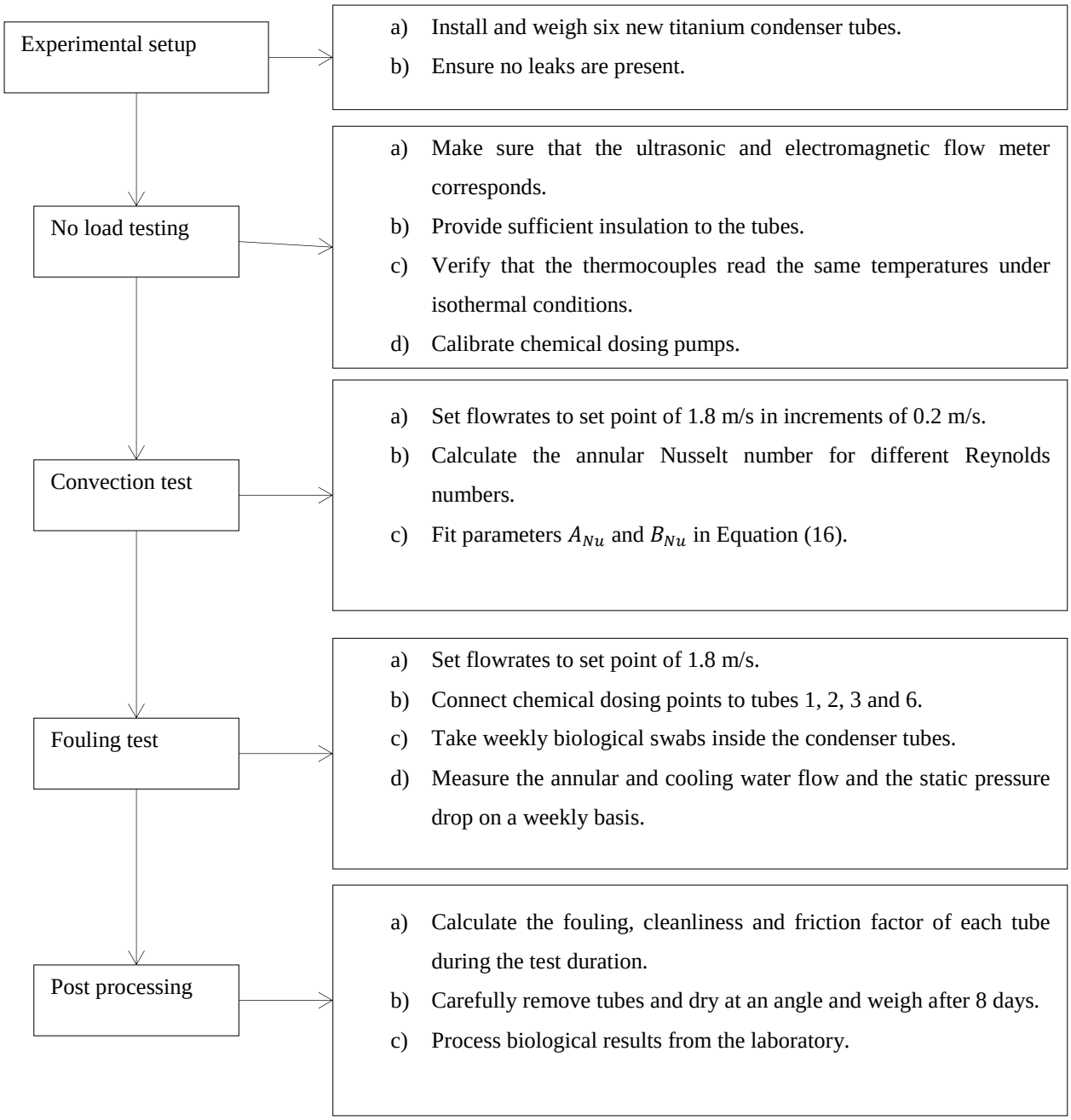


Figure 18: A flow chart explaining the experimental procedure.

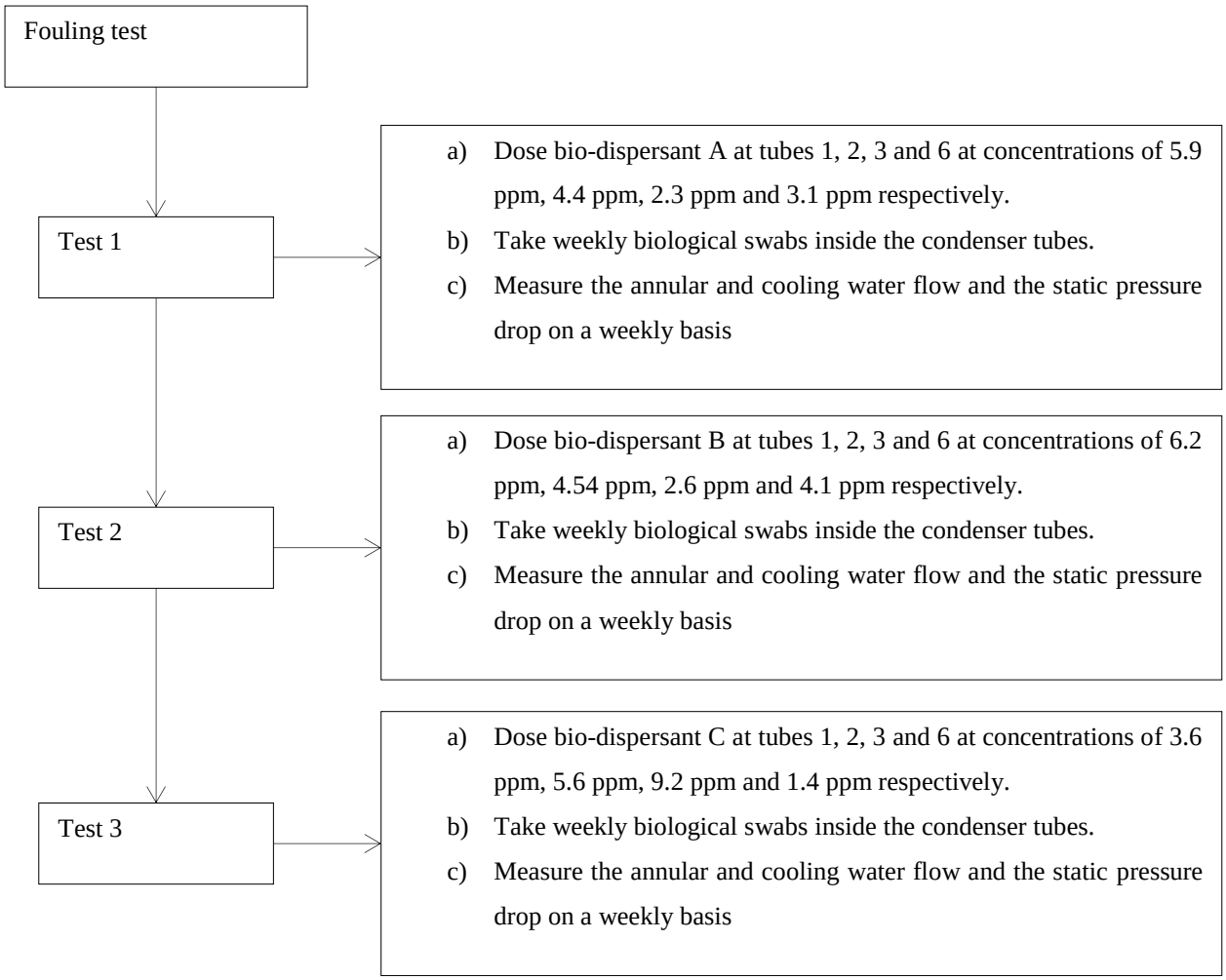


Figure 19: A flow chart explaining the three fouling tests in the experimental procedure (Figure 18).

4.7 Uncertainty analysis

The analysis of the experiments depends on the amount of uncertainty associated with the different measuring techniques. The fouling factor depends on the following 14 measured values:

$$R_f = \mathrm{f}\,(D_{ANN}, D_O, D_i, L_{eff}, L_p, T_{CW_{in}}, T_{CW_{out}}, T_{ANN_{in}}, T_{ANN_{out}}, F_{CW}, F_{ANN}, \Delta H, A_{Nu}, B_{Nu}) \quad (21)$$

Goodenough (2017) determined the annular convection coefficient experimentally and the errors of $D_{ANN}, D_O,\ D_i$ and L_{eff} were combined together in the annular coefficient regression. The fouling factor thus depends on the following 10 reduced parameters:

$$R_f = \mathrm{f}\,(L_p, T_{CW_{in}}, T_{CW_{out}}, T_{ANN_{in}}, T_{ANN_{out}}, F_{CW}, F_{ANN}, \Delta H, A_{Nu}, B_{Nu}) \quad (22)$$

Coleman & Steele (2009) and Holman (2012) estimated the overall uncertainty in the measured fouling factor as described in Equation (23) where X_i is the i^{th} variable of Equation (22).

$$R_f = \pm \sqrt{\sum_{i=1}^{10} \left(\frac{\partial {R_f}^2}{\partial X_i} {\Delta X_i}^2 \right)} \quad (23)$$

Holman (2012) described that Equation (23) can be very tedious to solve especially when large systems of equations are used. Holman (2012) provided an adaption to Equation (23) where the partial differential equation sections can be evaluated by using Equation (24).

$$\frac{\partial R_f}{\partial X_i} \approx \frac{\left(R_{f_{Xi+\Delta Xi}}\right) - R_{f_{Xi}}}{\Delta Xi} \quad (24)$$

Moffat (1988) stated that ΔXi must be arbitrarily small to calculate the most accurate estimate for the partial derivative. Moffat (1988) states that $\Delta X_i = W_i$ (W_i is described as the uncertainty in independent variable) is acceptable and are therefore applied in this study.

Table 3: Uncertainty variables and values

Measured variable	Symbol	Uncertainty in variable
Annulus external diameter	D_{ANN}	0.005 mm
Tube inside and outside diameter	D_i, D_O	0.1 mm
Dosing rate	F_{dose}	5 %
Length between pressure tappings	L_p	5 mm
Effective heat transfer length	L_{eff}	1 mm
Temperature	$T_{CW_{in}}, T_{CW_{out}}$	0.01 °C
	$T_{ANN_{in}}, T_{ANN_{out}}$	
Flowrate	F_{CW}, F_{ANN}	0.01 L/s
Pressure[1]	ΔH	5 mm
Annulus heat transfer coefficient[1]	A_{Nu}	6 %
Annulus heat transfer coefficient	B_{Nu}	1.6 %

[1] (Goodenough, 2017)

4.8 Cooling water analysis

The average cooling water results for the cooling water that flowed through the titanium condenser tubes during each test are shown in Table 4. The values shown are the average of the daily values over the duration of each test.

Table 4: Average cooling water properties for the duration of each test.

Description	Test		
	1	2	3
Cycles of concentration	35.03	26.95	20.51
Calcium hardness as $CaCO_3$ mg/l	464.81	313.59	305.40
Chemical oxygen demand mg/l	269.29	140.80	597.40
Chloride (Cl) mg/l	245.65	117.57	130.81
Electrical conductivity @ 25 °C µS/m	3590.27	1975.63	2352.20
Fluorine (F) mg/l	1.36	1.13	1.41
M Alkalinity	113.75	102.72	119.59
Magnesium hardness as $CaCO_3$ mg/l	492.36	219.05	280.38
Nitrate (NO_3) as N mg/l	6.28	2.98	3.69
P Alkalinity	4.77	3.57	6.39
pH @ 25 °C	8.51	8.42	8.42
Potassium (K) mg/l	102.31	58.38	57.34
Sodium (Na) mg/l	475.41	306.34	238.01
Sulphate (S) mg/l	1368.76	655.42	785.16
Turbidity (NTU)	14.43	13.89	15.42

The chemical oxygen demand (COD) is one of the few parameters that are measured on a daily basis at the power plant that indicates organic matter present in the cooling water. The Department of Water Affairs and Forestry (1996) indicated that evaporative cooling cycles with a COD larger than 70 mg/l will experience major damage due to biological fouling and that microbiologically-infused corrosion (MIC) will be experienced. The COD should also be interpreted in relation to turbidity measurements.

The turbidity of the water will increase as the amount of suspended solids in the water increases. Water will thus lose its transparency with a larger presence of suspended particles. It is important to note that turbidity is not only increased by the presence of organic matter but also by sediments form erosion, resuspended particles or any small particles entering the water for example fly ash (Lenntech, 2019).

The calcium hardness, magnesium hardness, conductivity, P alkalinity and M alkalinity parameters indicate the possibility for precipitation fouling. Goodenough (2017) indicated that precipitation fouling at the power plant only occurs after 70 days of operation. This study is therefore not focussed on the precipitation fouling.

5 Results and discussion

5.1 Fouling factor

The measured fouling factors for test 1, 2 and 3 are plotted in Figure 20, Figure 21 and Figure 22 respectively against the time duration of each test. The uncertainty in the data is shown in the error bars on each graph and is explained in Section 4.7 .The uncertainties of the different measured variables are shown in Table 3. Note that the dosing concentrations are not exactly the same for the tubes in the individual tests due to the difficulty in setting the peristaltic dosing pumps on exactly the same dosing rates during each test. The dosing rates are shown in Table 2. A peristaltic dosing pump with an adjustable dosing set point would have been a better option but was not economical feasible for this study. Appendix D shows which individual tube of each test can be compared to each other before the increase in dosing concentration as well as after the increase in dosing concentration. Note that this is a comparison study between the three different tests and that the different test results should rather be compared to each other than the results of the individual tubes.

The fouling factor is calculated by solving the fouling factor with the use of Equation (5). It should be noted that the fouling factors for each test started off at 0 m^2K/W and then became negative (when the uncertainties in the data are also considered): the surface roughness of the deposits was greater than the titanium metal surface roughness which lead to a slight increase in cooling water turbulence. A negative fouling factor is calculated as a result thereof (Crittenden and Alderman, 1988) (Mostafa, 2011). All the tests show an exponential increase in the fouling factor. The fouling factor in test 1 (Figure 20) and test 3 (Figure 22) follows a sigmoidal curve, a pattern normally observed for biological fouling (Reuter, Owen and Goodenough, 2017) (Nebot *et al.*, 2007).

The fouling results for test 1, 2 and 3 have the same general trend compared to the results observed Reuter, Owen and Goodenough (2017) using the same test apparatus at the same power plant but with a much larger fouling rate. The maximum fouling factor observed by Goodenough (2017) for non-dosed titanium condenser tubes was 3 m^2K/W after a period of 120 days. The maximum fouling factor for non-dosed titanium condenser tubes observed during this study was approximately 4 m^2K/W after a period of 60 days. The discrepancy between the maximum fouling factors observed during the Goodenough (2017) study and this study can be due to a change in make-up water chemistry as well as the availability of

clarifiers during the two studies. Only one of the two clarifiers was in service during this study where both were in service during the Goodenough (2017) study. The role of the clarifier is to remove any solids or suspended solids from the water. This can include any biological material that will aggravate the biological fouling inside the system.

It is important to note from Figure 20 that tube 4 (non-dosed tube) has a lower fouling factor than observed for tube 1, 2, 3 and 6 (dosed tubes) over the test duration. This indicates that bio-dispersant A dosed in tube 1, 2, 3 and 6 worsened the heat transfer inside the condenser tubes. The energy balance difference Equation (21) of tube 5 increased from an average of 1.03 % to 7.3 % on day 28, this was due to a cooling water inlet temperature thermocouple with a loose connection which was only noticed when the test was completed. The data observed from tube 5 is therefore inconclusive. The difference in energy balance as in Equation (22) is shown in Appendix E.

No change in fouling factor is observed when the bio-dispersant dosing concentration of tube 1, 2, 3 and 6 was increased on day 41 (Table 2). The chemistry department at the power plant dosed the bulk cooling water system, which was untreated, with 5 ppm non-oxidising biocide with a retention time of 24 hours on day 39. No change in fouling factors is observed because of the occurrence.

The bio-dispersant A consists of an akyl aryl polyglycol eter and an unspecified polymer. The amount of fouling observed in the non-dosed tubes is not related to the dosing rates. There is thus no direct correlation between the fouling factors and the dosing rates further shown by the fact that the trends do not drastically change once the dosing rates are increased. It is however shown that the non-dosed tubes perform better than the dosed tubes and that the dosing of bio-dispersant A has an adverse effect on the fouling.

All six of the condenser tubes were batch dosed 10 times with 20 ppm sodium hypochlorite (NaOCl) on day 48 and 52 while still dosing the increased dosage of bio-dispersant into the dosed tubes. The NaOCl was applied into the system by closing the main cooling water supply to the test apparatus, pouring 20 ppm NaOCl into the strainers and then slowly opening the cooling water supply to the test apparatus to have the largest possible retention time (15 s) of NaOCl inside the six condenser tubes. The goal was to determine if the biofilm inside the condenser tubes can be removed by using an oxidising biocide. A significant reduction in fouling factors of tube 1, 3 and 6 was observed when the NaOCl was introduced

into the system. No reduction in fouling factor is observed at tube 2. The energy balance difference Equation (21) for tube 2 increased from 1.46 % to 8.7 % (Appendix E) from day 52 to day 56. The reason was that hot water outlet thermocouple was found to be faulty which was repaired immediately. A slight reduction in tube 4 and 5 was observed when the NaOCl was introduced into the system. The reduction of fouling factors when the NaOCl was introduced into the system confirmed that biofilms were present inside the condenser tubes. Note that there was no correlation between the dosing rates and the fouling rates during the first test. It can be noted that the larger the increase in fouling factor the larger the drop after dosing the NaOCl expect for tube 2 which had the defective thermocouple.

The piping and heat exchanger equipment on the plant consist of parts constructed of stainless steel. NaOCl is highly corrosive to stainless steel and can therefore not be dosed into the cooling water system of the actual plant to remove any biofilms (Laycock, Newman and Newman, 1997) (Yamamoto and Hosoya, 1995).

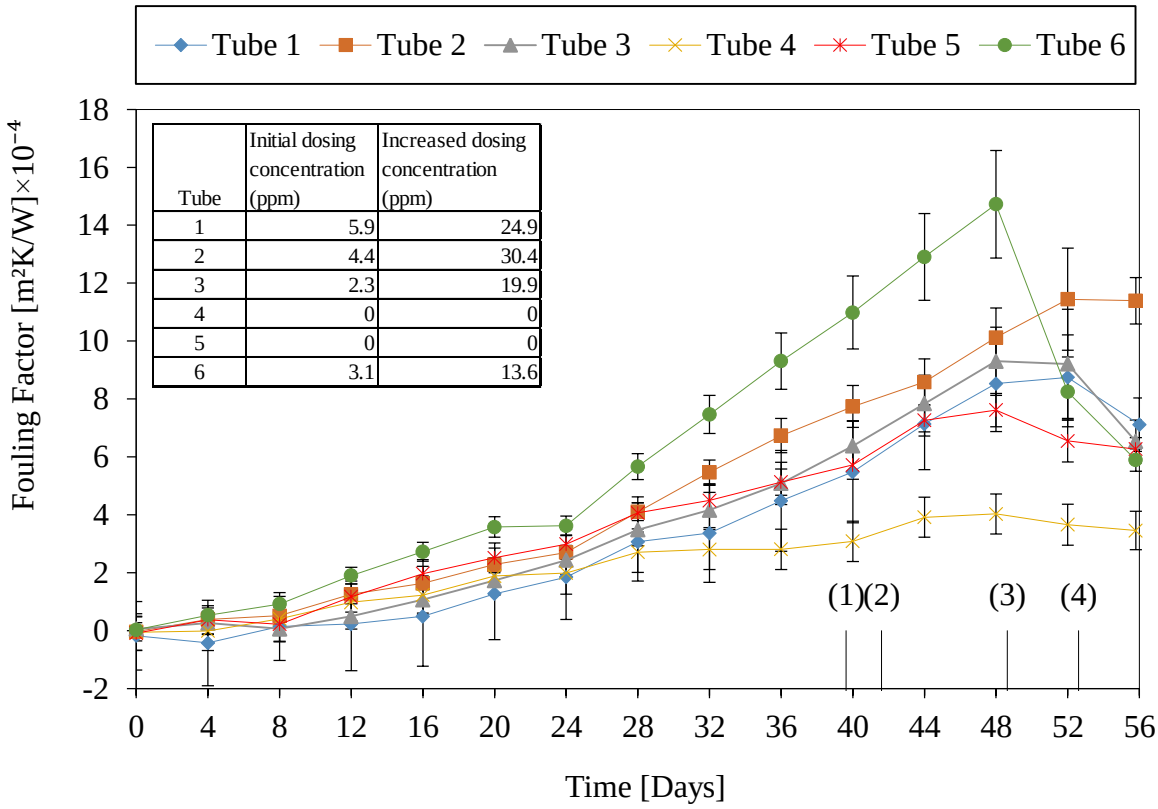
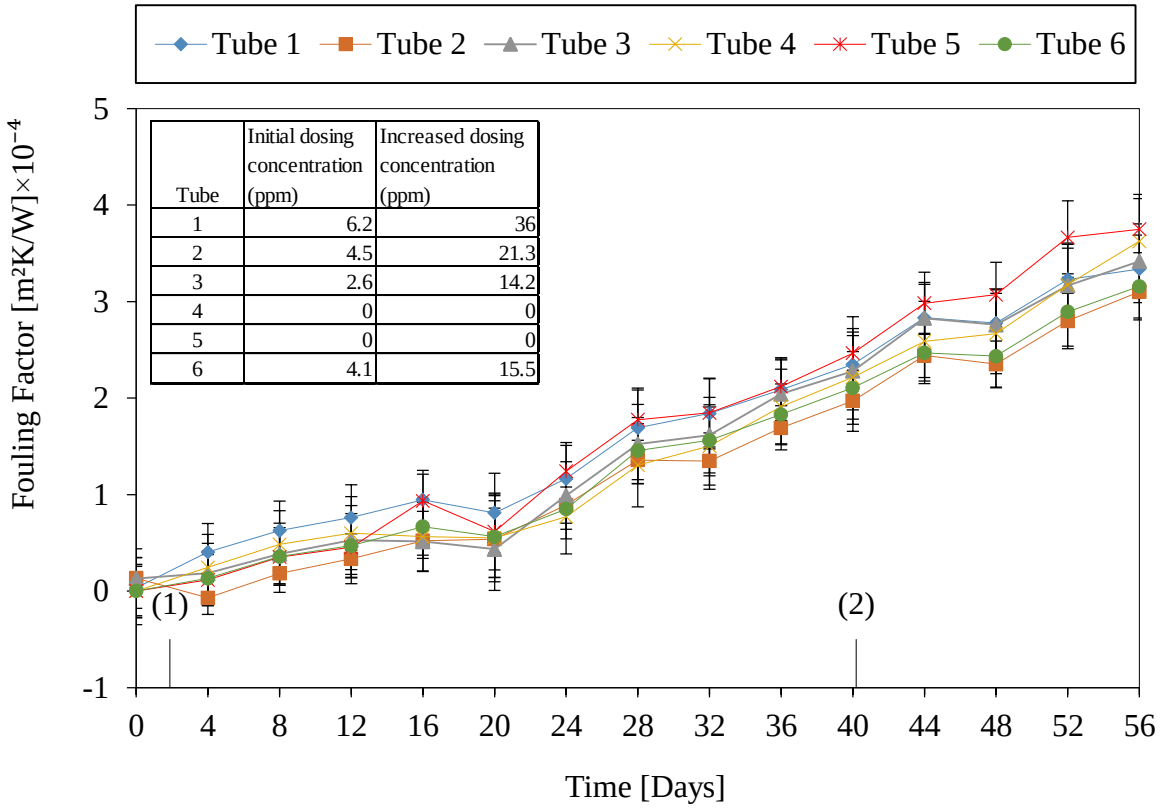


Figure 20: Measured fouling factors for tube 1, 2, 3, 4, 5 and 6 during test 1 – (1) Plant dosed biocide – (2) Increase dosing concentration in tube 1, 2, 3 and 6 – (3) Dosed NaOCl in strainers – (4) Dosed NaOCl in strainers

From Figure 21, it is clear that there is little to no difference in fouling factors is observed for tubes 1, 2, 3 and 6 with bio-dispersant B during test 2 especially when the uncertainty of the data is incorporated. No change in fouling rates was observed when the dosing concentration of tube 1, 2, 3 and 6 was increased on day 40 (Table 2). There is also no correlation between the dosing concentrations and the fouling rates.

The active ingredient in bio-dispersant B was an alkylene oxide block polymer. This type of bio-dispersant is widely used. There can be several reasons why it did not have any influence on the fouling rates including a bad batch of chemicals or that the organic matter in the cooling water is resistant to the active ingredient.



Tube	Initial dosing concentration (ppm)	Increased dosing concentration (ppm)
1	6.2	36
2	4.5	21.3
3	2.6	14.2
4	0	0
5	0	0
6	4.1	15.5

Figure 21: Measured fouling factors for tube 1, 2, 3, 4, 5 and 6 during test 2 – (1) Plant dosed biocide – (2) Increase dosing concentration in tube 1, 2, 3 and 6

The fouling factors of the six condenser tubes in test 3 (Figure 22) followed a similar trend to those of test 1 until the dosing concentrations were increased (Point (2)). The chemistry

department at the power plant dosed the bulk cooling water system with 5 ppm non-oxidising biocide with a retention time of 24 hours on day 21. No change in fouling factors is observed because of the occurrence. This indicates that the dosing of the biocide is ineffective and does not improve the heat transfer on the actual plant. The reason for the fouling factor of tube 3 having a value of 0 m^2K/W on day 12 – 28 was because of a problem with an isolating valve which shut the cooling water supply to the tube. The valve was repaired. Taking the trend from before and after this period suggested that tube 3 could have had a much higher fouling factor at day 44, probably as high as 20 m^2K/W.

It was observed that the fouling factors were dependant on the dosing concentrations of bio-dispersant C. The dosing concentrations increased from tube 4 = tube 5 < tube 6 < tube 1 < tube 2 < tube 3. The fouling factors of tube 4 = tube 5 < tube 6 < tube 1 < tube 2 < tube 3. Bio-dispersant C consists of several active ingredients as indicated in Table 1. The active ingredients in bio-dispersant C had an influence on the biofilm development and removal during this test.

The dosing concentrations of bio-dispersant C were increased on day 44 from where the fouling factors of tubes 1, 2 and 3 initially decreased. These fouling factors immediately started to deteriorate again. Tube 6 only showed a marginal drop in fouling factor by the increase in dosing concentration of bio-dispersant C. The dosing concentration of tube 6 was increased from 1.4 ppm to 16.3 ppm. The 16.3 ppm is lower than the next highest dosing concentration of tube 1 of 22 ppm. It is suspected that a dosing shock is observed above the 22 ppm dosing concentration which will break down the biological fouling inside the tubes and improve the heat transfer. It is also noted that tube 1, 2 and 3 had the same gradient of increase in fouling factors when it recovered from the increase in dosing concentration.

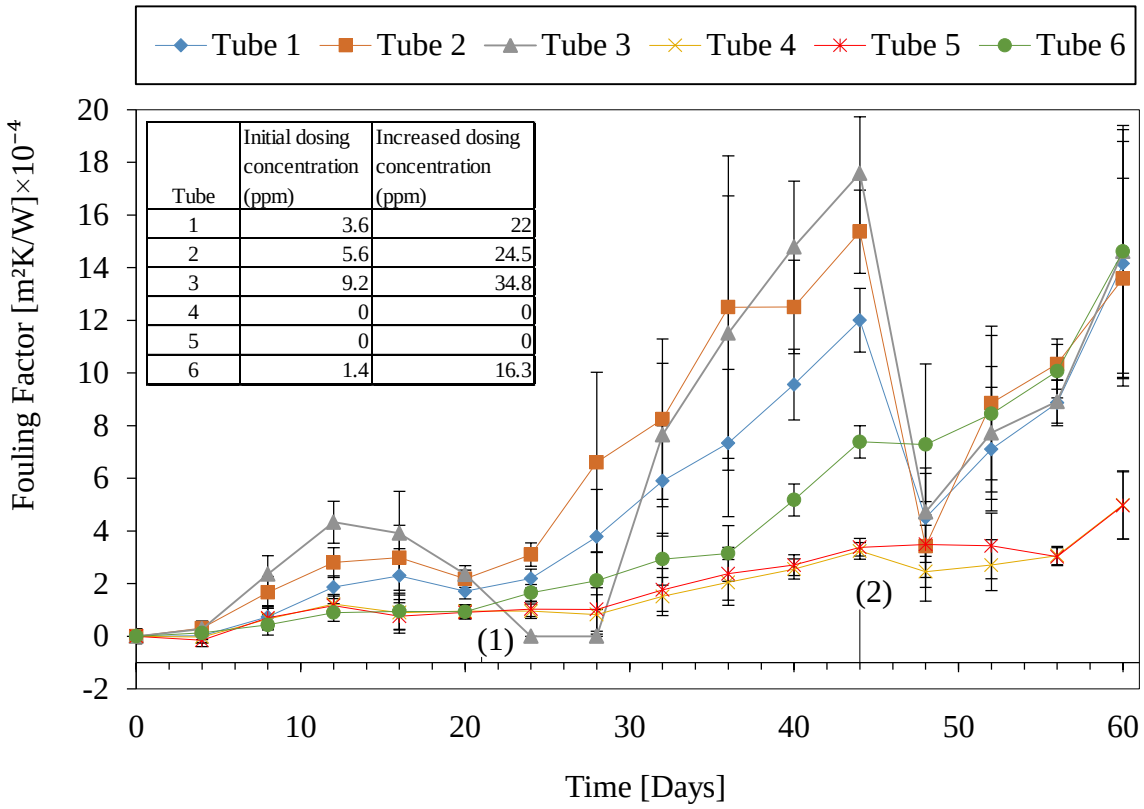


Figure 22: Measured fouling factors for tube 1, 2, 3, 4, 5 and 6 during test 3 – (1) Plant dosed biocide – (2) Increase dosing concentration in tube 1, 2, 3 and 6

5.2 Cleanliness factor

The calculated cleanliness factors for test 1, 2 and 3 are graphed in Figure 23, Figure 24 and Figure 25 respectively over the time duration of each test. The cleanliness factors for the first test correspond with the results obtained from Figure 20. It is clear that the non-dosed tubes have a higher cleanliness factors than the dosed tubes. It can also be seen that the cleanliness factors of all the tubes increased when the NaOCl was introduced to the test apparatus.

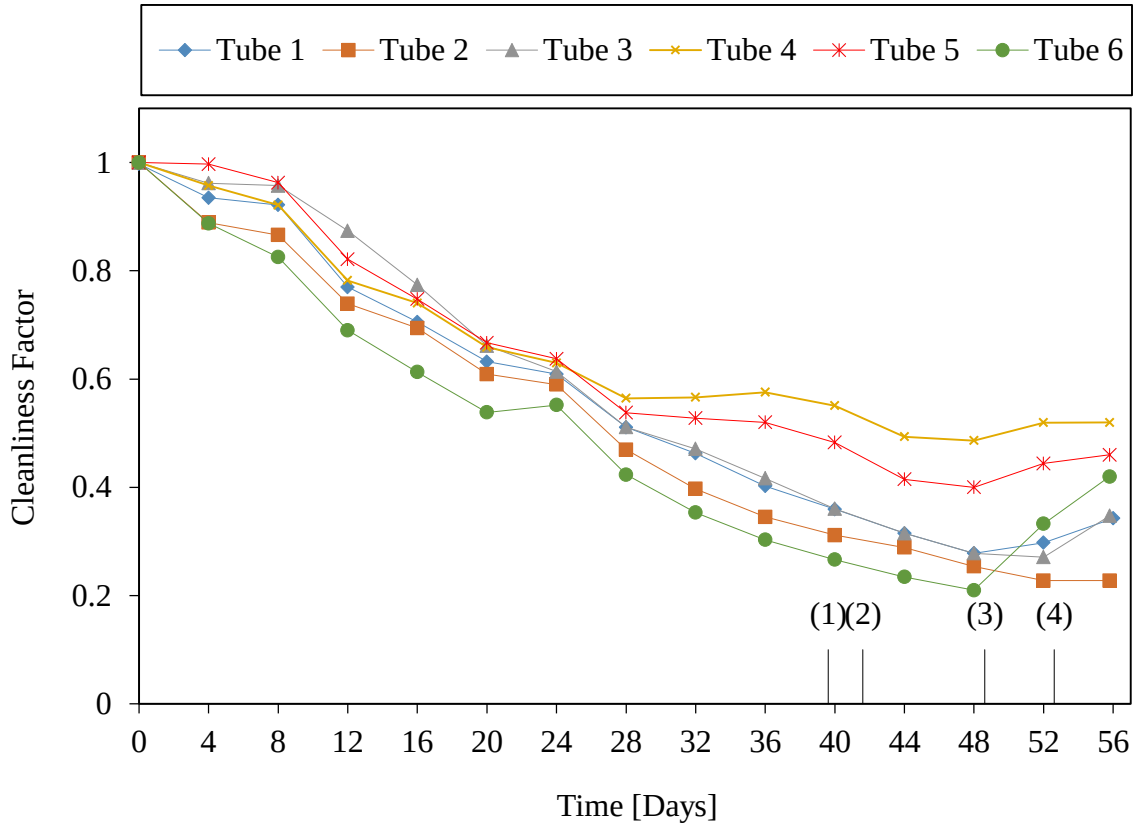


Figure 23: Calculated cleanliness factors for tube 1, 2, 3, 4, 5 and 6 during test 1 – (1) Plant dosed biocide – (2) Increase dosing concentration in tube 1, 2, 3 and 6 – (3) Dosed NaOCl in strainers – (4) Dosed NaOCl in strainers

The cleanliness factors of test 2 trended the same for all six condenser tubes during the time duration. This also proves the observations made at Figure 21. The cleanliness factors for test 1 and test 2 show an asymptotic approach to zero over an extended period of time.

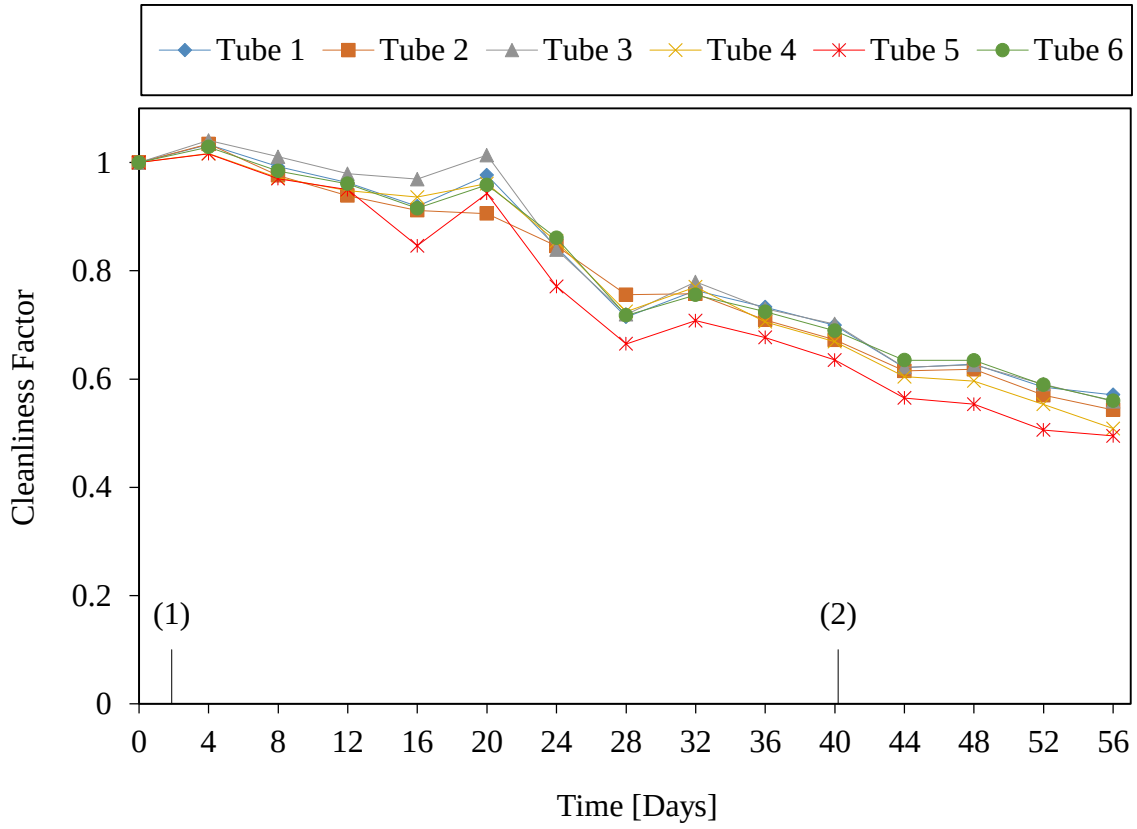


Figure 24: Calculated cleanliness factors for tube 1, 2, 3, 4, 5 and 6 during test 2 –(1) Plant dosed biocide –(2) Increase dosing concentration in tube 1, 2, 3 and 6

The results obtained from Figure 25 shows that the non-dosed condenser tubes have higher cleanliness factors than the dosed condenser tubes. The results also show that the cleanliness factors of the dosed condenser tubes are dependent on the chemical dosage concentration of bio-dispersant C. A higher chemical dosage concentration will result in a lower thermal performance of the dosed condenser tubes. It is also clear that an increase in bio-dispersant C initially improved the cleanliness factors of the dosed condenser tubes from where the cleanliness factors deteriorated again. The cleanliness factors in test 3 show an asymptotic approach to zero from day 0 to 44 from the cleanliness factors of tube 1, 2 and 3 increased due to the increase in bio-dispersant dosing and then started to decrease again. It is suspected that the cleanliness factors of tube 1, 2, 3 and 6 would approach the zero asymptotic value much quicker as before the increase in dosing concentration.

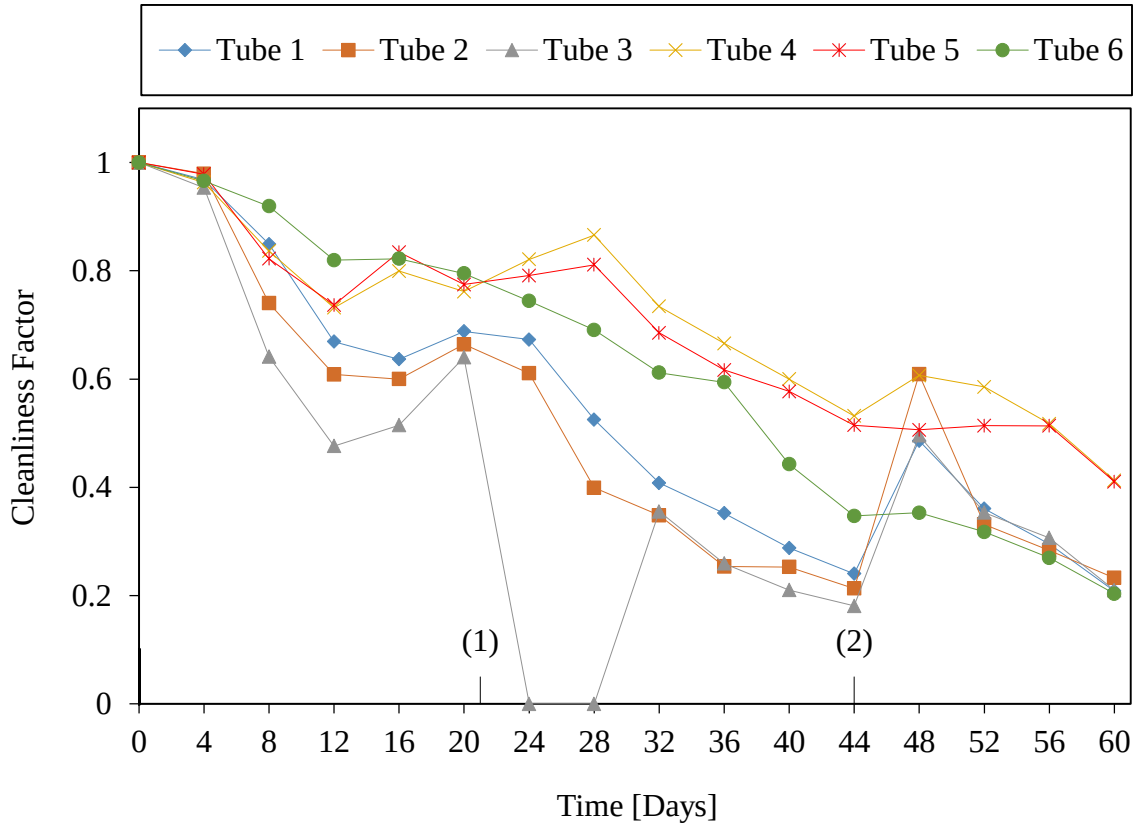


Figure 25: Calculated cleanliness factors for tube 1, 2, 3, 4, 5 and 6 during test 3 – (1) Plant dosed biocide – (2) Increase dosing concentration in tube 1, 2, 3 and 6

5.3 Friction factor

Furthermore, the friction factors calculated during test 1 (Figure 26), test 2 (Figure 27) and test 3 (Figure 28) followed the similar trends as their corresponding fouling factor figures. The fouling factors in each case increased as the fouling resistances increased and vice versa.

The increase of the dosing concentration of bio-dispersant A did not have any influence on the friction factors calculated during test 1. A decrease in friction factors are observed during the dosing of NaOCl as explained in Section 5.1 . This indicates that some of the biofilm was removed when the NaOCl was applied to the system and therefore decreased the pressure drop over the tube section.

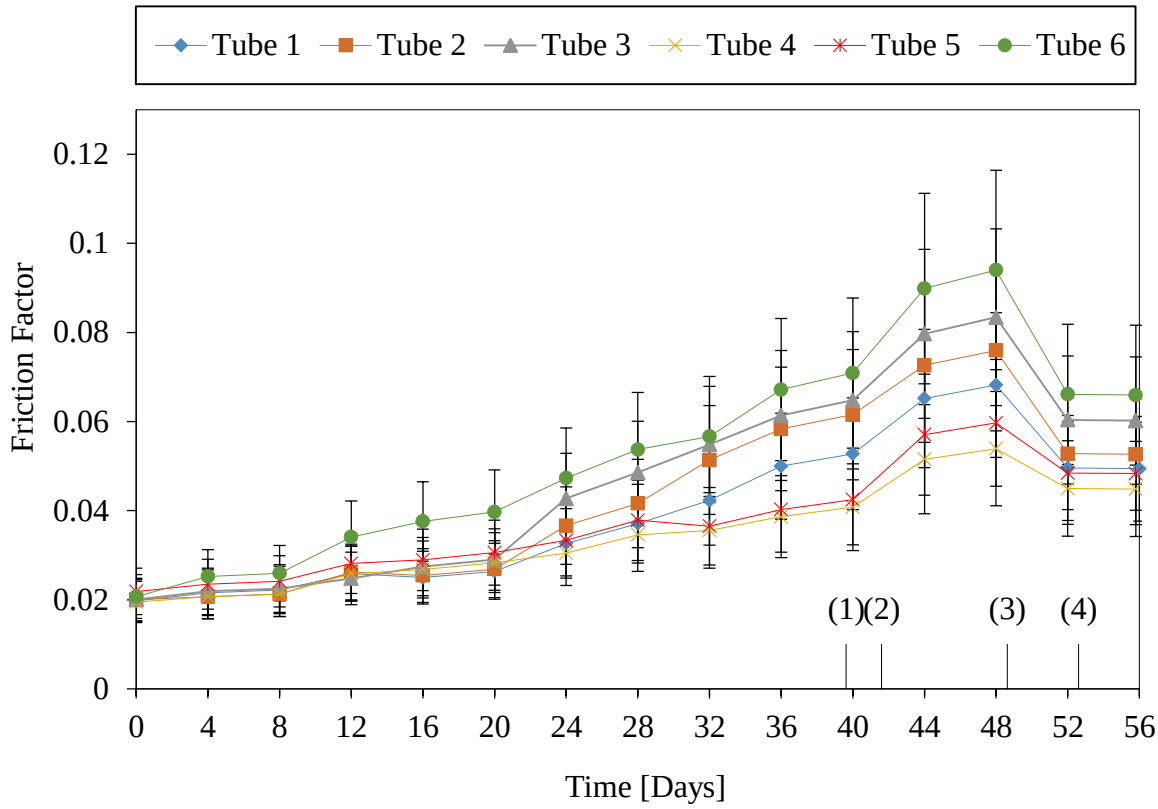


Figure 26: Measured friction factors for tube 1, 2, 3, 4, 5 and 6 during test 1 – (1) Plant dosed biocide – (2) Increase dosing concentration in tube 1, 2, 3 and 6 – (3) Dosed NaOCl in strainers – (4) Dosed NaOCl in strainers

The friction factors calculated during test 2 showed that the dosing of bio-dispersant B does not have an impact on the surface roughness inside the condenser tubes. These results also correspond to the fouling factor results obtained in Section 5.1 , showing that the dosing of bio-dispersant B does not have an influence on the heat transfer of the condenser tubes.

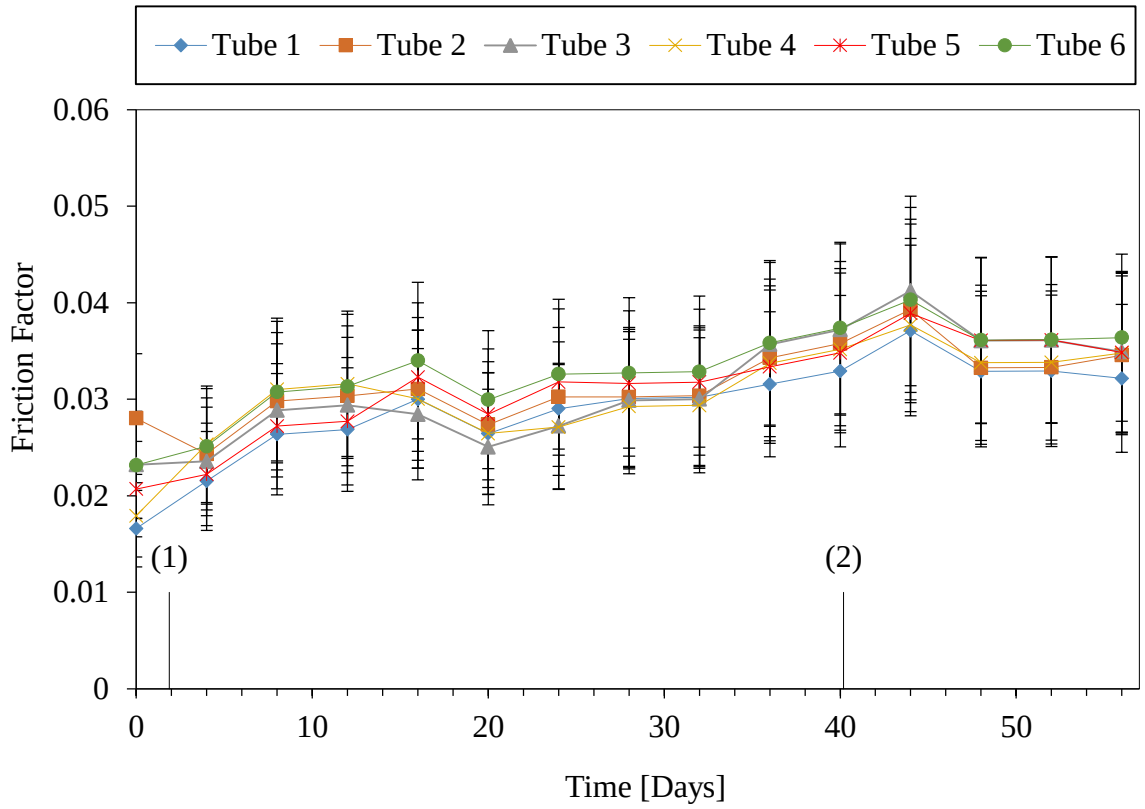


Figure 27: Measured friction factors for tube 1, 2, 3, 4, 5 and 6 during test 2 – (1) Plant dosed biocide – (2) Increase dosing concentration in tube 1, 2, 3 and 6

It is clear that the dosing concentration increase of bio-dispersant C led to a decrease in the calculated friction factors during test 3. Some biofilms were removed after the increase in dosing concentrations which lead to a decrease in pressure drop over the dosed condenser tubes. As result, the biofilms in the dosed condenser tubes started to grow and return to their original state after the increase in dosing concentrations resulting in a higher pressure drop over the test tube.

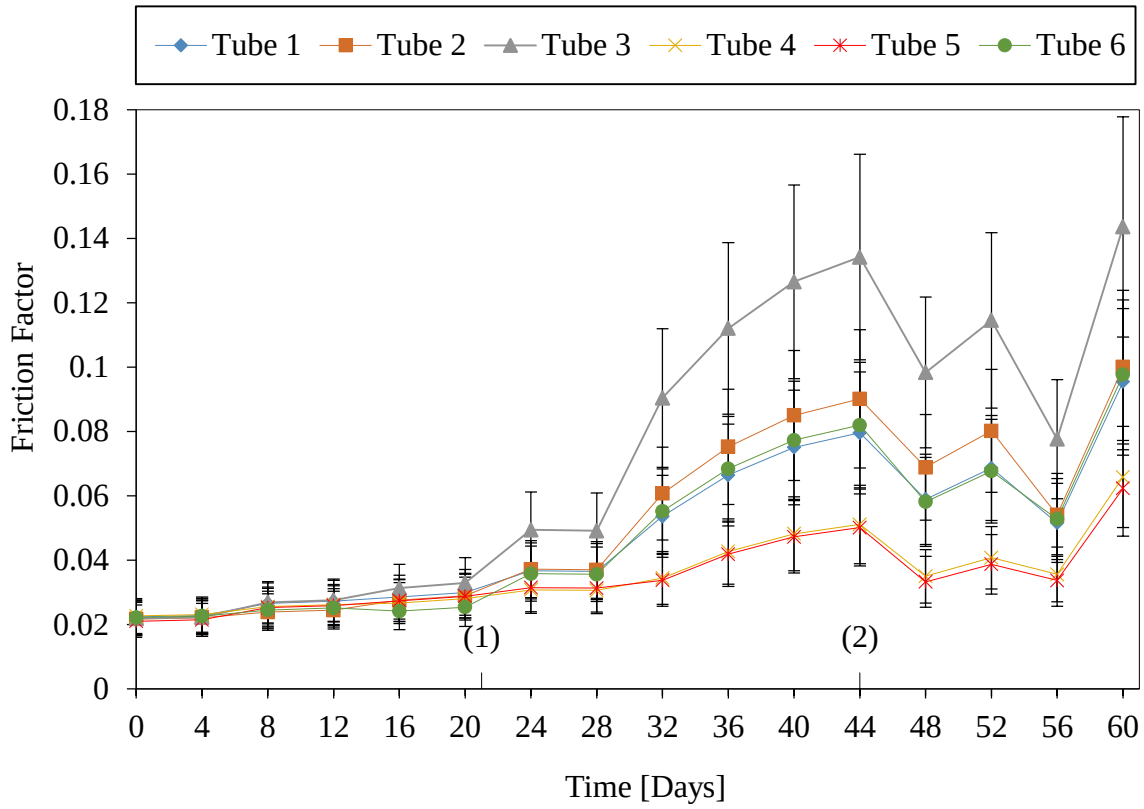


Figure 28: Measured friction factors for tube 1, 2, 3, 4, 5 and 6 during test 3 – (1) Plant dosed biocide – (2) Increase dosing concentration in tube 1, 2, 3 and 6

5.4 Mass gain

Each condenser tube was weighed before each test and naturally dried for 8 days at an angle after each test and then weighted again. The mass gain of the individual tubes during each test is shown in Figure 29.

The gain in mass of the individual condenser tubes during each test corresponds to the results obtained in Section 5.1 and 5.2 . There is no significant difference in mass gained between the dosed and non-dosed condenser tubes during test 2. This proves that the mass gained from the two non-dosed tubes (tube 4 and 5) is significantly less than the mass gained of the dosed tubes when dosed with bio-dispersant A and C during test 1 and 3 respectively.

Dissolved minerals inside the cooling water, such as, calcium, magnesium, silica and iron react with the carboxyl groups in the polymer biofilm layer. The biofilm layer is thickened by the minerals from where the mass of the tube increases (Horn and Richards, 2010)

(Christophersen, 2006). This indicates that the dosed condenser tubes during test 1 and 3 have thicker biofilms than the non-dosed tubes and explain why the dosed condenser tubes during test 1 and 3 gained more mass than the non-dosed tubes.

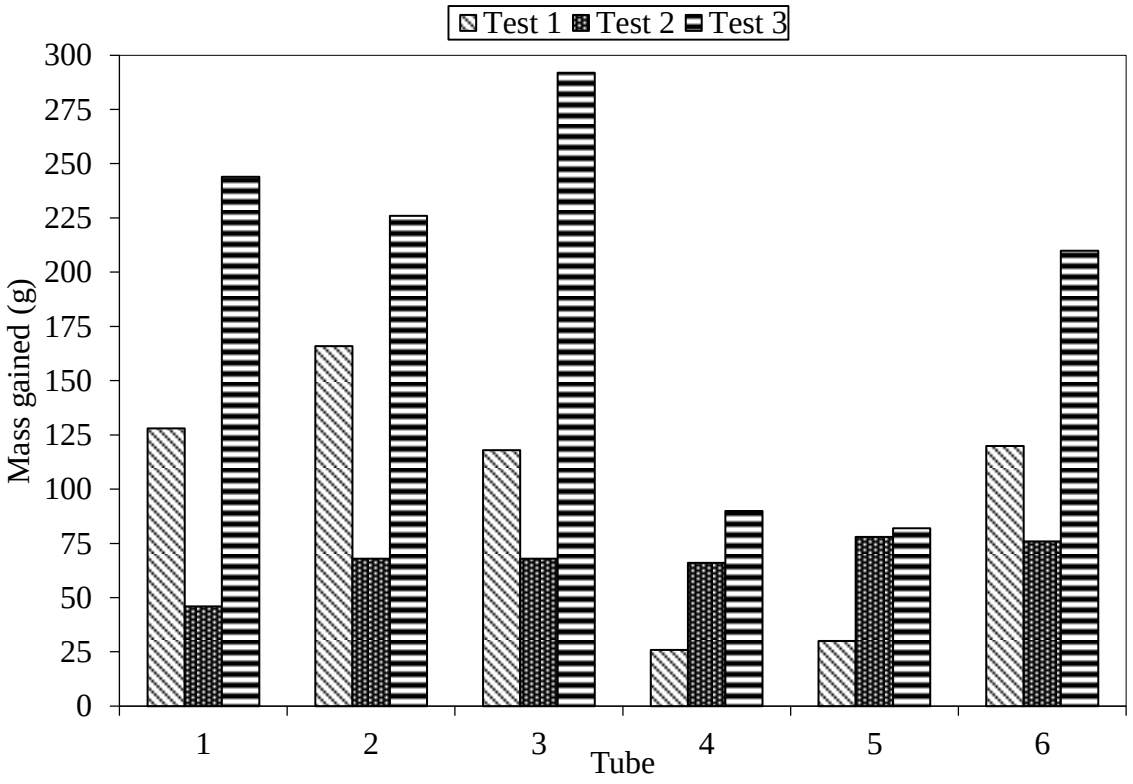


Figure 29: Mass gained for tube 1, 2, 3, 4, 5 and 6 during test 1, 2 and 3.

5.5 Bacterial counts

The bacterial counts of the individual tubes are averaged for each test and are shown in Figure 30 and Figure 31. There are no significant differences in anaerobic bacterial counts between the dosed and non-dosed condenser tubes for each of the tests (Figure 30). These bacterial counts indicate that a biofilm is present. The anaerobic bacteria film is the film below the aerobic film which is oxygen deprived. The aerobic bacteria film then develops on top of the anaerobic film which causes the resistance in heat transfer as explained below.

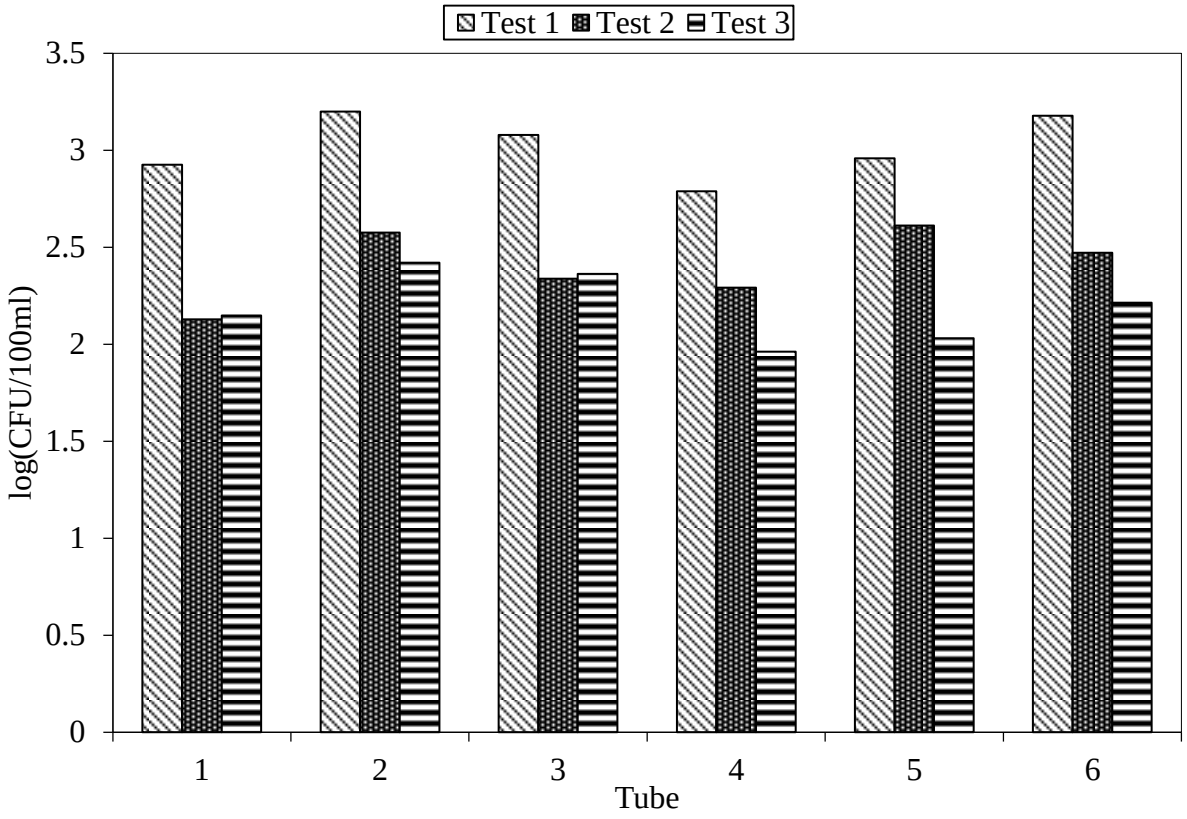


Figure 30: Anaerobic bacterial counts for tube 1, 2, 3, 4, 5 and 6 during test 1, 2 and 3.

The aerobic bacterial counts (Figure 31) for test 1 and 3 show that the dosed condenser tubes (tube 1, 2, 3 and 6) for test 1 and test 3 have much larger aerobic bacterial counts than the non-dosed (tube 4 and 5) condenser tubes. This indicates that a thicker biofilm is present when bio-dispersant A and C are dosed in the titanium condenser tubes, respectively. No significant differences in aerobic bacterial counts for the individual condenser tubes during test 2 are observed which indicates that bio-dispersant B does not remove any biofilms nor accelerates the growth of the biofilms. The aerobic counts for each tube during each test qualitatively correspond to the fouling factors. A higher aerobic count will also lead to a higher fouling factor value.

Several literature studies indicate that bio-dispersants have to be dosed in conjunction with a biocide (Mohseni and Berijani, 2018)(Di Pippo *et al.*, 2017) (Horn and Richards, 2010) (Buckman, 2017). The bio-dispersant will break the biofilm particles in the water and on the surface walls into smaller particles for more effective elimination by the biocides. A reason why the increase in biofilm formation was noted by using bio-dispersant A and C could be

because the biofilms inside the incoming water was dispersed into smaller particles which easier attached to the surface walls, after which the biofilms colonize in other regions downstream the titanium condenser tube as described in Section 2.8 . Bio-dispersant B has been ineffective. Bio-dispersant A and C should therefore be used in conjunction with a biocide to disperse the biofilms into smaller partials for more effective elimination by the biocide.

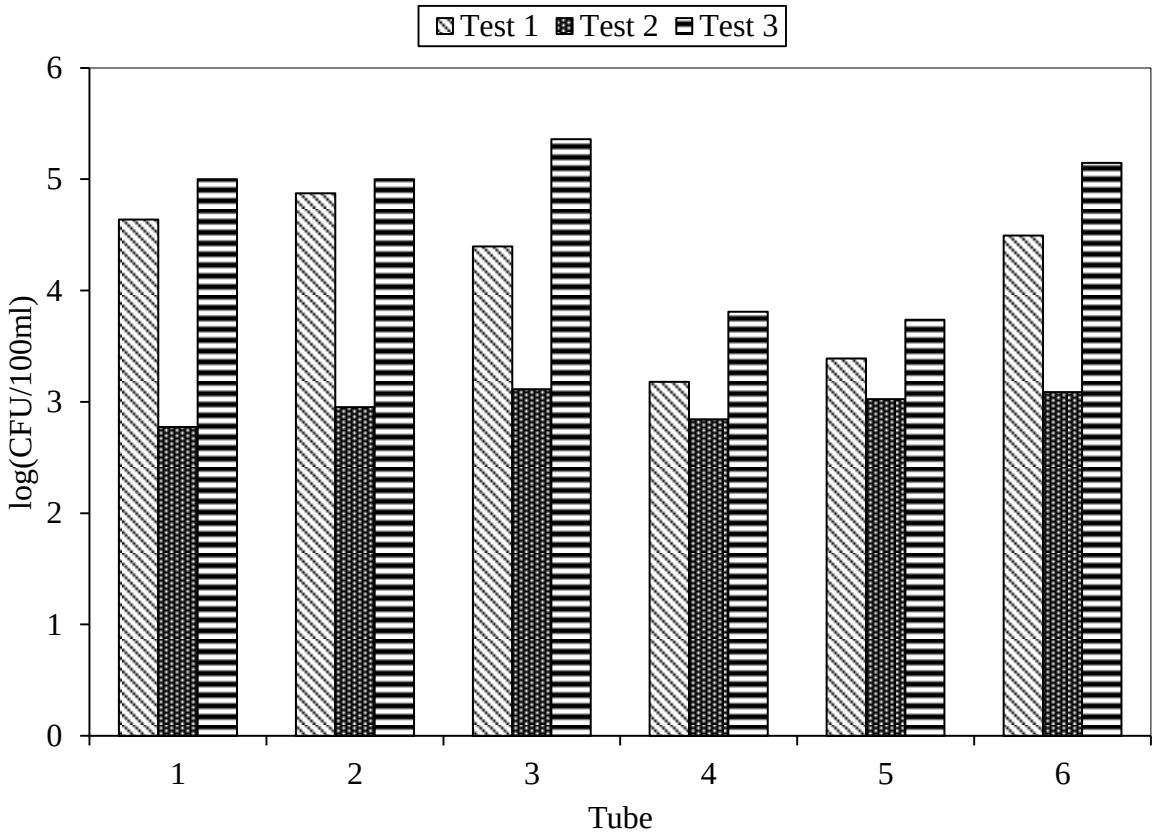


Figure 31: Aerobic bacterial counts for tube 1, 2, 3, 4, 5 and 6 during test 1, 2 and 3.

6 Relating the impact of single tube fouling to the actual main turbine condenser

It is important to translate the fouling resistances obtained from Section 5.1 to the actual condenser saturation pressures to evaluate the potential financial impact of chemical dosing on the thermal performance of the actual power plant. This section describes a hypothetical study to determine the potential financial gain or loss if bio-dispersant A, B and C are dosed at the actual power plant.

6.1 Heat transfer inside the actual main turbine condensers

The actual condenser at the coal fired power plant has a church window configuration with two passes and consists of 26000 titanium tubes.

The same assumptions as made in Section 4.6.1 together with the following were made during the analysis of the actual main turbine condenser:

1. Condensation occurs throughout the entire condenser at a constant rate.
2. The condenser hotwell temperature is equal to the saturation temperature inside the condenser.
3. The actual main turbine condenser is modelled as a single horizontal tube.

The log mean temperature difference method is applicable to determine the heat transfer inside the actual main turbine condenser when the assumptions in Section 4.6.1 are made (Cengel and Ghajar, 2011). The rate of heat transfer is expressed as:

$$\mathrm{Q} = \mathrm{U}A_S \, \Delta \, T_{LM} \tag{25}$$

Where U is the overall heat transfer coefficient, A the available heat transfer surface of all the condenser tubes and $\Delta \, T_{LM}$ is the log mean temperature difference expressed in Equation (3). Cengel and Ghajar (2011) describes that the overall heat transfer for a unit area is equal to the inverse of the total thermal resistance as explained in Equation (4).

The total thermal resistance for the single horizontal tube is the sum of the thermal resistances of the: convectional resistance of the cooling water inside the condenser tubes,

conduction resistance of the tube material, fouling resistance inside the condenser tube and the convectional heat transfer resistance of the steam exiting the low pressure turbine.

$$\sum R = R_{CW} + R_{tube} + R_f + R_{shell} \tag{26}$$

Equation (27) is expanded to into its individual variables in Equation (5).

$$\sum R = \frac{1}{h_{CW} \cdot A_s} + \frac{ln\left(\frac{D_O}{D_i}\right)}{2 \cdot \pi \cdot k_t \cdot L_{eff}} + R_f + \frac{1}{h_{shell} \cdot A_{shell}} \tag{27}$$

6.1.1 Inside tube convection coefficient

The friction factor of single horizontal tube is calculated by using the Petukhov correlation in Equation (28) (Petukhov, 1970):

$$f_{CW} = (0.79 \cdot \ln(Re_{CW}) - 1.64)^{-2} \tag{28}$$

The friction factor influence the Nusselt number (Equation (7)) which has an impact on the convectional heat transfer coefficient (Equation (8)) inside the condenser tubes (Cengel and Ghajar, 2011). The Reynolds number for the cooling water flowing inside the condenser tubes is calculated by using Equation (9) (Cengel and Ghajar, 2015).

6.1.2 Shell side convection coefficient

The average convection heat transfer coefficient for film condensation on the outer surface of a single horizontal tube is calculated as (Cengel and Ghajar, 2011).

$$h_{shell} = 0.729 \cdot \left(\frac{{h_{fg}}^* \cdot {\rho_c}^2 \cdot g \cdot {k_c}^3}{\mu_c \cdot (T_{Sat} - T_{Wall_o}) \cdot D_O}\right)^{0.25} \tag{29}$$

Film condensation takes place on a vertical tier of horizontal tubes and Equation (29) is, therefore, modified to with a correction factor as indicated in Equation (30).

$$h_{shell} = 0.729 \cdot \left(\frac{{h_{fg}}^* \cdot {\rho_c}^2 \cdot g \cdot {k_c}^3}{\mu_c \cdot (T_{Sat} - T_{Wall_o}) \cdot D_O} \right)^{0.25} \cdot N^{-0.25} \quad (30)$$

The main turbine condenser tubes have a church window design layout and the correction factor N was obtained from the original condenser design documents.

${h_{fg}}^*$ is calculated assuming that no superheat in the steam is entering the condenser as (Cengel and Ghajar, 2011):

$${h_{fg}}^* = h_{fg} \cdot 1000 + 0.68 \cdot Cp_c \cdot (T_{Sat} - T_{Wall_o}) \quad (31)$$

The outside tube area available for heat transfer is calculated as:

$$A_c = \pi \cdot D_0 \cdot L_t \cdot N_t \quad (32)$$

With D_0 the outer diameter of the condenser tube, L_t the length of the condenser tube and N_t the total number of condenser tubes.

6.1.3 Condenser heat transfer performance analysis

The condenser saturation pressure is calculated by solving the saturation temperature T_{Sat} from Equation (29) and translating the saturation temperature to the saturation pressure by using steam tables (Cooper and Le Fevre, 1969). The iterative process and sample calculations are shown in Appendix F.

6.2 Relating the experimentally determined fouling resistances to its impact on an actual power generating unit.

The measured fouling resistances from each test were used for the analysis:

- Test 1: Tube 4 as the control tube and tube 6 as the dosed tube. Tube 6 was chosen because it had the highest fouling resistances to obtain the worst impact on the actual power generating unit.

- Test 2: Tube 4 as the control tube and tube 1 as the dosed tube. All six tubes had very similar fouling resistances during this test.
- Test 3: Tube 4 as the control tube and tube 2 as the dosed tube. Tube 2 was chosen because it had the second highest fouling resistances to obtain the worst impact on the actual power generating unit. Tube 3 which yielded the highest fouling resistances was problematic during the test and was therefore not used.

These fouling resistances were used to calculate the corresponding saturation pressures inside the actual main turbine condenser if the actual main turbine condensers fouled at the same rate as the tubes in the test apparatus chosen above by using the model explained in Section 6.1 . The following design parameters were used during the simulation:

- The maximum power generating unit design generated load is 503 MW.
- The maximum allowed condenser operating saturation pressure is 20 kPa.
- The cooling water inlet temperature to the condenser is 24 °C.
- Cooling water at a design flowrate of 9.8 m^3/s flows through the condenser.
- The titanium condenser tubes have an external diameter of 24 mm and an internal diameter of 23 mm.
- The condenser consists of 26000 tubes with a length of 12 m each and the condenser has two passes.
- The energy rejected by the condenser as a function of saturation pressure at a generated load of 503 MW is obtained from the original heat balance diagrams and are expressed as:

$$E_{reg} = 9.36065 \cdot P_{sat} + 544.27055 \tag{33}$$

- The generated load as a function of the energy rejected for loads below 503 MW obtained from the original heat balance diagrams is expressed as:

$$P_{gen} = 0.7687 \cdot E_{reg} - 52.703 \tag{34}$$

- The net unit heat rate is a function of the enthalpy of the water in the condenser hotwell (Putman and Harpster, 2000). This expression is obtained from the original heat balance diagrams as:

$$\mathrm{HR} = 5.467 \cdot H_{hotwell} + 6278.5 \quad (35)$$

- Auxiliary power is approximately 4.5% of the generated power.

The following information was obtained from the power station at which the research was conducted:

- The average calorific value (CV) of the coal used is 20 MJ/kg.
- The power station pays R 800 per ton of coal.
- The selling price per MWh electricity is approximately R700 per unit send out.

The effect of the fouling resistances obtained from each test is done by using the actual condenser model, the condenser and plant design conditions as well as the information about the coal and cost per megawatt send out as described above.

6.2.1 Results obtained from the fouling resistances obtained from test 1:

The calculated actual condenser saturation pressure and generated unit load is shown in Figure 32 for test 1. The actual condenser saturation pressure for the non-dosed tube (ND) and dosed tube (D) are calculated by using the fouling resistance data obtained from tube 4 and tube 6 respectively from the first test.

The condenser saturation pressure for the non-dosed tube follows the exact same trend as the fouling resistance obtained in Figure 20 for tube 4. It can also be seen that the generated load for the saturation pressure for the non-dosed tube is at the maximum 503 MW because the saturation pressure is below the 20 kPa maximum value (Figure 32).

The condenser saturation pressure for the dosed tube also follows the exact same trend as the fouling resistance obtained in Figure 20 for tube 6 up to day 28 where it reaches the maximum condenser saturation pressure of 20 kPa. The unit generated load for the dosed tube then starts to decline until day 48 where it reaches a generated load of 270 MW. A 233 MW load loss would have been taken on the power generating unit if the actual condenser tubes were chemically dosed. The test tubes in the test apparatus were dosed with NaOCl on day 48 which decreased the fouling resistances of the tubes, therefore, the increase in generated load for the dosed tube from day 48 to day 56 in Figure 32.

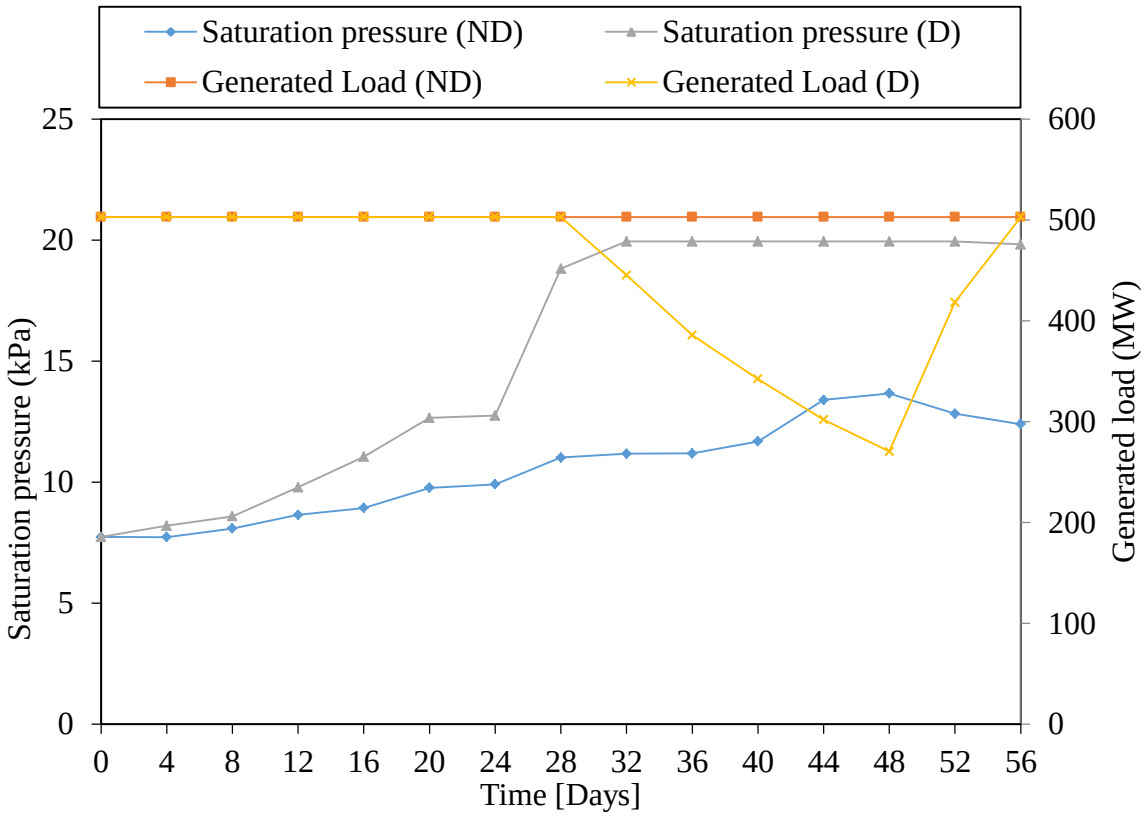


Figure 32: Generated load and actual condenser saturation pressure for test 1- (D) Dosed tube-6, (ND) Non dosed tube-4

Figure 33 shows the financial impacts of the increase in condenser backpressure for the non-dosed and dosed tube as well as the financial impacts of the decreased capability to generate the maximum design load of 503 MW.

Figure 33 consists of three parts:

- Increased coal usage impact: This is the Rands loss per day due to the impact on increased coal usage (decrease in overall cycle efficiency) due to the increase in condenser saturation pressure.
- Load loss impact: This is the Rands loss per day due to the inability of the power generation unit to produce its maximum load of 503 MW. This is the financial loss due to not having the designed production output.
- Total loss: The sum of the increased coal usage impact and load loss impact.

It can be seen that the non-dosed tube only have a loss due to an increase in coal usage. The impact of the fouling when the tube is not dosed does not affect the production output but only an increase in coal cost per day can be seen because of the decrease in cycle efficiency.

The fouling resistance inside a condenser tube due to the dosing of a bio-dispersant has a significant financial impact on the power generation company. An increase in loss due to increase coal usage is observed while the maximum saturation pressure has not been reached (day 28). The financial loss per day increases severely when the production output of the power generation unit is limited whereby the coal usage decreases. The financial loss due to the production limit is far more than the financial gain due to the decrease in coal consumption. The dosing of NaOCl at day 48 had a significant impact by reducing the daily financial loss.

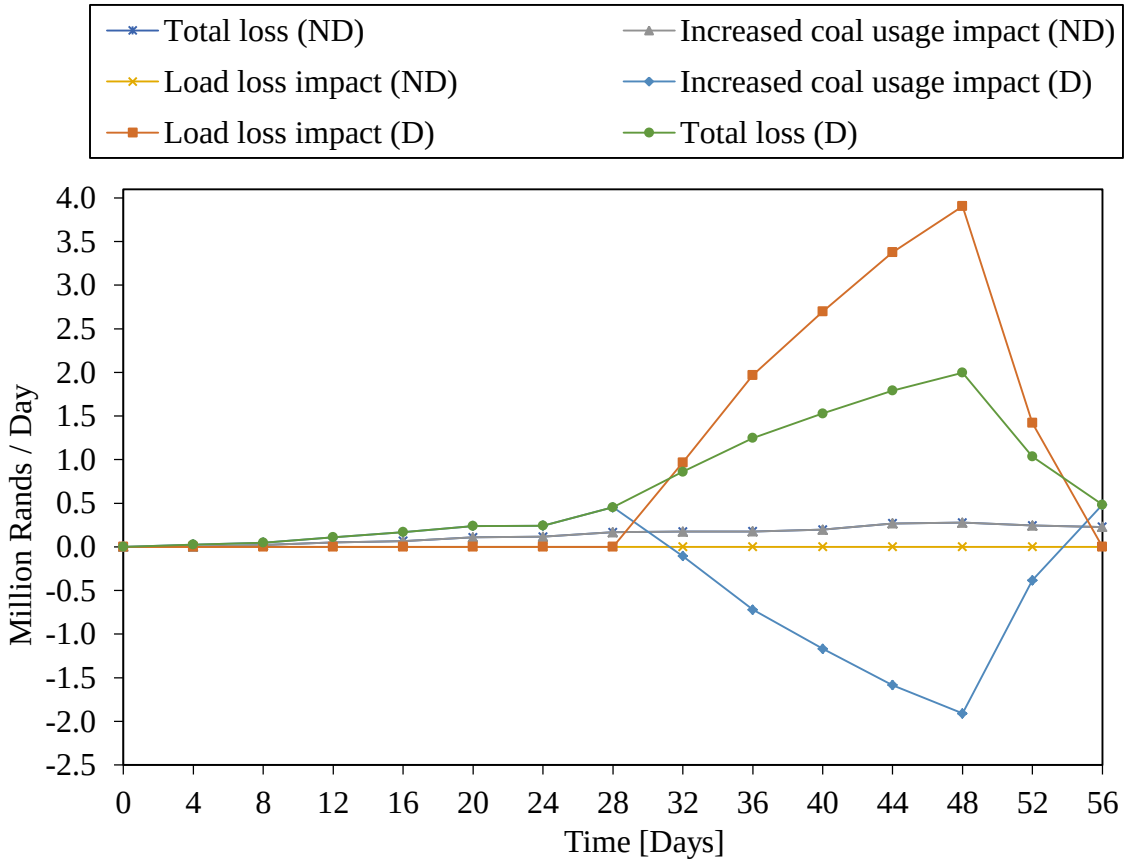


Figure 33: Financial impacts of chemical dosing for test 1: non-dosed tube – 4 (ND) and dosed (D) tube-6.

The non-dosed tube showed a cumulative loss over the 56 day test period of R 2.1 million and the dosed tube showed a cumulative loss of R 10.23 million. This showed that the power generation company would have suffered a net loss of R 8.13 million per power generating unit if the bulk cooling water system was dosed by only a bio-dispersant over a period of 56 days.

6.2.2 Results obtained from the fouling resistances obtained from test 2:

The calculated actual condenser saturation pressure and generated unit load is shown in Figure 34 for test 2. The actual condenser saturation pressure for the non-dosed tube (ND) and dosed tube (D) are calculated by using the fouling resistance data obtained from tube 4 and tube 1 respectively from the second test.

The condenser saturation pressure for the non-dosed and dosed tube follows the exact same trend as the fouling resistance obtained in Figure 21 for tube 4 and 1 respectively. It can also be seen that the generated load for the saturation pressure for the non-dosed and dosed tube is at the maximum 503 MW because the saturation pressure is below the 20 kPa maximum value (Figure 34). This shows that the dosing of bio-dispersant B had no effect on the thermal efficiency of a power generating unit.

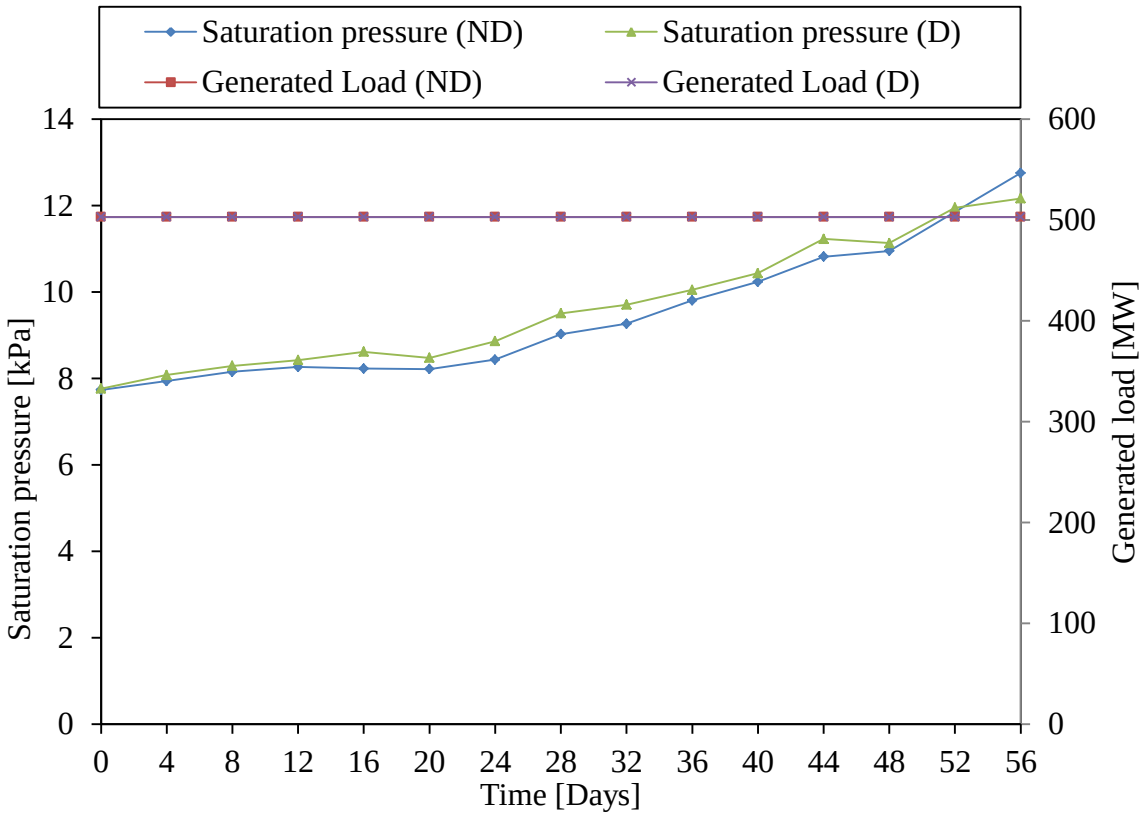


Figure 34: Generated load and actual condenser saturation pressure for test 2- (D) Dosed tube-1, (ND) Non dosed tube-4.

Figure 35 shows the financial impacts of the increase in condenser backpressure for the non-dosed and dosed tube.

It can be seen that the non-dosed and dosed tube only have a loss due to an increase in coal usage. The impact of the fouling when the tube is not dosed or dosed does not affect the production output but only an increase in coal cost per day can be seen.

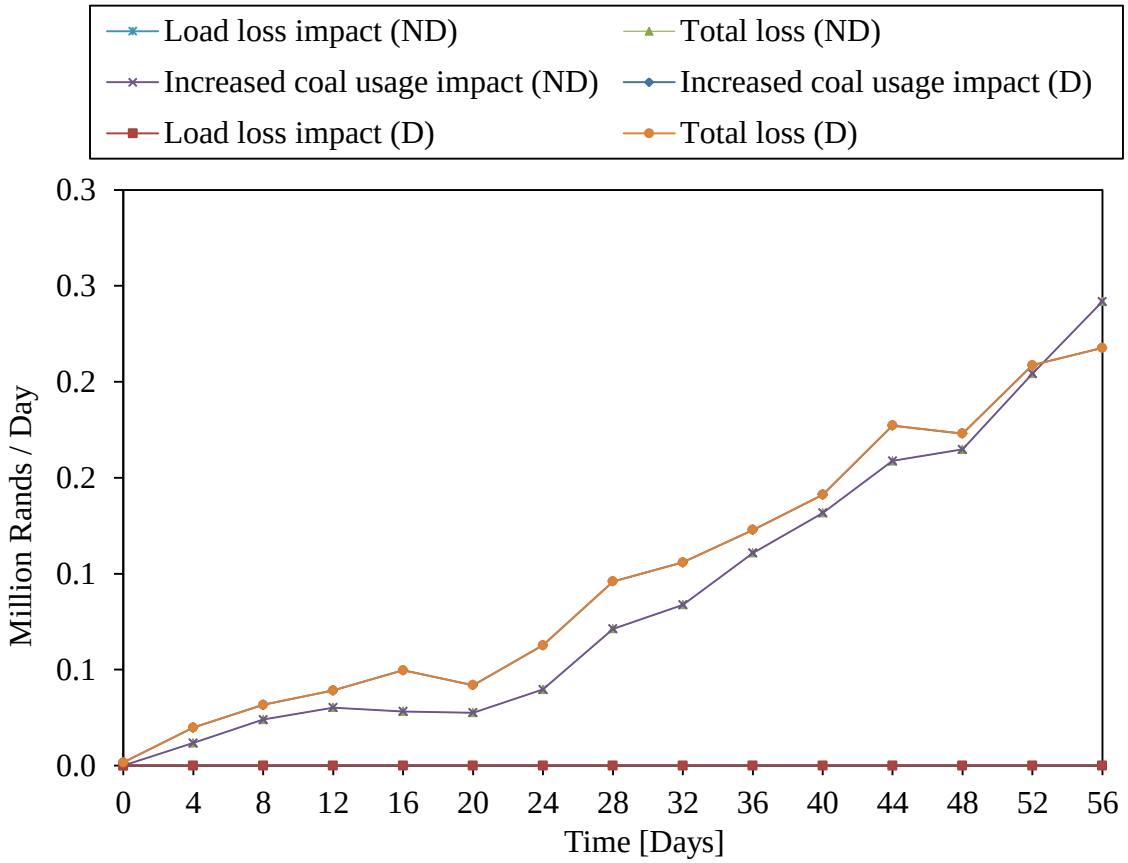


Figure 35: Financial impacts of chemical dosing for test 2: non-dosed tube – 4 (ND) and dosed (D) tube-1.

The non-dosed tube showed a cumulative loss over the 56 day test period of R 1.33 million and the dosed tube showed a cumulative loss of R 1.49 million. This shows that the dosing of bio-dispersant B has not led to any nett financial loss over the 56 day period.

6.2.3 Results obtained from the fouling resistances obtained from test 3:

The calculated actual condenser saturation pressure and generated unit load is shown in Figure 36 for test 3. The actual condenser saturation pressure for the non-dosed tube (ND) and dosed tube (D) are calculated by using the fouling resistance data obtained from tube 4 and tube 2 respectively from the third test.

The condenser saturation pressure for the non-dosed tube follows the exact same trend as the fouling resistance obtained in Figure 22 for tube 4. It can also be seen that the generated load

for the saturation pressure for the non-dosed tube is at the maximum 503 MW because the saturation pressure is below the 20 kPa maximum value (Figure 36).

The condenser saturation pressure for the dosed tube also follows the exact same trend as the fouling resistance obtained in Figure 20 for tube 2 up to day 28 where it reaches the maximum condenser saturation pressure of 20 kPa. The unit generated load for the dosed tube then starts to decline until day 44 at a generated load of 260 MW. A 243 MW load loss would have been taken on the power generating unit if the actual condenser tubes were chemically dosed. The dosing concentration of bio-dispersant C was increase on day 44 from where the generated load increased to 503 MW from where it decreased again to 290 MW on day 60 (Figure 36).

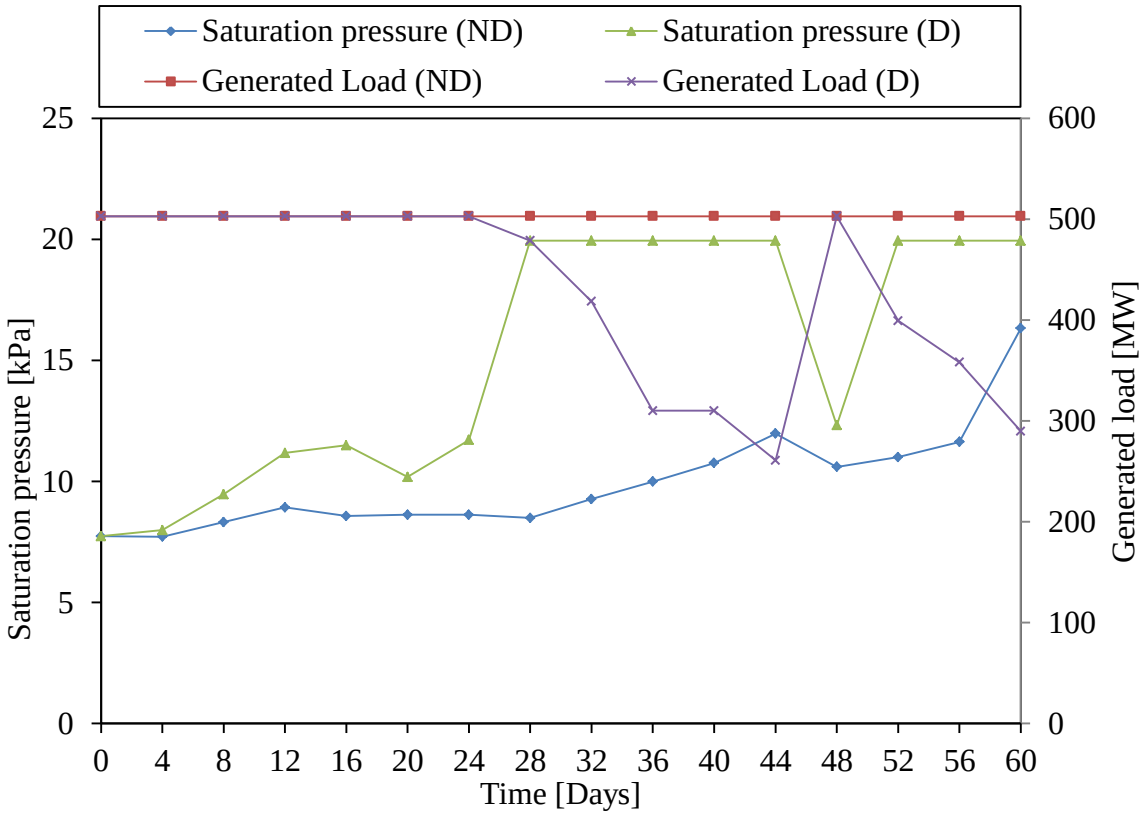


Figure 36: Generated load and actual condenser saturation pressure for test 3- (D) Dosed tube-3, (ND) Non dosed tube-4.

Figure 37 shows the financial impacts of the increase in condenser backpressure for the non-dosed and dosed tube as well as the financial impacts of the decreased capability to generate the maximum design load of 503 MW.

It can be seen that the non-dosed tube only have a loss due to an increase in coal usage. The impact of the fouling when the tube is not dosed does not affect the production output but only an increase in coal cost per day can be seen.

The fouling resistance inside a condenser tube due to the dosing of a bio-dispersant has a significant financial impact on the power generation company. An increase in loss due to increase coal usage is observed while the maximum saturation pressure has not been reached (day 28). The financial loss per day increases severely when the production output of the power generation unit is limited whereby the coal usage decreases. The financial loss due to the production limit is far more than the financial gain due to the decrease in coal consumption. The increase of the dosing concentration of bio-dispersant C at day 44 had a significant impact by reducing the total daily financial losses the total losses increases again until day 60 after the dosing concentration of bio-dispersant C was increased.

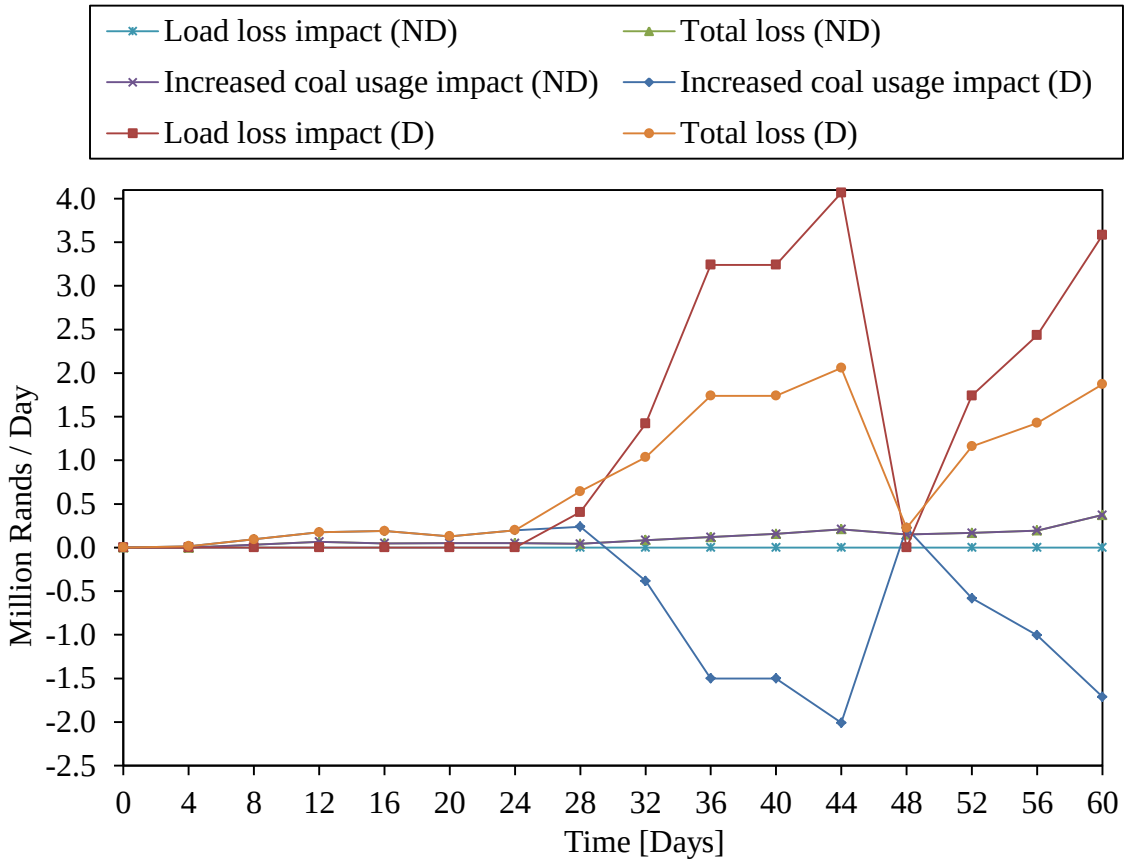


Figure 37: Financial impacts of chemical dosing for test 3: non-dosed tube – 4 (ND) and dosed (D) tube-3.

The non-dosed tube showed a cumulative loss over the 60 day test period of R 1.7 million and the dosed tube showed a cumulative loss of R 12.7 million. This showed that the power generation company would have suffered a net loss of R 11 million per power generating unit if the bulk cooling water system was dosed by only bio-dispersant C over a period of 60 days.

7 Conclusions and recommendations

Fouling was measured in six parallel titanium condenser tubes using a co-current double pipe heat exchanger at a wet cooled coal-fired power station. Three test runs were done, each with a different bio-dispersant. Four of the six condenser tubes, in the test apparatus, were chemically dosed during each test at different concentrations. The condenser test apparatus was effective to determine the effect of bio-dispersants on the fouling, friction, and cleanliness factor of each tube. Problems with some of the thermocouples were observed during the tests but were corrected between the tests to minimize the effect on the results. The anaerobic and aerobic counts as well as the mass gained by each tube were measured which correlated to the fouling, friction, and cleanliness factor of the tubes. It was also noted that the biocide dosing by the chemical services department at the power utility had no effect on any of the above mentioned parameters which indicated that the frequency of dosing and the current dosing regimen are ineffective and should be revised.

The dosing of bio-dispersant A and C during test 1 and 3 respectively increased the fouling and friction factors and decreased cleanliness factors inside the condenser tubes and worsened the heat transfer. Test 1 where bio-dispersant A was dosed showed a difference of 10.69 m^2K/W in fouling factor between the worst performing dosed and non-dosed tube after a period of 48 days. Test 3 where bio-dispersant C was dosed showed a difference of 14.2 m^2K/W in fouling factor between the worst performing dosed and the two non-dosed tubes after a period of 44 days. An increase in dosing concentration of bio-dispersant A during test 1 showed no effect on the fouling factors of the dosed tubes. The fouling factors of three of the four dosed tubes decreased when the dosing concentrations of bio-dispersant C were increased during test 3 from the fouling factors increased again. The dosing of bio-dispersant A and C led to a significant mass gain of the condenser tubes and higher aerobic bacterial counts are observed for these tubes.

The dosing of bio-dispersant B during test 2 had no measurable effect on the fouling and friction factors, mass gained and aerobic bacterial counts when the dosed and non-dosed tubes are compared. Test 2 showed an average fouling factor of 3.41 m^2K/W after a period of 56 days for the dosed and non-dosed tubes. It is also revealed that the supplier recommendation of bio-dispersant and dosing rates may not be appropriate and could cause the power utility to commit to expenses that are not leading to any desired results.

All three of the bio-dispersants are currently being used to dose the bulk cooling water system at the power utility. These bio-dispersants are dosed in a continuous way and are alternated approximately every three months. The dosing of bio-dispersant A and C are likely to reduce the heat transfer inside the main turbine condensers which will lead to a reduction in cycle efficiency. A reduction in cycle efficiency is currently observed by the power utility because of the incorrect dosing regimens where a bio-dispersant should be dosed in conjunction with a biocide. The biofilms inside the main turbine condensers will not be removed by using only bio-dispersant A or C. Bio-dispersant B does not have any measurable influence on the biofilms inside the main turbine. The growing biofilms in the system will increase the system resistance of the system which lead to a reduction in cooling water flow through the cooling water circuit. It has become clear that the type and dosing concentration of bio-dispersants has a significant effect on the rate of dosing. The tests conducted mirrored the actual bulk cooling water system dosing where only bio-dispersants are dosed with ineffective dosing of biocides. Hence a similar deterioration is observed in the actual condenser and the test tubes. No dosing of a bio-dispersant by the power utility took place during the tests, the dosing of only a bio-dispersant is therefore a wasteful expenditure and the supplier recommended dosing regimen is not effective at the power utility.

The hypothetical impact study on the actual condenser showed that the dosing of bio-dispersant A, B and C will lead to a condenser related load losses of 233 MW, 0 MW and 243 MW respectively. The total net financial losses due to the dosing of bio-dispersant A, B and C are R 8.13 million, R 0 and R 11 million respectively over the different test durations per power generating unit. The sole dosing of two of the three different bio-dispersants therefore could lead to severe financial losses. The power utility currently experiences load losses in the order of 180 MW per fouled condenser because of fouling that is present due to incorrect dosing regimens.

The research question: “What is the change in fouling rate inside titanium condenser tubes as a result of chemical dosing?” has therefore been answered. It has been shown that the fouling rates are influenced by the dosing of bio-dispersants and that the incorrect chemical dosing can lead to significant financial losses.

It is recommended that:

- Bio-dispersant A and C are systematically tested at different concentrations in parallel with biocides to determine if the biofilms present in the cooling water cycle will be removed.
- Bio-dispersants and biocides are tested on a small scale before it is used on an actual cooling water cycle at a wet-cooled power plant. This should become practice before any chemicals that are dosed into the cooling water cycle at the power utility.
- The power utility should evaluate the actual condenser backpressures against chemical dosing to evaluate the effectiveness of the chemical dosing. This should be logged to determine the optimum chemical dosing regimen.
- The power utility should revise the dosing of biocides because no effect on the fouling factors on the tubes could have been seen when it was dosed into the main cooling water system.
- Similar work should be repeated to determine the effectiveness of anti-scalants in the cooling water systems at the power utility.
- The personnel at the power utility need to become more aware and knowledgeable about chemical dosing of cooling water systems and should become less reliant on the supplier recommendations.
- The test facility should be maintained and kept in a good working condition for further analysis of chemical additives.

References

Accepta Water Treatment (2018) *Accepta 2321 Bio-Dispersant for Cooling Water Systems*. Available at: https://accepta.com/product/water-treatment-chemicals-wastewater-effluent-treatment-products/cooling-water-treatment-chemicals/biodispersants-cooling-water-treatment-chemicals/477-bio-dispersant-for-cooling-water-systems-2321 (Accessed: 11 October 2018).

Acuro Organics Limited (2018) *Cooling Tower Chemicals*. Available at: http://www.chemicals99.com/cooling-tower-chemicals-range.html (Accessed: 11 October 2018).

Ahmed, B. and Zubair, S. M. (2016) 'Predicting the impact of heat exchanger fouling in power systems', *Energy*. Elsevier Ltd, 107, pp. 595–602. Vol: 107.

Amjad, Z. and Hooley, J. P. (1994) 'Effect of antiscalants on the precipitation of calcium carbonate in aqueous solutions', *Tenside, Surfactants, Detergents*, pp. 12–17.

Bio-Source (2018) *Biodispersants*. Available at: https://biosourceinc.com/products/biodispersants-specialty-product/ (Accessed: 11 October 2018).

Buckman (2017) *Biofilms*. Available at: https://www.buckman.com/wp-content/uploads/2018/04/E297W-Biofilms.pdf.

Cengel, Y. A. and Ghajar, A. J. (2011) *Heat and Mass Transfer: Fundamentals & Applications*. 4th edn. New York: McGraw-Hill.

Characklis, W. and Marshall, K. (1990) *Biofilms Volume 5 of Wiley Series in Ecological and Applied Microbiology*. California: Wiley. Available at: https://books.google.co.za/books?id=soAXAQAAIAAJ.

Chemtex (2018) *Dispersant and Biodispersant*. Available at: http://www.chemtexlimited.com/dispersant-and-biodispersant.html (Accessed: 10 October 2018).

Chemworld.com (2018) *Bio Dispersant*. Available at:

https://www.boilerandcoolingwater.com/Bio-Dispersant-p/cw64-5.htm (Accessed: 10 October 2018).

Christophersen, D. (2006) 'Biodetergents for Cooling Water', (November), pp. 223–226.

Christophersen, D. (2018) *Microbiological Control Strategy in Cooling Tower Systems*. Available at: http://www.veoliawatertech.com/crownsolutions/ressources/documents/2/21852,Issue-19-Microbiological-Control-S.pdf (Accessed: 10 October 2018).

Cloete, T. E. (2003) 'Resistance mechanisms of bacteria to antimicrobial compounds', *International Biodeterioration and Biodegradation*, 51(4), pp. 277–282. Vol: 51.

Cloete, T. E., Jacobs, L. and Brözel, V. S. (1999) 'The chemical control of biofouling in industrial water systems', *Biodegradation*, 9(1), pp. 23–27. Vol: 9.

Coleman, H W, Steele, G. W. (2009) *Experimentation, Validation, and Uncertainty Anylysis for Engineers*. 3rd edn. New Jersey: John Wiley and Sons, Inc.

Cooper, J. R. and Le Fevre, E. J. (1969) *Thermophysical Properties of Water Substance*. 1st edn. Amsterdam: Elsevier.

Crittenden, B. and Alderman, N. J. (1988) 'Negative Fouling Resistances : The Effect of Surface Roughness', *Chemical Engineering Science*, 43(4), pp. 829–838. Vol: 43.

Dave, H., John, P., Sarkar, A. and Mehta, B. (1999) 'Operating Experience of Non Chromate Based Cooling Water Treatment at Iffco Kalol unit', *Enviormental Science*, pp. 1–10.

Department of Water Affairs and Forestry (1996) 'South African Water Quality Guidelines', *Industrial Use*, 3(2), p. 123. Available at: http://www.dwa.gov.za/iwqs/wq_guide/Pol_saWQguideMARINEIndustrialusevol3.pdf.

Deziani, M., Rahmani, K., Roudaki, S. J. M. and Kordloo, M. (2017) 'Feasibility study for reduce water evaporative loss in a power plant cooling tower by using air to Air heat exchanger with auxiliary Fan', *DES*. Elsevier B.V., 406, pp. 119–124. Vol: 406.

Elsmore, R. (1994) 'Development of bromine chemistry in controlling microbial growth in water systems', *International Biodeterioration and Biodegradation*, 33(3), pp. 245–253. Vol:

33.

Fernandez-Torres, M. J., Fitzgerald, A. M., Paterson, W. R. and Wilson, D. I. (2001) ‘A theoretical study of freezing fouling: Limiting behaviour based on a heat and mass transfer analysis’, *Chemical Engineering and Processing*, 40(4), pp. 335–344. Vol: 40.

French Creek Software, I. (2017) ‘French Creek Software’.

Gnielinski, V. (2009) ‘Heat Transfer Coefficients for Turbulent Flow in Concentric Annular Ducts’, *Heat Transfer Engineering*, 30(6), pp. 431–436. Vol: 30.

Goodenough, J. L. (2017) *The effects of paint-based protective films on the actual temporal water-side performance characteristics of steam surface condenser tubes*. Stellenbosch. Available at: http://scholar.sun.ac.za/handle/10019.1/101009.

Goodenough, J. L. and Reuter, H. C. R. (2014) ‘Performance characteristics of artificial coatings applied to steam surface condensers’, *International Journal of Thermal Sciences*. Elsevier Masson SAS, 85, pp. 123–137. Vol: 85.

Green, W. G. and Perry, H. R. (2013) *Perry’s Chemical Engineers’ Handbook*, *Journal of Chemical Information and Modeling*. Vol: 53.

Holman, J. P. (2012) *Experimental Methods for Engineers*. 8th edn, *Notes and Queries*. 8th edn. New York: Mc Graw Hill.

Horn, B. and Richards, G. (2010) ‘Use Of Degradable, Non-Oxidizing Biocides and Biodispersants for the Maintenance of Capacity in Nutrient Injection Wells’, *Proceedings of the Annual International Conference on Soils, Sediments, Water and Energy*, 13(2008).

Ibrahim, S. M. A. and Attia, S. I. (2015) ‘The influence of condenser cooling seawater fouling on the thermal performance of a nuclear power plant’, *Annals of Nuclear Energy*. Elsevier Ltd, 76, pp. 421–430. Vol: 76.

Jamal, M., Tasneem, U., Hussain, T. and Andleeb, and S. (2015) ‘Bacterial Biofilm: Its Composition, Formation and Role in Human Infections’, *Research & Reviews: Journal of Microbiology and Biotechnology*, 4(3), pp. 1–14. Available at: http://www.rroij.com/open-access/bacterial-biofilm-its-composition-formation-and-role-in-human-infections.php?aid=61426.

Kotzé, P. (2015) ‘How much water will we need to keep the lights on?’, *Water and energy*, 14(3), pp. 22–25. Available at: https://journals.co.za/docserver/fulltext/waterb/14/3/waterb_v14_n3_a9.pdf?expires=1550480542&id=id&accname=guest&checksum=B894904BB70B23555BD563F7C100D125.

Laycock, N. J., Newman, R. C. and Newman, R. C. (1997) ‘The initiation of crevice corrosion steels in stainless’, *Corrosion Science*, 39(1), pp. 1791–1809. Vol: 39.

Lenntech (2019) *Turbidity*. Available at: https://www.lenntech.com/turbidity.htm#:~:targetText=Turbidity is a measure of,of the quality of water.

Li, J., Zhai, Z., Wang, J. and Huang, S. (2016) ‘On-line fouling monitoring model of condenser in coal-fired power plants’, *Applied Engineering*. Elsevier Ltd, 104, pp. 628–635. Vol: 104.

Liengen, T., Féron, R., Basséguy, R., Beech, I. B. (2018) *Understanding Biocorrosion Fundamentals and Applications*. 1st edn. Cambridge, United Kingdom: Elsevier Science& Technology.

Love, N. D., Szybist, J. P. and Sluder, C. S. (2012) ‘Effect of heat exchanger material and fouling on thermoelectric exhaust heat recovery’, *Applied Energy*. Elsevier Ltd, 89(1), pp. 322–328. Vol: 89.

Macdonald, R., Santa, M. and Bro, V. S. (2001) ‘The response of a bacterial biofilm community in a simulated industrial cooling water system to treatment with an anionic dispersant’, *Journal of Applied Microbiology*, 89(2), pp. 225–235. Vol: 89.

Mardones, L. E., Legnoverde, M. S., Pereyra, A. M. and Basaldella, E. I. (2018) ‘Long-lasting isothiazolinone-based biocide obtained by encapsulation in micron-sized mesoporous matrices’, *Progress in Organic Coatings*. Elsevier, 119(July 2017), pp. 155–163. Vol: 119.

Moffat, R. J. (1988) ‘Describing the Uncertainties in Experimental Results’, *Experimental Thermal and Fluid Science*, 1, pp. 3–17.

Mohseni, A. and Berijani, S. (2018) ‘Importance of water & wastewater reuse in different industries as an effective solution in dehydration crisis’, pp. 1–10. Available at:

http://absunpalayesh.com/wp-content/uploads/Manuscript-1.pdf.

Morkus, P., Zolfaghari, M., Parrello, D., Csordas, M., Malikov, M., Rose, J., Choi, K. B., Fillipe, C. D. . and Latulippe, D. R. (2018) 'Optimization of microorganism preservation conditions for the development of an acute toxicity bioassay for biocides', *Chemosphere*. Elsevier Ltd, 221, pp. 45–54. Vol: 221.

Mostafa, M. A. (2011) *Heat Transfer: Theoretical Analysis, Experimental Investigations and Industrial Systems*. 1st edn. CC BY-NC-SA 3.0.

Mueller, S. A., Gaines, W. A., Kendall, A. M., Anderson, J. E. and Kim, B. R. (2002) 'Literature review—efficacy of various disinfectants against Legionella in water systems', *Water Research*, 36(18), pp. 4433–4444. Vol: 36.

Murthy, P. S., Venkatesan, R., Nair, K. V. K. and Ravindran, M. (2004) 'Biofilm control for plate heat exchangers using surface seawater from the open ocean for the OTEC power plant', *International Biodeterioration & Biodegradation*, 53, pp. 133–140. Vol: 53.

Murthy, P. S., Venkatesan, R. Ã., Nair, K. V. K., Inbakandan, D., Jahan, S. S., Peter, D. M. and Ravindran, M. (2005) 'Evaluation of sodium hypochlorite for fouling control in plate heat exchangers for seawater application', *International Biodeterioration & Biodegradation*, 55, pp. 161–170. Vol: 55.

Mwaba, M. G., Golriz, M. R. and Gu, J. (2006) 'A semi-empirical correlation for crystallization fouling on heat exchange surfaces', *Applied Thermal Engineering*, 26(4), pp. 440–447. Vol: 26.

Nebot, E., Casanueva, J. F., Casanueva, T. and Sales, D. (2007) 'Model for fouling deposition on power plant steam condensers cooled with seawater: Effect of water velocity and tube material', *International Journal of Heat and Mass Transfer*, 50(17–18), pp. 3351–3358. Vol: 50.

Nimmons, M. J. (1979) *Heat transfer effects in turbulent flow due to biofilm development.* Rice University.

Olariu, R. (2015) *Treatment of cooling tower blowdown water. The effect of biodispersant on the ultrafiltration membrane*. Delft University of Technology.

Pääkkönen, T. M., Riihimäki, M., Simonson, C. J., Muurinen, E. and Keiski, R. L. (2015) 'Modeling CaCO3 crystallization fouling on a heat exchanger surface – Definition of fouling layer properties and model parameters', *International Journal of Heat and Mass Transfer*, 83, pp. 84–98. Vol: 83.

Pattanayak, L., Padhi, B. N. and Kodamasingh, B. (2019) 'Thermal performance assessment of steam surface condenser', *Case Studies in Thermal Engineering*. Elsevier Ltd, 14(September 2018), p. 100484. Vol: 14.

Petukhov, B. S. (1970) 'Heat Transfer and Friction in Turbulent Pipe Flow with Variable Physical Properties', *Advances in Heat Transfer*, 6, pp. 503–564. Vol: 6.

Di Pippo, F., de Tora, F., Di Gregorio, L., Buccolini, M., Capocecera, R., Rossetti, S. and Tandoi, V. (2017) 'Green bio-dispersant removal efficacy estimation for controlling biofilms in cooling towers', *Annals of Microbiology*. Annals of Microbiology, 67(11), pp. 779–784. Vol: 67.

Di Pippo, F., Di Gregorio, L., Congestri, R., Tandoi, V. and Rossetti, S. (2018) 'Biofilm growth and control in cooling water industrial systems', *FEMS Microbiology Ecology*. Oxford University Press, 94(5), pp. 1–13. Vol: 94.

Prakash, B., Veeregowda, B. M. and Krishnappa, G. (2003) 'Biofilms : A survival strategy of bacteria', *Current Science*, 85(9), pp. 1299–1307.

Putman, R. E. and Harpster, J. W. (2000) 'The economic effects of condenser backpressure on heat rate, condensate subcooling and feedwater dissolved oxygen', *CONCO*. Available at: http://remote1.concosystems.net/sites/default/files/userfiles/files/techical-papers/economic-effects-condenser-backpressure-heat-rate-condensate-subcooling-and-feedwater-dissolved-oxyg.pdf.

Rahmani, K. (2017) 'Reducing water consumption by increasing the cycles of concentration and Considerations of corrosion and scaling in a cooling system', *Applied Thermal Engineering*. Elsevier Ltd, 114, pp. 849–856. Vol: 114.

Rahmani, K., Jadidian, R. and Haghtalab, S. (2016) 'Evaluation of inhibitors and biocides on the corrosion, scaling and biofouling control of carbon steel and copper–nickel alloys in a power plant cooling water system', *Desalination*. Elsevier B.V., 393, pp. 174–185. Vol: 393.

Reuter, H. C. R., Owen, M. and Goodenough, J. L. (2017) ‘Experimental evaluation of the temporal effects of paint-based protective films on composite fouling inside admiralty brass and titanium steam surface condenser tubes’, *Applied Thermal Engineering*. Elsevier Ltd, 126, pp. 848–857. Vol: 126.

Shandong Taihe Water Treatment Technologies Co (2013) ‘HPMA, Polymaleic Acid, PMA, HPMA (Solvent Based), Polymaleic Acid, Belclene 200 - Shandong Taihe Water Treatment’. Available at: http://www.thwater.net/03-PMA.htm.

Shen, C., Cirone, C., Jacobi, A. M. and Wang, X. (2015) ‘Fouling of enhanced tubes for condensers used in cooling tower systems : A literature review’, *Applied Thermal Engineering*. Elsevier Ltd, 79, pp. 74–87. Vol: 79.

Smith, J.M , Van Ness, H.C, Abbott, M. M. (2015) *Introduction to Chemical Engineering Thermodynamics*. 7th edn. McGraw Hill Higher Education.

Somerscales, E. F. C. (1997) ‘Fundamentals of corrosion fouling’, *Experimental Thermal and Fluid Science*, 14(4), pp. 335–355. Vol: 14.

SUEZ (2018) *Cooling water systems chemicals*. Available at: https://www.suezwater.co.uk/cooling-water-systems-chemicals/ (Accessed: 11 October 2018).

Tuo, H. and Hrnjak, P. (2014) ‘Effect of venting the periodic reverse vapor flow on the performance of a microchannel evaporator in air-conditioning systems’, *International Journal of Heat and Mass Transfer*, 69, pp. 66–76. Vol: 69.

Urbaniec, K., Markowski, M. and Trafczynski, M. (2011) ‘Identification of the Influence of Fouling on the Heat Recovery in a Heat Exchanger Network’, *Applied Energy*, 102, p. 2011. Vol: 102.

Vedran, M.-V., Branimir, P. and Vedran, M. (2018) ‘Numerical model for on-condition monitoring of condenser in coal-fired power plants’, *International Journal of Heat and Mass Transfer*, 117, pp. 912–923. Vol: 117.

Venkatnarayanan, S., Sriyutha Murthy, P., Kirubagaran, R. and Venugopalan, V. P. (2017) ‘Chlorine dioxide as an alternative antifouling biocide for cooling water systems: Toxicity to

larval barnacle Amphibalanus reticulatus (Utinomi)', *Marine Pollution Bulletin*. Elsevier Ltd, 124(2), pp. 803–810. Vol: 124.

Walker, M. E., Safari, I., Theregowda, R. B., Hsieh, M., Abbasian, J., Arastoopour, H., Dzombak, D. A. and Miller, D. C. (2012) 'Economic impact of condenser fouling in existing thermoelectric power plants', *Energy*. Elsevier, 44(1), pp. 429–437. Vol: 44.

Watkinson, A. P. and Wilson, D. I. (1997) 'Chemical reaction fouling: A review', *Experimental Thermal and Fluid Science*, 14(4), pp. 361–374. Vol: 14.

Yamamoto, K. and Hosoya, K. (1995) 'Corrosivity of Br- and C1- on duplex stainless steel', *materials Science and Engineering*, 198(1–2), pp. 239–243. Vol: 198.

Zaslavschi, I., Shemer, H., Hasson, D. and Semiat, R. (2013) 'Rotating cylinder technique for assessing the effectiveness of anti-scalants', *Water Research*. Elsevier Ltd, 47(11), pp. 3716–3722. Vol: 47.

Appendix A

ANSYS® R18.2 was used to simulate how mixing takes place inside a condenser tube once dosed with a bio-dispersant using a peristaltic dosing pump.

The entrance section where the cooling water is distributed through the manifold is simulated as per geometry in Figure 38 and Figure 39. The length between the manifold and the T-piece is 200 mm and a 500 mm entrance section into the tube as selected. The internal diameter of the PVC pipes as shown in Figure 38 is 21.01 mm. The inside diameter of the chemical injection point indicated in Figure 39 is 5 mm.

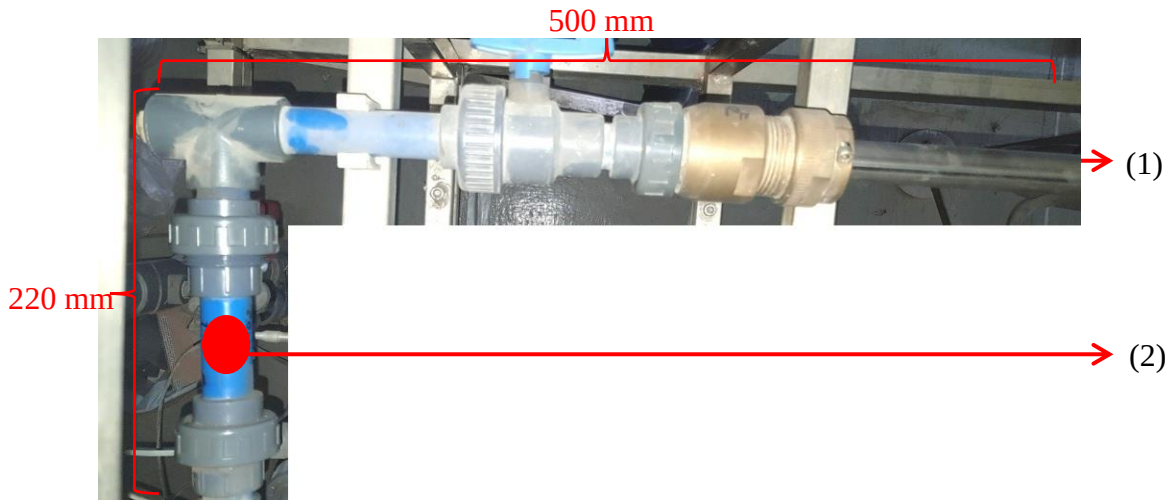


Figure 38: Cooling water tube section modelled – (1) Section where CFD was performed, (2) Proposed chemical injection point

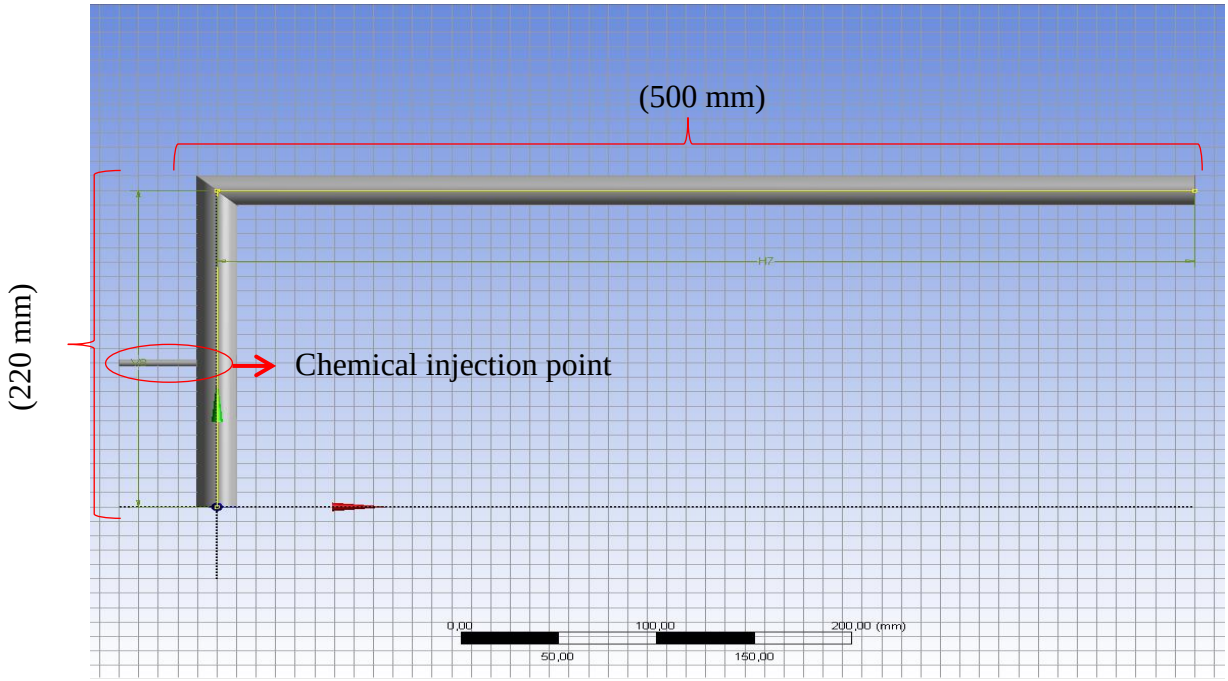


Figure 39: CFD geometry as per Figure 10.

The geometry in Figure 39 was meshed using a mesh size of 0.002 mm and a quadrilateral mesh type was used. The mesh was refined using a refinement setting of one. The meshed geometry is shown in Figure 40.

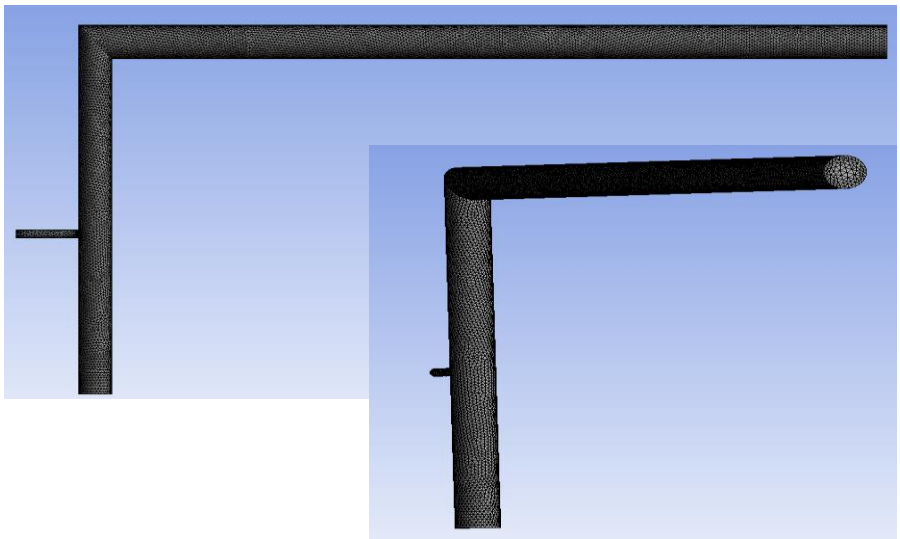


Figure 40: Meshed geometry as in Figure 39.

The data inputs were as follow:

- The energy equation was used to perform an energy balance.
- A realizable k-epsilon viscous model was chosen with standard wall functions.
- The species model was selected. The density model was chosen as the volume-weighted-mixing-law. The specific heat and thermal conductivity of the bio-dispersant were chosen to be the same as water. This assumption is valid because of the extremely low bio-dispersant concentrations inside the water. The unity Lewis number approximation was used to calculate the mass diffusivity. This mass diffusivity approximation using the unity Lewis number method is the only approximation that lets the model converge to an error below 5 %.
- Two fluids were selected, water and the bio-dispersant. The build in default properties for water was used. The viscosity, density and thermal conductivity for the bio-dispersant are 0.011 kg/m·s, 1030 kg/m³ and 0.6 W/m·K respectively.
- The bio-dispersant entered the geometry at 6.238 e-06 kg/s at a temperature of 300 K (the average temperature of the chemicals inside the test apparatus). The bio-dispersant flowrate was varied during the analysis. No cooling water enters the geometry at the chemical inlet point.
- The cooling water enters the geometry at 1.8 m/s and at 320 K.
- The solution methods were as follow:
    - Pressure-velocity coupling: SIMPLE
    - Spartial Discretization
        - Gradient: Least squares cell based
        - Pressure: Standard
        - Momentum: Second order upwind
        - Turbulent kinetic energy: Second order upwind
        - Turbulent dissipation rate: Second order upwind
        - Species: Second order upwind
        - Energy: Second order upwind

The model was solved and the results are shown in Figure 41, Figure 42 and Figure 43.

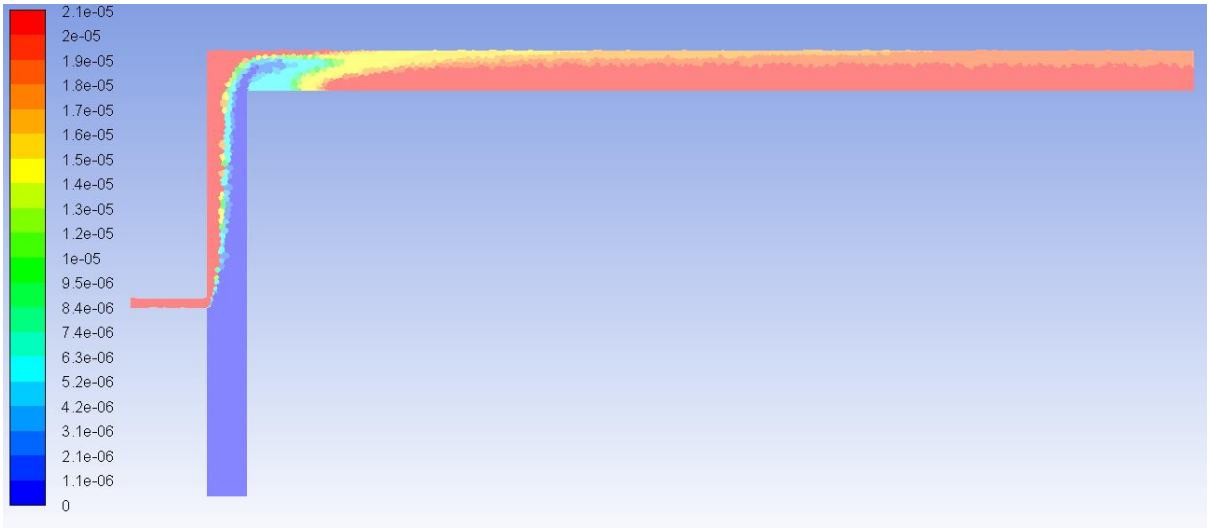


Figure 41: CFD results for a bio-dispersant flowrate of 1.24761e-05 kg/s (Final mixing concentration of 20 ppm). The scale indicates the bio-dispersant concentration in mg bio-dispersant per 1 L water.

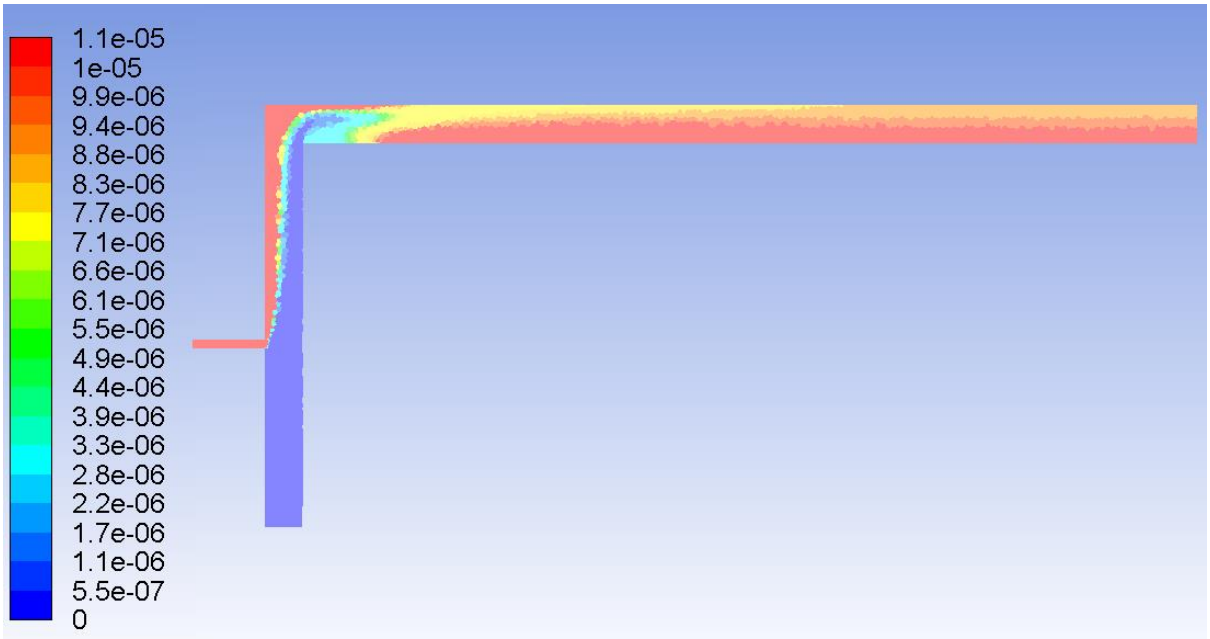


Figure 42: CFD results for a bio-dispersant flowrate of 6.238056e-06 kg/s (Final mixing concentration of 10 ppm). The scale indicates the bio-dispersant concentration in mg bio-dispersant per 1 L water.

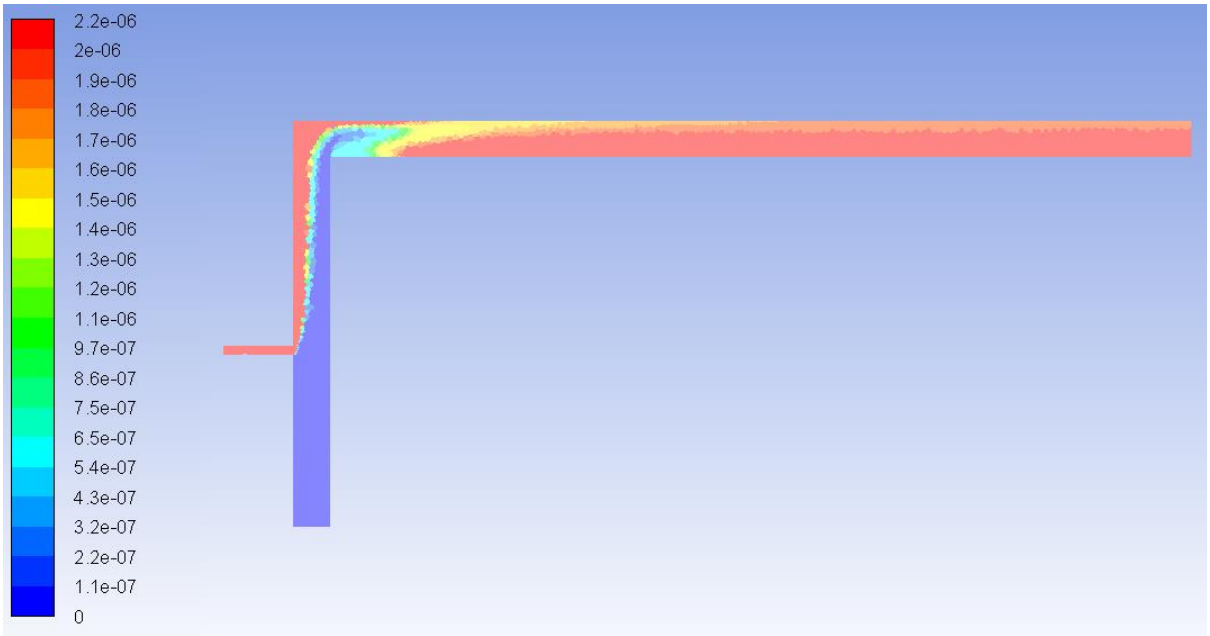


Figure 43: CFD results for a bio-dispersant flowrate of 1.24761e-06 kg/s (Final mixing concentration of 2 ppm). The scale indicates the bio-dispersant concentration in mg bio-dispersant per 1 L water.

It can be seen from Figure 41, Figure 42 and Figure 43 that the bio-dispersant is mixed well within the first 500 mm of the entrance length of the test apparatus which is before it reaches the point where heat transfer occurs in the tube section. It is therefore concluded that the chemical injection point can be installed to the test apparatus as per geometry in Figure 39. The installed injection point is shown in Figure 14.

Appendix B

B.1 Fluid properties

The density of water (kg/m³) as a function of temperature (°C) is expressed as (Green and Perry, 2013, 2-103):

$$\rho_W = \left(17.863 + 58.606 \cdot \left(1 - \frac{T + 273.15}{647.096}\right)^{0.35} - 95.396 \cdot \left(1 - \frac{T + 273.15}{647.096}\right)^{\frac{2}{3}} + 213.89 \cdot \left(1 - \frac{T + 273.15}{647.096}\right) - 141.26 \cdot \left(1 - \frac{T + 273.15}{647.096}\right)^{\frac{4}{3}}\right) \cdot 18.015 \quad (36)$$

The viscosity of water (kg/m·s) as a function of temperature (°C) is expressed as (Green and Perry, 2013, 2-432):

$$\mu_W = e^{\left(-52.843 + \left(\frac{3703.6}{T + 273.15}\right)\right)} + 5.866 \cdot \log(T + 273.15) + (-5.879E - 29) \cdot (T + 273.15)^{10} \quad (37)$$

The thermal conductivity of water (W/m·K) as a function of temperature (°C) is expressed as (Green and Perry, 2013, 2-315):

$$k_W = -432 + 0.0057255 \cdot (T + 273.15) - 0.000008078 \cdot (T + 273.15)^3 \quad (38)$$

The thermal heat capacity of water (J/kg·K) as a function of temperature (°C) is expressed as (Green and Perry, 2013, 2-153)

$$Cp_W = (276370 - 2090.1 \cdot (T + 273.15) + 8.125 \cdot (T + 273.15)^2 - 0.014116 \cdot (T + 273.15)^3 + 0.0000093701 \cdot (T + 273.15)^4)/18.01 \quad (39)$$

Appendix C

C.1 Sample calculations

C.1.1 Measured variables:

Table 5: Measured variables of tube 6 during test 1 at day 8. These values are used in the sample calculations.

Cooling water inlet temperature	$T_{CW_{in}}$	=	40.50	°C
Cooling water outlet temperature	$T_{CW_{out}}$	=	41.70	°C
Tube hot water inlet temperature	$T_{ANN_{in}}$	=	46.64	°C
Tube hot water outlet temperature	$T_{ANN_{out}}$	=	45.45	°C
Tube cooling water flow rate	F_{CW}	=	0.54	L/s
Flow through annulus	F_{ANN}	=	0.53	L/s
Manometric height difference	ΔH	=	340	mm
Experimentally determine coefficient	A_{Nu}	=	0.888	(1)
Experimentally determine coefficient	B_{Nu}	=	0.455	(1)
Tube inside diameter	D_i	=	0.023	m
Tube outside diameter	D_O	=	0.024	m
Annulus external diameter	D_{ANN}	=	0.0353	m
Length between pressure tapings	L_p	=	3.5	m
Effective heat transfer length	L_{eff}	=	3.199	m
Tube thermal conductivity	k_t	=	20	$\frac{W}{m \cdot K}$

C.1.2 Fluid thermodynamic properties

The bulk mean temperature for the cooling water inside the condenser tube is calculated as:

$$T_{CW_m} = \frac{T_{CW_{in}} + T_{CW_{out}}}{2} \quad (40)$$

$$T_{CW_m} = \frac{40.504 + 41.699}{2} = 41.101\ ^\circ\text{C}$$

The density of the cooling water inside the condenser tube is calculated by using Equation (36).

$$\rho_{CW} = 988.34\ \frac{kg}{m^3}$$

The specific heat capacity of the cooling water inside the condenser tube is calculated by using Equation (39).

$$Cp_{W\,CW} = 4177.65\ \frac{J}{kg \cdot K}$$

The thermal conductivity of the cooling water inside the condenser tube is calculated by using Equation (38).

$$k_{CW} = 0.521\ \frac{W}{m \cdot K}$$

The viscosity of the cooling water inside the condenser tube is calculated by using Equation (37).

$$\mu_{CW} = 0.000657\ \frac{kg}{s \cdot m}$$

The Prandtl number for the cooling water inside the condenser tube is calculated as (Cengel and Ghajar, 2015):

$$Pr_{CW} = \frac{\mu_{CW} \cdot Cp_{CW}}{k_{\mathrm{CW}}}$$

$$Pr_{CW} = \frac{0.000657 \cdot 4177.65}{0.521} = 5.269$$

The thermodynamic properties for the water flowing through the annulus are similarly calculated as:

T_{ANN_m} = 46.05 °C

ρ_{ANN} = 986.12 $\frac{kg}{m^3}$

$Cp_{W_{ANN}}$ = 4177.48 $\frac{J}{kg \cdot K}$

k_{ANN} = 0.5119 $\frac{W}{m \cdot K}$

μ_{ANN} = 0.0006 $\frac{kg}{s \cdot m}$

Pr_{ANN} = 4.9 (-)

C.1.3 Flow rates

The cooling water mass flow rate is calculated as:

$$m_{CW} = \frac{F_{CW} \cdot \rho_{CW}}{1000} \quad (41)$$

$$m_{CW} = \frac{0.54 \cdot 988.34}{1000} = 0.534 \ \frac{kg}{s}$$

The cross sectional area of the inside of the condenser tube is calculated as:

$$A_i = \pi \cdot \left(\frac{D_i}{2}\right)^2 \tag{42}$$

$$A_i = \pi \cdot \left(\frac{0.023}{2}\right)^2 = 0.000415\ m^2$$

The cooling water linear velocity inside the condenser tube is calculated as:

$$u_{CW} = \frac{F_{CW}}{A_i \cdot 1000} \tag{43}$$

$$u_{CW} = \frac{0.54}{0.000415 \cdot 1000} = 1.3\ \frac{m}{s}$$

The mass flow rate of the water in the annulus section is calculated as:

$$m_{ANN} = \frac{F_{ANN} \cdot \rho_{ANN}}{1000} \tag{44}$$

$$m_{ANN} = \frac{0.532 \cdot 986.12}{1000} = 0.525\ \frac{kg}{s}$$

The cross sectional area of the inside of the annulus tube is calculated as:

$$A_{ANN} = \pi \cdot \left(\left(\frac{D_{ANN}}{2}\right)^2 - \left(\frac{D_O}{2}\right)^2\right) \tag{45}$$

$$A_{ANN} = \pi \cdot \left(\left(\frac{0.0353}{2}\right)^2 - \left(\frac{0.024}{2}\right)^2\right) = 0.000526\ m^2$$

The linear velocity of the water in the annulus section is calculated as:

$$u_{ANN} = \frac{F_{ANN}}{A_{ANN} \cdot 1000} \tag{46}$$

$$u_{ANN} = \frac{0.532}{0.000526 \cdot 1000} = 1.011\ \frac{m}{s}$$

C.1.4 Friction factor and Reynolds numbers

The Reynolds number for the cooling water is calculated as (Cengel and Ghajar, 2015):

$$Re_{CW} = \frac{D_i \cdot u_{CW} \cdot \rho_{CW}}{\mu_{CW}} \quad (9)$$

$$Re_{CW} = \frac{0.023 \cdot 1.3 \cdot 986.12}{0.000657} = 44959$$

The friction factor inside the condenser tube is calculated by using Equation (6):

$$f_{CW} = \frac{\rho_{CW} \cdot g \cdot \left(\frac{\Delta H}{1000}\right)}{\frac{L_p \cdot \rho_{CW} \cdot {u_{CW}}^2}{2 \cdot D_i}} \quad (6)$$

$$f_{CW} = \frac{988.34 \cdot 9.807 \cdot \left(\frac{340.5}{1000}\right)}{\frac{3.5 \cdot 988.34 \cdot 1.3^2}{2 \cdot 0.023}} = 0.0259$$

The Reynolds number for the water flowing through the annulus section is calculated (Cengel and Ghajar, 2015):

$$Re_{ANN} = \frac{(D_{ANN} - D_O) \cdot u_{ANN} \cdot \rho_{ANN}}{\mu_{ANN}} \quad (10)$$

$$Re_{ANN} = \frac{(0.0353 - 0.024) \cdot 1.011 \cdot 986.12}{0.0006} = 18773$$

C.1.5 Nusselt numbers and convection heat transfer coefficients

The Nusselt number for the cooling water is calculated by using Equation (7).

$3000 < Re < 10^6$:

$$Nu_{CW} = \frac{\left(\frac{f_{CW}}{8}\right) \cdot (Re_{CW} - 1000) \cdot Pr_{CW}}{\left(1 + 12.7 \cdot \left(\frac{f_{CW}}{8}\right)^{0.5} \cdot \left(Pr_{CW}{}^{\frac{2}{3}} - 1\right)\right)} \quad (7)$$

$$Nu_{CW} = \frac{\left(\frac{0.0259}{8}\right) \cdot (44959 - 1000) \cdot 5.269}{\left(1 + 12.7 \cdot \left(\frac{0.0259}{8}\right)^{0.5} \cdot \left(5.269^{\frac{2}{3}} - 1\right)\right)} = 304.75$$

The convection heat transfer coefficient for the cooling water is calculated by using Equation (8):

$$h_{CW} = \frac{Nu_{CW} \cdot k_{CW}}{D_i} \quad (8)$$

$$h_{CW} = \frac{304.75 \cdot 0.521}{0.023} = 6904.76 \ \frac{W}{m^2 \cdot K}$$

The convection heat transfer coefficient for the water flowing through the annulus section is calculated as Equation (15) (Goodenough, 2017):

$$h_{ANN} = A_{Nu} \cdot Re_{ANN}{}^{B_{Nu}} \cdot Pr_{ANN}{}^{0.3} \cdot \left(\frac{k_{ANN}}{D_{ANN} - D_O}\right) \quad (15)$$

$$h_{ANN} = 0.888 \cdot 18773^{0.455} \cdot 4.9^{0.3} \cdot \left(\frac{0.509}{0.0353 - 0.024}\right) = 5716.79 \frac{W}{m^2 \cdot K}$$

C.1.6 Thermal resistances

The cooling water thermal resistance is calculated as:

$$R_{CW} = \frac{1}{h_{CW} \cdot A_s} \quad (47)$$

$$R_{CW} = \frac{1}{6904.76 \cdot 0.231} = 6.27 \cdot 10^{-4} \frac{K}{W}$$

Where the total tube inside area available for heat transfer is:

$$A_s = 2 \cdot \pi \cdot \left(\frac{D_i}{2}\right) \cdot L_{eff} \tag{48}$$

$$A_s = 2 \cdot \pi \cdot \left(\frac{0.023}{2}\right) \cdot 3.199 = 0.231\ m^2$$

The thermal resistance for the water flowing through the annulus section is calculated as:

$$R_{ANN} = \frac{1}{h_{ANN} \cdot A_{ANN_S}} \tag{49}$$

$$R_{ANN} = \frac{1}{5716.79 \cdot 0.241} = 7.26 \cdot 10^{-4}\,\frac{K}{W}$$

Where the total annulus area available for heat transfer is:

$$A_{ANN_S} = 2 \cdot \pi \cdot \left(\frac{D_o}{2}\right) \cdot L_{eff} \tag{50}$$

$$A_{ANN_S} = 2 \cdot \pi \cdot \left(\frac{0.024}{2}\right) \cdot 3.199 = 0.241\ m^2$$

The thermal resistance for the tube wall is calculated as:

$$R_{tube} = \frac{ln\left(\frac{D_O}{D_i}\right)}{2 \cdot \pi \cdot k_t \cdot L_{eff}} \tag{51}$$

$$R_{tube} = \frac{ln\left(\frac{0.024}{0.023}\right)}{2 \cdot \pi \cdot 20 \cdot 3.199} = 1.058 \cdot 10^{-4}\,\frac{K}{W}$$

The total thermal resistance minus the fouling resistance is calculated by using Equation (1):

$$\sum R\ -\ R_f = R_{CW} + R_{tube} + R_{ANN}$$

$$\sum R\ -\ R_f = 6.27 \cdot 10^{-4} + 1.058 \cdot 10^{-4} + 7.26 \cdot 10^{-4} = 1.45\ \cdot 10^{-3}\,\frac{K}{W}$$

C.1.7 Heat transfer

The rate of heat transfer inside the condenser tubes is calculated as Equation (18):

$$Q_{CW} = m_{CW} \cdot Cp_{W_{CW}} \cdot \left(T_{CW_{out}} - T_{CW_{in}}\right) \quad (18)$$

$$Q_{CW} = 0.534 \cdot 4177.65 \cdot (41.699 - 40.504) = 2664.43\ W$$

The rate of heat transfer side the annulus section is calculated as Equation (19):

$$Q_{ANN} = m_{ANN} \cdot Cp_{W_{ANN}} \cdot \left(T_{ANN_{in}} - T_{ANN_{out}}\right) \quad (19)$$

$$Q_{ANN} = 0.525 \cdot 4177.48 \cdot (46.642 - 45.452) = 2608.32\ W$$

The energy balance is calculated as Equation (20):

$$EB = \frac{Q_{CW} - Q_{ANN}}{\max(Q_{CW}, Q_{ANN})} \quad (20)$$

$$EB = \frac{2664.43 - 2608.32}{2664.43} \cdot 100 = 2.1\ \%$$

The log mean temperature difference is calculated using Equation (3):

$$\Delta T_{LM} = \frac{\left(T_{ANN_{in}} - T_{CW_{in}}\right) - \left(T_{ANN_{out}} - T_{CW_{out}}\right)}{\ln\left(\frac{T_{ANN_{in}} - T_{CW_{in}}}{T_{ANN_{out}} - T_{CW_{out}}}\right)} \quad (3)$$

$$\Delta T_{LM} = \frac{(46.642 - 40.504) - (45.453 - 41.699)}{\ln\left(\frac{46.642 - 40.504}{45.453 - 41.6991}\right)} = 4.84\ ^{\circ}\mathrm{C}$$

The overall heat transfer coefficient is calculated by using Equation (2):

$$\mathrm{U} = \frac{average(Q_{CW}, Q_{ANN})}{A_{ANN_S} \cdot \Delta\, T_{LM}} \tag{2}$$

$$\mathrm{U} = \frac{2636.37}{0.241 \cdot 4.84} = 2254.34\ \frac{W}{m^2 \cdot K}$$

$$\mathrm{U} \cdot A_{ANN_S} = 543.74 \frac{W}{K}$$

The fouling resistance inside the condenser tube is then calculated by substituting the equations above:

$$R_f = A_{ANN_S} \cdot \left(\frac{1}{\mathrm{U} \cdot A_{ANN_S}} - (\sum R\ -\ R_f) \right) \tag{52}$$

$$R_f = 0.241 \cdot \left(\frac{1}{543.74} - (1.457\ \cdot 10^{-3}) \right) = 9.2\ \cdot 10^{-5} \frac{m^2 \cdot K}{W}$$

The fouling resistance inside the condenser tube can also be evaluated by comparing the overall heat transfer to the overall heat transfer at the start of the test. The overall heat transfer coefficient at the beginning at the test was $2790.1\ \frac{W}{m^2 \cdot K}$.

$$R_f = \frac{1}{\mathrm{U}_t} - \frac{1}{\mathrm{U}_{t_0}} \tag{16}$$

$$R_f = \frac{1}{2254.34} - \frac{1}{2790.1} = 8.517\ \cdot 10^{-5} \frac{m^2 \cdot K}{W}$$

This leads to a 7.4 % error.

The cleanliness factor is calculated as:

$$CF = \frac{\mathrm{U}_t}{\mathrm{U}_{t_0}} \cdot 100 \tag{17}$$

$$CF = \frac{2254.34}{2790.1} \cdot 100 = 80.8\ \%$$

Appendix D

Appendix D shows which individual tube of each test can be compared to each other before the increase in dosing concentration as well as after the increase in dosing concentration.

D.1 Before increase in dosing concentration

The difference between the maximum and minimum dosing concentration, including the uncertainty parameters, into each of the tubes indicated in Figure 44 is 2.31 ppm.

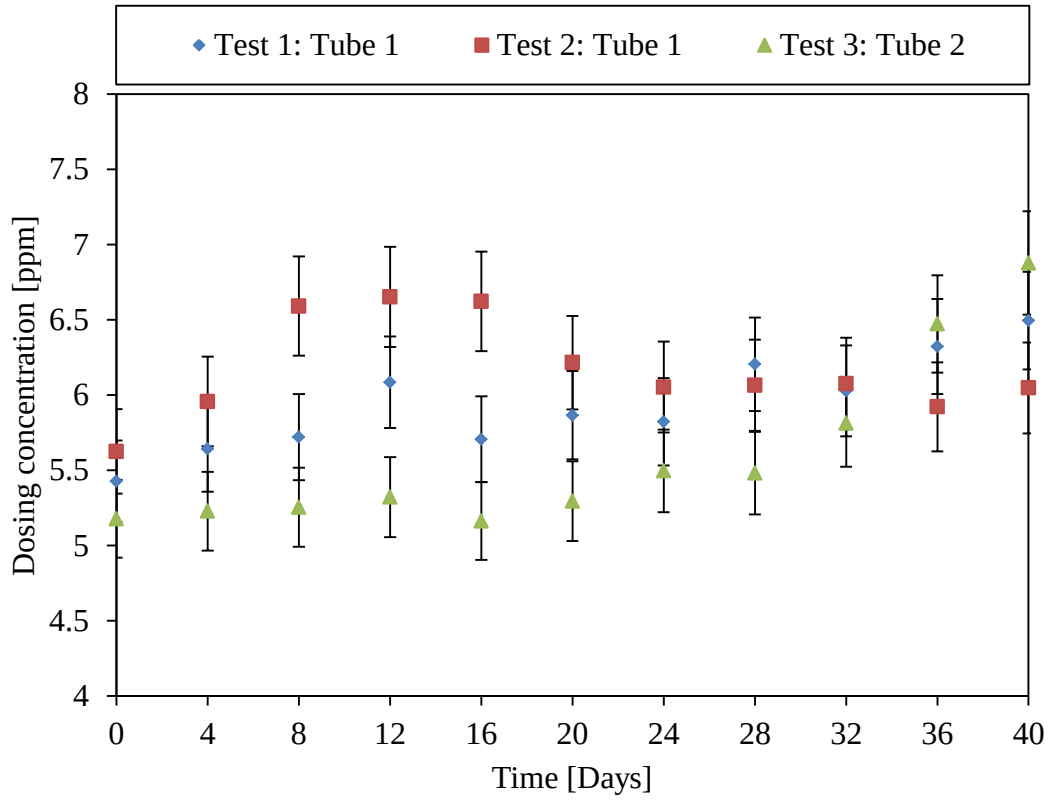


Figure 44: Bio-dispersant dosing concentration: Test 1: Tube 1 (5.9 ml/h), Test 2: Tube 1 (6.2 ml/h) and Test 3: Tube 2 (5.6 ml/h).

The difference between the maximum and minimum dosing concentration, including the uncertainty parameters, into each of the tubes indicated in Figure 45 is 1.98 ppm.

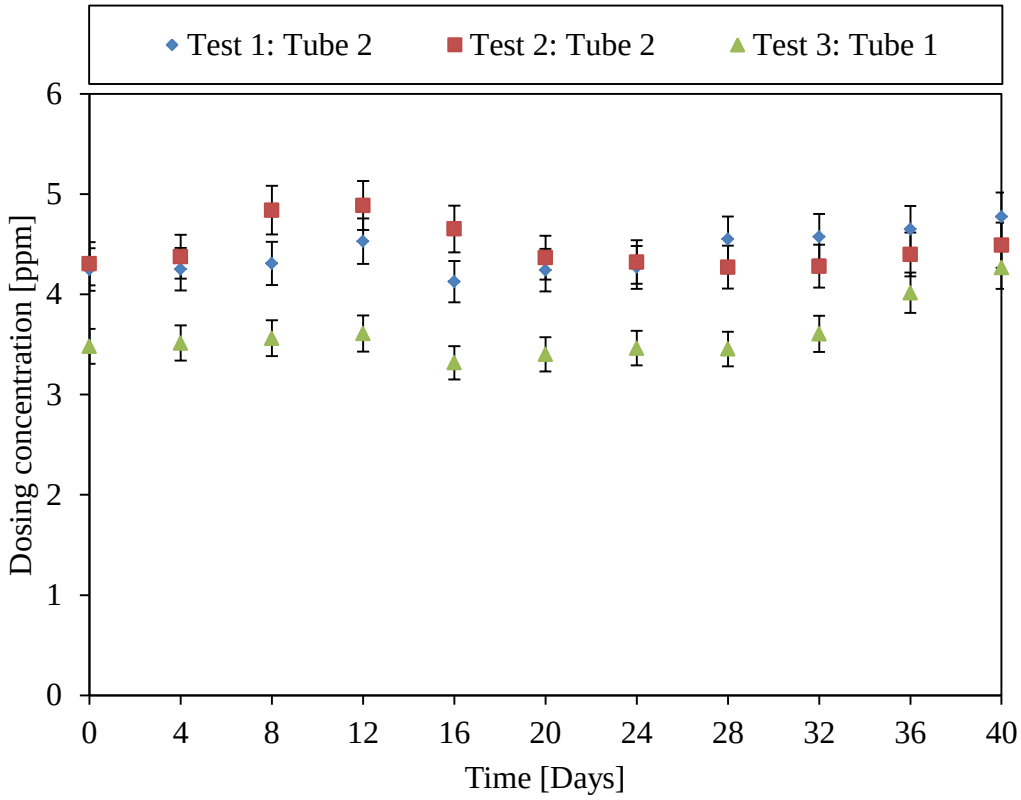


Figure 45: Bio-dispersant dosing concentration: Test 1: Tube 2 (4.4 ml/h), Test 2: Tube 2 (4.5 ml/h) and Test 3: Tube 1 (3.6 ml/h).

The difference between the maximum and minimum dosing concentration, including the uncertainty parameters, into each of the tubes indicated in Figure 46 is 1.82 ppm.

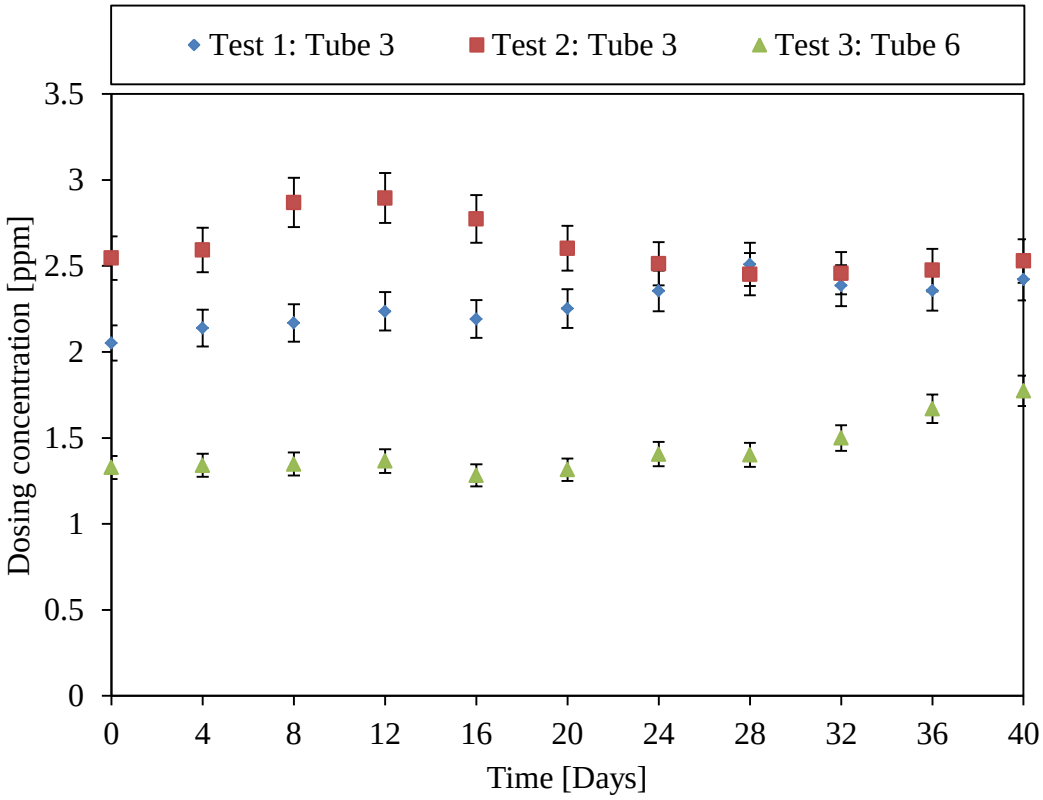


Figure 46: Bio-dispersant dosing concentration: Test 1: Tube 3 (2.3 ml/h), Test 2: Tube 3 (2.6 ml/h) and Test 3: Tube 6 (1.4 ml/h).

The difference between the maximum and minimum dosing concentration, including the uncertainty parameters, into each of the tubes indicated in Figure 47 is 9.58 ppm. The difference is very high. It is therefore recommended that only Test 1: Tube 6 and Test 2: Tube 6 are compared with each other (difference between the maximum and minimum dosing concentration: 1.99 ppm.

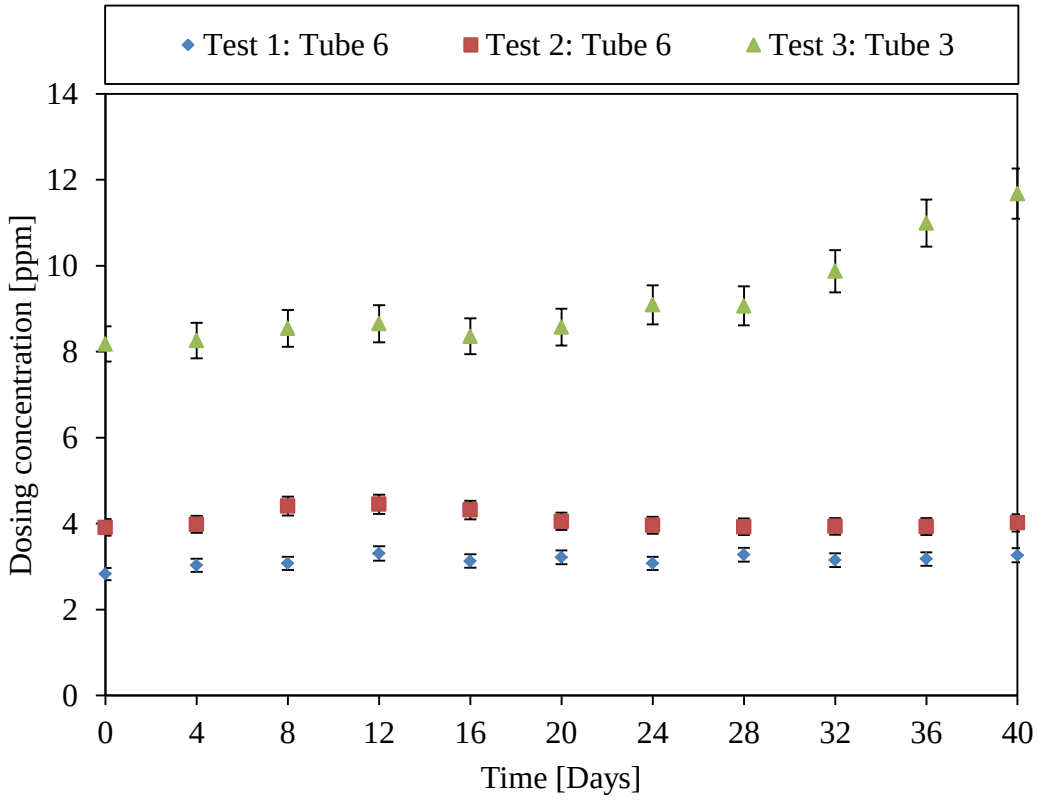


Figure 47: Bio-dispersant dosing concentration: Test 1: Tube 6 (3.1 ml/h), Test 2: Tube 6 (4.1 ml/h) and Test 3: Tube 3 (9.2 ml/h).

D.2 After increase in dosing concentration

The difference between the maximum and minimum dosing concentration after the initial increase in concentration, including the uncertainty parameters, into each of the tubes indicated in Figure 48 is 19.5 ppm. The 19.5 ppm is high and it is therefore not recommended to compare the results of these individual tubes to each other but to rather compare the results of the individual tests to each other.

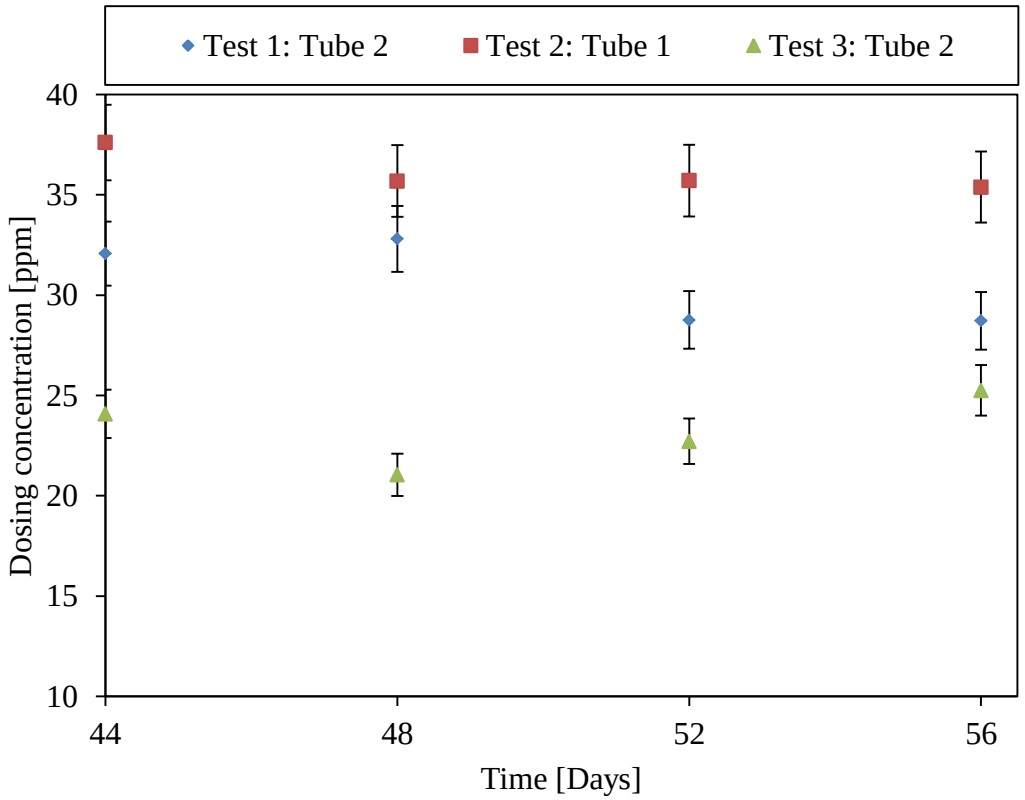


Figure 48: Bio-dispersant dosing concentration: Test 1: Tube 2 (30.4 ml/h), Test 2: Tube 1 (36 ml/h) and Test 3: Tube 2 (24.5 ml/h).

The difference between the maximum and minimum dosing concentration after the initial increase in concentration, including the uncertainty parameters, into each of the tubes indicated in Figure 49 is 14.78 ppm. The 14.78 ppm is high and it is therefore not recommended to compare the results of these individual tubes to each other but to rather compare the results of the individual tests to each other.

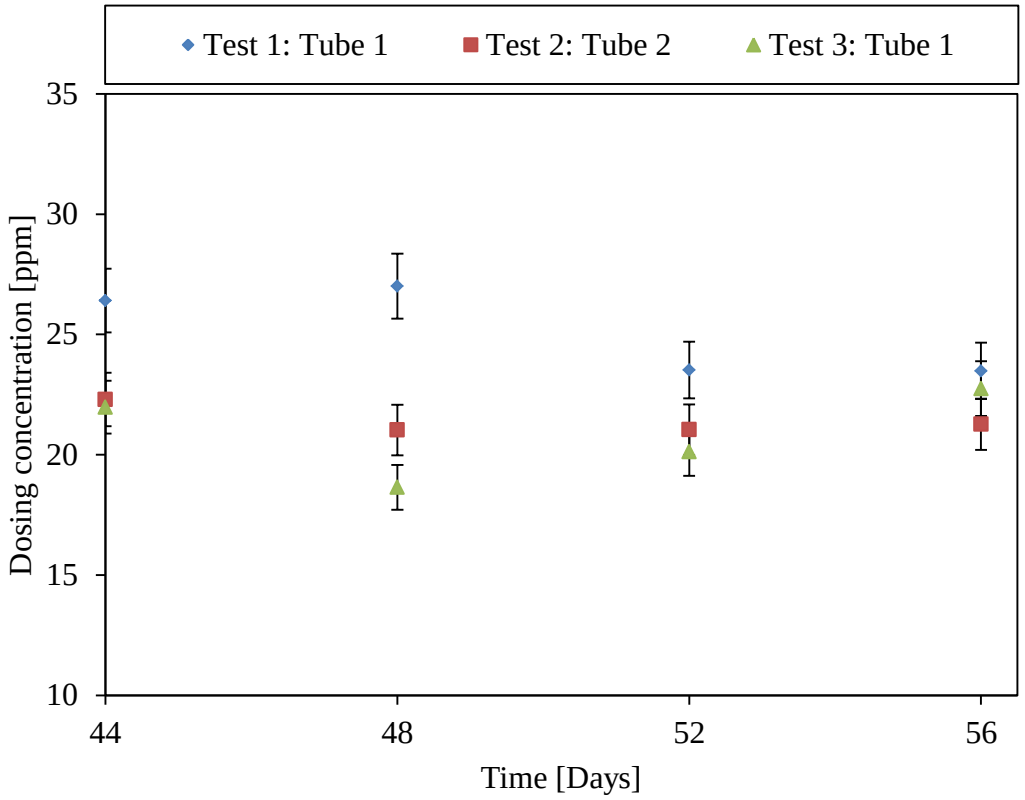


Figure 49: Bio-dispersant dosing concentration: Test 1: Tube 1 (24.9 ml/h), Test 2: Tube 2 (21.3 ml/h) and Test 3: Tube 1 (22 ml/h).

The difference between the maximum and minimum dosing concentration after the initial increase in concentration, including the uncertainty parameters, into each of the tubes indicated in Figure 49 is 10.35 ppm. The 10.35 ppm is high and it is therefore not recommended to compare the results of these individual tubes to each other but to rather compare the results of the individual tests to each other.

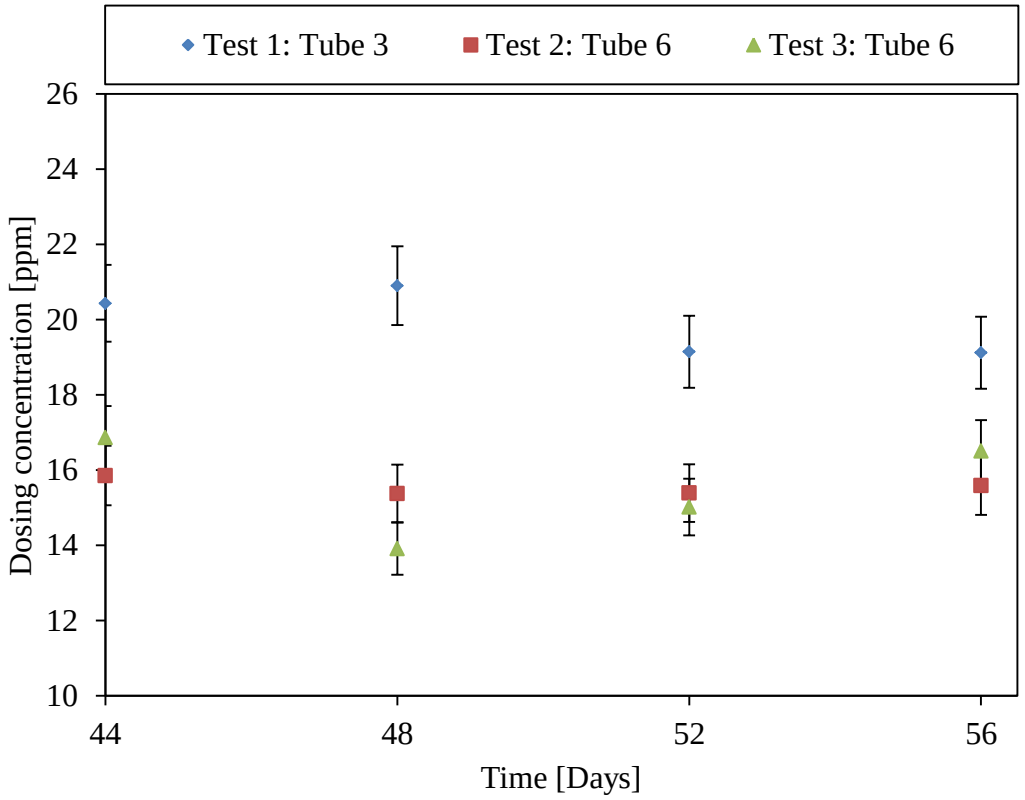


Figure 50: Bio-dispersant dosing concentration: Test 1: Tube 3 (19.9 ml/h), Test 2: Tube 6 (15.5 ml/h) and Test 3: Tube 6 (16.3 ml/h).

The difference between the maximum and minimum dosing concentration after the initial increase in concentration, including the uncertainty parameters, into each of the tubes indicated in Figure 51 is 37.68 ppm. The 37.68 ppm is high and it is therefore not recommended to compare the results of these individual tubes to each other but to rather compare the results of the individual tests to each other. Test 1: Tube 6 and Test 2: Tube 3 can however be compared to each other with a difference between the maximum and minimum dosing concentrations of 3.17 ppm.

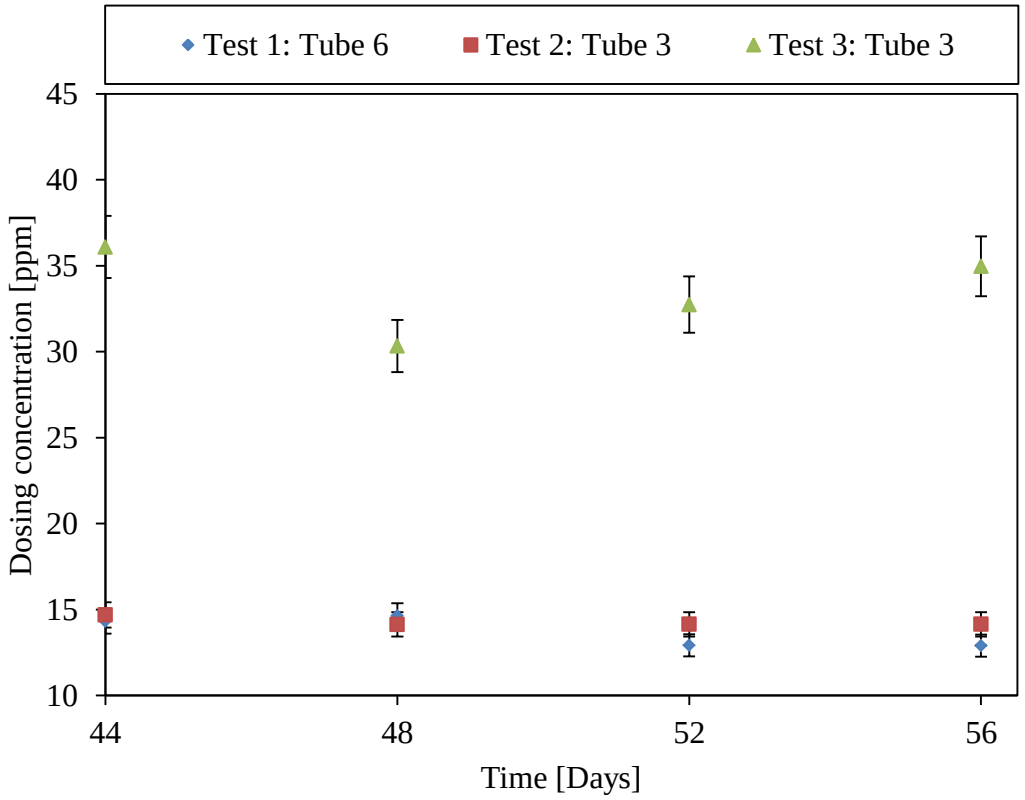


Figure 51: Bio-dispersant dosing concentration: Test 1: Tube 6 (13.6 ml/h), Test 2: Tube 3 (14.2 ml/h) and Test 3: Tube 3 (34.8 ml/h).

Appendix E

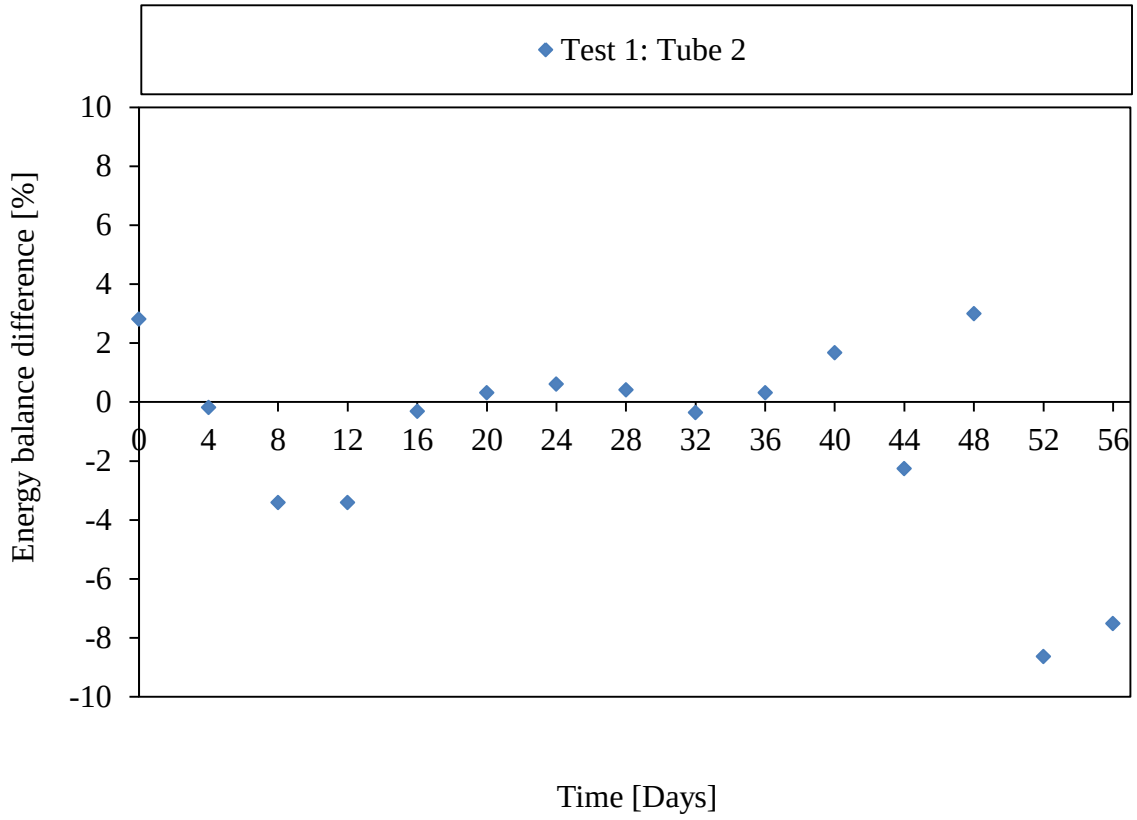


Figure 50: Difference in energy balance Equation (21) of Test 1: Tube 2

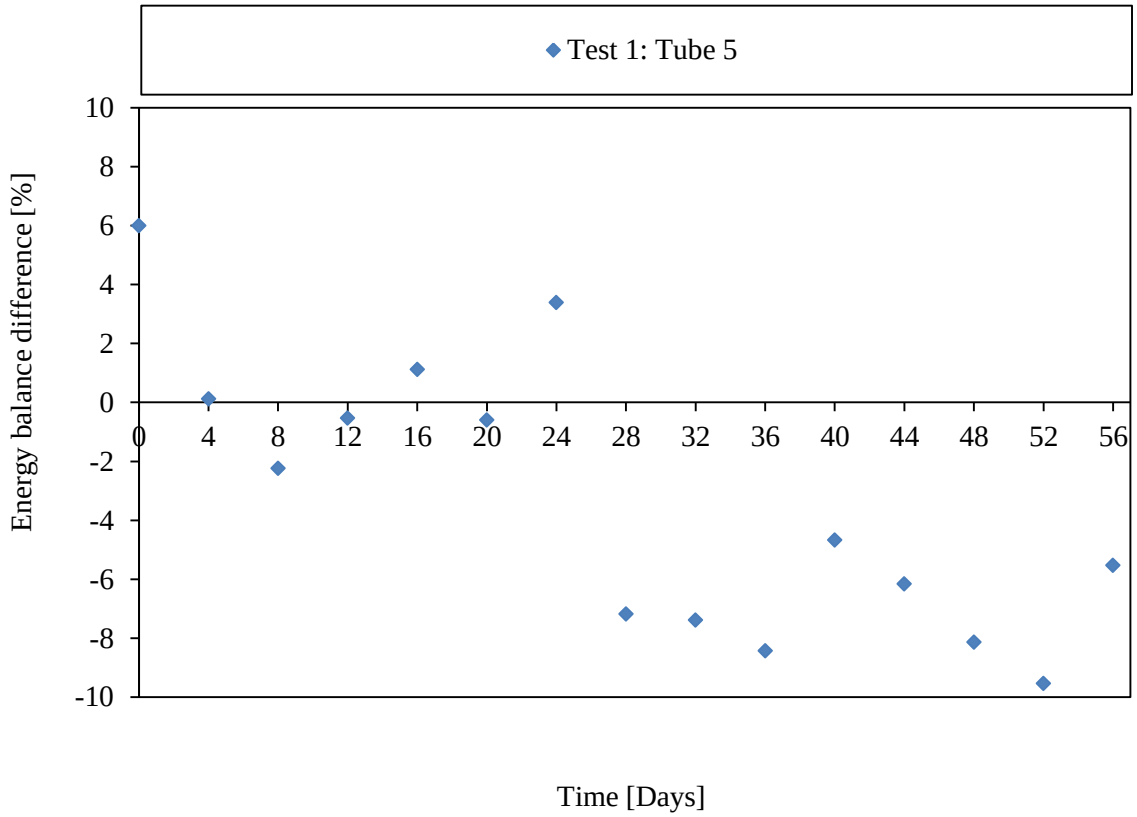


Figure 50: Difference in energy balance Equation (21) of Test 1: Tube 5

Appendix F

F.1 Main turbine condenser sample calculations

Table 6: Inputs used for the main turbine condenser sample calculations

Cooling water inlet temperature	$T_{CW_{in}}$	=	30	°C
Energy transferred from steam to cooling water	E_{Reg}	=	624.07	MW
Fouling resistance inside condenser tube as per data (reference to tube outside area)	R_{f_D}		4.96E-6	$\frac{m^2 \cdot K}{W}$
Tube outside diameter	D_O	=	0.024	m
Tube inside diameter	D_i	=	0.023	m
Tube thermal conductivity	k_t	=	20	$\frac{W}{m \cdot K}$
Total number of tubes	N_t	=	26000	-
Total number of passes	N_p	=	2	-
Total cooling water flowrate through condenser	F_{CW}	=	10.43	$\frac{m^3}{s}$
Total tube length	L_t	=	12	m
Incoming steam quality	q	=	1	-

Table 7: Guess values used for the main turbine condenser sample calculations

Cooling water outlet temperature	$T_{CW_{out}}$	=	50	°C
Steam saturation temperature	T_{Sat}	=	60	°C
Tube outside wall temperature	T_{Wall_o}	=	50	°C

F.1.1 Fluid thermodynamic properties

It is first necessary to calculate the mass flow rate of the incoming cooling water using the guess values in Table 6.

The bulk mean temperature for the cooling water inside the condenser tube is calculated as:

$$T_{CW_m} = \frac{T_{CW_{in}} + T_{CW_{out}}}{2} \tag{40}$$

$$T_{CW_m} = \frac{30 + 50}{2} = 40\ °C$$

The density of the cooling water inside the condenser tube is calculated by using Equation (36).

$$\rho_{CW} = 988.80\ \frac{kg}{m^3}$$

The specific heat capacity of the cooling water inside the condenser tube is calculated by using Equation (39).

$$Cp_{CW} = 4177.82\ \frac{J}{kg \cdot K}$$

The cooling water mass flow rate is calculated as:

$$m_{CW} = F_{CW} \cdot \rho_{CW} \tag{41}$$

$$m_{CW} = 10.43 \cdot 988.80 = 10313.21\ \frac{kg}{s}$$

The cooling water outlet temperature is then calculated as:

$$T_{CW_{out}} = \frac{E_{Reg} \cdot 1000000}{m_{CW} \cdot Cp_{CW}} + T_{CW_{in}} \tag{53}$$

$$T_{CW_{out}} = \frac{624.07 \cdot 1000000}{10325.12 \cdot 4178.48} + 30 = 44.48\ °C$$

The new bulk mean temperature for the cooling water is calculated as:

$$T_{CW_m} = \frac{T_{CW_{in}} + T_{CW_{out}}}{2} \quad (40)$$

$$T_{CW_m} = \frac{30 + 44.48}{2} = 37.24\ °C$$

The density of the cooling water inside the condenser tubes is calculated by using Equation (36) and the bulk cooling water temperature.

$$\rho_{CW} = 989.94\ \frac{kg}{m^3}$$

The specific heat capacity of the cooling water inside the condensers tube is calculated by using Equation (39) and the bulk cooling water temperature.

$$Cp_{W\,CW} = 4178.48\ \frac{J}{kg \cdot K}$$

The thermal conductivity of the cooling water inside the condensers tube is calculated by using Equation (38) and the bulk cooling water temperature.

$$k_{CW} = 0.623\ \frac{W}{m \cdot K}$$

The viscosity of the cooling water inside the condenser tubes is calculated by using Equation (37) and the bulk cooling water temperature.

$$\mu_{CW} = 0.000708\ \frac{kg}{s \cdot m}$$

The Prandtl number for the cooling water inside the condenser tubes is calculated as (Cengel and Ghajar, 2015):

$$Pr_{CW} = \frac{\mu_{CW} \cdot Cp_{CW}}{k_{\mathrm{CW}}} \quad (54)$$

$$Pr_{CW} = \frac{0.000708 \cdot 4178.48}{0.623} = 4.75$$

The density of the condensate exiting the condenser is calculated by using Equation (36) and the steam saturation temperature.

$$\rho_c = 979.67\ \frac{kg}{m^3}$$

The specific heat capacity of the condensate exiting the condenser is calculated by using Equation (39) and the steam saturation temperature.

$$Cp_c = 4181.68\ \frac{J}{kg \cdot K}$$

The thermal conductivity of the condensate exiting the condenser is calculated by using Equation (38) and the steam saturation temperature.

$$k_c = 0.647\ \frac{W}{m \cdot K}$$

The viscosity of the condensate exiting the condenser is calculated by using Equation (37) and the steam saturation temperature.

$$\mu_c = 0.000474\ \frac{kg}{s \cdot m}$$

The Prandtl number for the condensate exiting the condenser tubes is calculated as Equation (36) (Cengel and Ghajar, 2015):

$$Pr_c = \frac{\mu_c \cdot Cp_c}{k_c} \tag{55}$$

$$Pr_c = \frac{0.000407\ \cdot 4181.68}{0.647} = 3$$

The latent heat available to be transferred from the steam to the cooling water based on the steam saturation temperature is calculated as (Cooper and Le Fevre, 1969):

$$h_{fg} = h_V(T_{Sat}) - h_L(T_{Sat}) \tag{56}$$

$$h_{fg} = 2584.21 - 192.71 = 2391.56\ \frac{kJ}{kg}$$

The enthalpy of the steam entering the condenser is calculated as:

$$h_s = h_V(T_{Sat}) \cdot \mathrm{q} - \ h_L(T_{Sat}) \cdot (1 - q) \tag{57}$$

$$h_s = 2584.21 \cdot 1 - 192.71 \cdot (1 - 1) = 2584.26\ \frac{kJ}{kg}$$

F.1.2 Flow rates

The cooling water mass flow rate is calculated as:

$$m_{CW} = F_{CW} \cdot \rho_{CW} \tag{41}$$

$$m_{CW} = 10.43 \cdot 989.94 = 10325.12\ \frac{kg}{s}$$

The cross sectional cooling water flow area of the inside of the condenser is calculated as:

$$A_i = \pi \cdot \left(\frac{D_i}{2}\right)^2 \cdot \left(\frac{N_t}{N_p}\right) \tag{42}$$

$$A_i = \pi \cdot \left(\frac{0.023}{2}\right)^2 \cdot \left(\frac{26000}{2}\right) = 5.40\ m^2$$

The cooling water linear velocity inside each of the tubes inside the condenser tube is calculated as:

$$u_{CW} = \frac{F_{CW}}{A_i \cdot 1000} \tag{43}$$

$$u_{CW} = \frac{10.43}{5.40} = 1.931\ \frac{m}{s}$$

The condensate mass flow is calculated as:

$$m_C = \frac{E_{Reg} \cdot 1000}{h_s - h_c} \tag{58}$$

$$m_c = \frac{624.07 \cdot 1000}{2608.8 - 192.7} = 260.95\ \frac{kg}{s}$$

F.1.3 Friction factor and Reynolds numbers

The Reynolds number for the cooling water is calculated as (Cengel and Ghajar, 2015):

$$Re_{CW} = \frac{D_i \cdot u_{CW} \cdot \rho_{CW}}{\mu_{CW}} \quad (10)$$

$$Re_{CW} = \frac{0.023 \cdot 1.931 \cdot 989.94}{0.000708} = 62106.64$$

The friction factor inside the condenser tube is calculated by using the Petukhov's correlation (Cengel and Ghajar, 2011):

$$f_{CW} = (0.79 \cdot \ln(Re_{CW}) - 1.64)^{-2} \quad (28)$$

$$f_{CW} = (0.79 \cdot \ln(62117.92) - 1.64)^{-2} = 0.02$$

F.1.4 Nusselt numbers and convection heat transfer coefficients

The Nusselt number for the cooling water is calculated by using (Cengel and Ghajar, 2015):

$3000 < Re > 10^6$:

$$Nu_{CW} = \frac{\left(\frac{f_{CW}}{8}\right) \cdot (Re_{CW} - 1000) \cdot Pr_{CW}}{\left(1 + 12.7 \cdot \left(\frac{f_{CW}}{8}\right)^{0.5} \cdot \left(Pr_{CW}{}^{\frac{2}{3}} - 1\right)\right)} \quad (7)$$

$$Nu_{CW} = \frac{\left(\frac{0.02}{8}\right) \cdot (62117.92 - 1000) \cdot 4.75}{\left(1 + 12.7 \cdot \left(\frac{0.02}{8}\right)^{0.5} \cdot \left(4.75^{\frac{2}{3}} - 1\right)\right)} = 335.58$$

The convection heat transfer coefficient for the cooling water is calculated by using:

$$h_{CW} = \frac{Nu_{CW} \cdot k_{CW}}{D_i} \tag{8}$$

$$h_{CW} = \frac{336.11 \cdot 0.622}{0.023} = 9083.17 \ \frac{W}{m^2 \cdot K}$$

The average convection heat transfer coefficient for film condensation on the outer surface of a single horizontal tube is calculated as (Cengel and Ghajar, 2011):

$$h_{shell} = 0.729 \cdot \left(\frac{{h_{fg}}^* \cdot {\rho_c}^2 \cdot g \cdot {k_s}^3}{\mu_c \cdot (T_{Sat} - T_{Wall_o}) \cdot D_O} \right)^{0.25} \tag{29}$$

Film condensation takes place on a vertical tier of horizontal tubes and Equation (29) is, therefore, modified to with a correction factor as indicated in Equation (30).

$$h_{shell} = 0.729 \cdot \left(\frac{{h_{fg}}^* \cdot {\rho_c}^2 \cdot g \cdot {k_s}^3}{\mu_c \cdot (T_{Sat} - T_{Wall_o}) \cdot D_O} \right)^{0.25} \cdot N^{-0.25} \tag{30}$$

The main turbine condenser tubes have a church window design layout and the correction factor N was obtained from the original condenser design documents.

${h_{fg}}^*$ is calculated as (Cengel and Ghajar, 2011):

$${h_{fg}}^* = h_{fg} \cdot 1000 + 0.68 \cdot Cp_c \cdot (T_{Sat} - T_{Wall_o}) \tag{31}$$

The outside tube area available for heat transfer is calculated as Equation (32):

$$A_c = 2 \cdot \pi \cdot \left(\frac{D_0}{2} \right) \cdot L_t \cdot N_t \tag{59}$$

$$A_c = 2 \cdot \pi \cdot \left(\frac{0.024}{2} \right) \cdot 12 \cdot 26000 = 23524.25 \, m^2$$

The tube outside wall temperature (T_{Wall_o}) need to be calculated by an iterative process as follow:

Step 1: Calculate ${h_{fg}}^*$

$${h_{fg}}^* = h_{fg} \cdot 1000 + 0.68 \cdot Cp_c.(T_{Sat} - T_{Wall_o}) \quad (31)$$

$${h_{fg}}^* = 2357.7 \cdot 1000 + 0.68 \cdot 4181.65 \cdot (60 - 50) = 2386126.22 \ \frac{J}{kg}$$

Step 2: Calculate h_{shell}

$$h_{shell} = 0.729 \cdot \left(\frac{{h_{fg}}^* \cdot {\rho_c}^2 \cdot g \cdot {k_s}^3}{\mu_c \cdot (T_{Sat} - T_{Wall_o}) \cdot D_O} \right)^{0.25} \cdot N^{-0.25} \quad (29)$$

$$h_{shell} = 0.729 \cdot \left(\frac{(2386126.22) \cdot (979.67)^2 \cdot (9.801) \cdot (0.647)^3}{(4.74E-4) \cdot (60 - 50) \cdot 0.024} \right)^{0.25} \cdot (3.8)^{-0.25}$$

$$= 5689.82 \frac{W}{m^2 \cdot K}$$

Step 3: Calculate the rate of heat transfer using h_{shell}

$$Q_C = \frac{h_{shell} \cdot A_c \cdot (T_{Sat} - T_{Wall_o})}{1000000} \quad (60)$$

$$Q_C = \frac{(5689.82) \cdot (23524.25) \cdot (60 - 50)}{1000000} = 1338.48 \ MW$$

Step 4: Compare Q_C and E_{Reg}. Repeat step 1 to 4 until $\left| Q_C - E_{Reg} \right| < 1E - 10$

h_{shell} and T_{Wall_o} is calculated as 7319.05 $\frac{W}{m^2 \cdot K}$ and 55.33 °C respectively after 22 iterations.

F.1.5 Thermal resistances

The cooling water thermal resistance is calculated as:

$$R_{CW} = \frac{1}{h_{CW} \cdot A_s} \tag{47}$$

$$R_{CW} = \frac{1}{9083.17 \cdot 22544.06} = 4.883 \cdot 10^{-9} \frac{K}{W}$$

Where the total tube inside area available for heat transfer is:

$$A_s = 2 \cdot \pi \cdot \left(\frac{D_i}{2}\right) \cdot L_t \cdot N_t \tag{48}$$

$$A_s = 2 \cdot \pi \cdot \left(\frac{0.023}{2}\right) \cdot 12 \cdot 26000 = 22544.06\, m^2$$

The thermal resistance of the tube wall is calculated as:

$$R_{tube} = \frac{ln\left(\frac{D_O}{D_i}\right)}{2 \cdot \pi \cdot k_t \cdot L_t \cdot N_t} \tag{51}$$

$$R_{tube} = \frac{ln\left(\frac{0.024}{0.023}\right)}{2 \cdot \pi \cdot 20 \cdot 12 \cdot 26000} = 1.086 \cdot 10^{-9} \frac{K}{W}$$

The fouling resistance respective to the condenser tube volume is calculated as:

$$R_f = \frac{R_{f_D}}{A_{shell_S}} \tag{61}$$

$$R_f = \frac{4.96\text{E} - 6}{23524.25} = 2.1084 \cdot 10^{-10} \frac{K}{W}$$

The thermal resistance for the steam flowing on the outside of the condenser tubes is given as:

$$R_{shell} = \frac{1}{h_{shell} \cdot A_{shell_S}} \tag{62}$$

$$R_{shell} = \frac{1}{731.05 \cdot 23524.25} = 5.808 \cdot 10^{-9} \frac{K}{W}$$

The total thermal resistance is calculated by using Equation (5):

$$\sum R = R_{CW} + R_{tube} + R_f + R_{shell} \quad (5)$$

$$\sum R = 4.883 \cdot 10^{-9} + 1.086 \cdot 10^{-9} + 2.1084 \cdot 10^{-10} + 5.808 \cdot 10^{-9}$$
$$= 1.198 \cdot 10^{-9} \frac{K}{W}$$

F.1.6 Heat transfer

The log mean temperature difference is calculated as (Cengel and Ghajar, 2011):

$$\Delta T_{LM} = \frac{\left(T_{CW_{out}} - T_{CW_{in}}\right)}{\ln\left(\frac{T_{\mathrm{Sat}} - T_{CW_{in}}}{T_{Sat} - T_{CW_{out}}}\right)} \quad (3)$$

$$\Delta T_{LM} = \frac{(44.48 - 30)}{\ln\left(\frac{60 - 30}{60 - 44.48}\right)} = 21.96\ ℃$$

The overall heat transfer coefficient is calculated as Equation (4):

$$U = \frac{1}{A_c \cdot \sum R} \quad (4)$$

$$U = \frac{1}{23524.25 \cdot 1.198 \cdot 10^{-9}} = 3546.02 \frac{W}{m^2 \cdot K}$$

The total heat transfer rate is calculated as Equation (2):

$$Q_{Calc} = \frac{U \cdot A_c \cdot \Delta T_{LM}}{1000000} \quad (2)$$

$$Q_{Calc} = \frac{3546.02 \cdot 23524.25 \cdot 21.96}{1000000} = 1832.50\ MW$$

The steam saturation temperature is calculated and compared to the actual steam saturation temperature in

Table 7 derived from Equation (3).

$$T_{Sat} = \frac{T_{CW_{in}} - T_{CW_{out}} \cdot e^{\frac{(T_{CW_{out}} - T_{CW_{in}})}{\Delta T_{LM}}}}{1 - e^{\frac{(T_{CW_{out}} - T_{CW_{in}})}{\Delta T_{LM}}}} \tag{63}$$

$$T_{Sat} = \frac{30 - 44.48 \cdot e^{\frac{(44.48-30)}{7.48}}}{1 - e^{\frac{(44.48-30)}{7.48}}} = 46.92\ ℃$$

The new values calculated in above are used as the values for the second iteration. This process is repeated until $\left|Q_{Calc} - E_{Reg}\right| < 1E - 10$. The condition was reached within 3 iterations in this case. The final values calculated after the iterations are shown in Table 8.

Table 8: Iterated values for the variables above.

Parameter		Value		Parameter		Value	
$T_{CW_{out}}$	=	44.46	°C	f_{CW}	=	0.2	-
T_{CW_m}	=	37.23	°C	Nu_{CW}	=	335.56	-
ρ_{CW}	=	989.95	$\frac{kg}{m^3}$	h_{CW}	=	9082.43	$\frac{W}{m^2 \cdot K}$
Cp_{CW}	=	4178.48	$\frac{J}{kg \cdot K}$	h_{shell}	=	7319.06	$\frac{W}{m^2 \cdot K}$
k_{CW}	=	0.623	$\frac{W}{m \cdot K}$	$h_{fg}{}^*$	=	2367997.7	$\frac{J}{kg}$
μ_{CW}	=	7.079E-4	$\frac{kg}{s \cdot m}$	A_c	=	23524.25	m^2
Pr_{CW}	=	4.75	-	Q_C	=	624	MW
ρ_c	=	985.82	$\frac{kg}{m^3}$	R_{CW}	=	4.884E-09	$\frac{K}{W}$
Cp_c	=	4177.55	$\frac{J}{kg \cdot K}$	A_s	=	22544.07	m^2
k_c	=	0.634	$\frac{W}{m \cdot K}$	R_{tube}	=	2.0855E-09	$\frac{K}{W}$
μ_c	=	5.908E-4	$\frac{kg}{s \cdot m}$	R_f	=	2.1084E-10	$\frac{K}{W}$
Pr_c	=	3.78	-	R_{shell}	=	5.8080E-09	$\frac{K}{W}$
h_{fg}	=	2389.42	$\frac{kJ}{kg}$	$\sum R$	=	1.1988E-08	$\frac{K}{W}$
h_s	=	2585.85	$\frac{kJ}{kg}$	ΔT_{LM}	=	7.481	°C
m_{CW}	=	10325.16	$\frac{kg}{s}$	U	=	3545.90	$\frac{W}{m^2 \cdot K}$
A_i	=	5.401	m^2	Q_{Calc}	=	624	MW
u_{CW}	=	1.931	$\frac{m}{s}$	T_{Sat}	=	46.911	°C
m_C	=	261.18	$\frac{kg}{s}$	P_{Sat}	=	10.57	kPa
Re_{CW}	=	62106.60	-	T_{Wall_o}	=	43.30	°C